Naval Research Laboratory

Washington, DC 20375-5320

Radio-Frequency Propagation Measurements in Confined Ship Spaces Aboard the ex-USS *Shadwell*

ERIC L. MOKOLE
MARK PARENT
SURENDRA N. SAMADDAR
EDMOND TOMAS
BRIAN T. GOLD
TOM T. STREET
JOHN VALENZI

Target Characteristics Branch
Radar Division

August 18, 2000

20000919135

REPORT DOCUMENTATION PAGE

Public reporting burden for this collection of information is estimated to average 1 hour per response, including the time for reviewing instructions, searching existing data sources, gathering and maintaining the data needed, and completing and reviewing the collection of information. Send comments regarding this burden estimate or any other aspect of this collection of information, including suggestions for reducing this burden, to Washington Headquarters Services, Directorate for Information Operations and Reports, 1215 Jefferson Davis Highway, Suite 1204, Arlington, VA 22202-4302, and to the Office of Management and Budget, Paperwork Reduction Project (0704-0188), Washington, DC 20503.

1. AGENCY USE ONLY (Leave Blank)	2. REPORT DATE August 18, 2000	3. REPORT TYPE AND DATES COVERED Final	
4. TITLE AND SUBTITLE Radio-Frequency Propagation Measurements in Confined Ship Spaces Aboard the ex-USS *Shadwell*			**5. FUNDING NUMBERS** PE — 603508N
6. AUTHOR(S) Eric L. Mokole, Mark Parent, Surendra N. Samaddar, Edmond Tomas, Brian T. Gold, Tom T. Street, and John Valenzi			
7. PERFORMING ORGANIZATION NAME(S) AND ADDRESS(ES) Naval Research Laboratory Washington, DC 20375-5320			**8. PERFORMING ORGANIZATION REPORT NUMBER** NRL/MR/5340--00-9951
9. SPONSORING/MONITORING AGENCY NAME(S) AND ADDRESS(ES) Office of Naval Research Arlington, VA 22203			**10. SPONSORING/MONITORING AGENCY REPORT NUMBER**

11. SUPPLEMENTARY NOTES

12a. DISTRIBUTION/AVAILABILITY STATEMENT Approved for public release; distribution is unlimited.	12b. DISTRIBUTION CODE

13. ABSTRACT (Maximum 200 words)

Understanding the propagation of RF energy in confined naval shipboard environments is extremely important to the operability and effectiveness of communication systems used by the Navy. Single-frequency communication systems are known to suffer from multipath interference that can render them ineffective in confined spaces. Spread-spectrum and frequency-hopping systems, currently used in wireless local area networks (LANs), have been shown to operate effectively in confined shipboard environments in the absence of other RF signals. However, the transfer characteristics of these signals relative to bulkheads, watertight doors, ducts, mast cable transits, compartment penetrations and obstructions, and steel deckplates are not well characterized. Also, the complex interactions of communication signals with competing RF signals are not well understood for confined ship spaces. To address these issues for systems between 800 MHz and 3 GHz, a broadband bistatic measurement system was designed, and initial measurements were taken on the ex-USS *Shadwell* (23-25 February 1998) in Mobile, Alabama. More than 100 sets of data were collected for various open/closed door configurations on three levels of the ex-USS *Shadwell*. The measurement system and the measurements are discussed. Initial observations indicate that received power levels over reasonably long propagation distances were sufficient to ensure communication, even when all closures were set.

14. SUBJECT TERMS			15. NUMBER OF PAGES 76
RF propagation Confined ship spaces Communication	Radar Electromagnetic interference Electromagnetic compatibility	Jamming Reduced manning Damage control	16. PRICE CODE

17. SECURITY CLASSIFICATION OF REPORT UNCLASSIFIED	18. SECURITY CLASSIFICATION OF THIS PAGE UNCLASSIFIED	19. SECURITY CLASSIFICATION OF ABSTRACT UNCLASSIFIED	20. LIMITATION OF ABSTRACT UL

NSN 7540-01-280-5500

CONTENTS

RADIO-FREQUENCY PROPAGATION MEASUREMENTS
IN CONFINED SHIP SPACES ABOARD THE EX-USS *SHADWELL*

INTRODUCTION

Understanding the propagation of radio-frequency (RF) energy in confined naval shipboard environments is extremely important to the operability and effectiveness of communication systems used by the Navy. Single-frequency communication systems are known to suffer from multipath interference that can render them ineffective in confined ship spaces without the use of leaky-wave antennas. Spread spectrum and frequency-hopping systems, currently used in wireless local area networks (LANs), have been shown to operate effectively in confined shipboard environments in the absence of competing RF sources. However, the transfer characteristics of these signals with respect to steel bulkheads, watertight doors, ducts, mast cable transits (MCTs), and steel deckplates are not fully understood. Good propagation in this environment does not ensure good communication, because signals in adjacent compartments may interfere with each other, thereby making them difficult to distinguish. The mechanisms that enable good propagation of communications signals also permit equally good propagation of competing radar and jamming signals. The complex interaction of these competing RF sources is not well understood for confined ship spaces.

To understand and characterize the underlying radiation and propagation mechanisms of signal sources at frequencies between 800 MHz and 3 GHz in confined ship spaces, a broadband bistatic measurement system was developed. This measurement system was tested on the USS *Barry* (28 January 1998) at the Washington Navy Yard in Washington, DC, and was subsequently refined. The improved system was transported to the ex-USS *Shadwell*, the Naval Research Laboratory's Advanced Fire Research Vessel,[1] where data were collected (23-25 February 1998) to ascertain how a ship's structure affects signal propagation over the frequencies of interest. The ex-USS *Shadwell* is moored at Little Sand Island in Mobile, AL, and serves as a test vessel for the Navy's Systems Commands, under the control of the Navy Technology Center for Safety and Survivability (NTCSS) at the Naval Research Laboratory (NRL).[2]

This work was sponsored by the ONR program, Damage Control – Automation for Reduced Manning (DC–ARM). The underlying purpose of this study was to determine the limitations of shipboard emergency communications during damage-control episodes when Condition Zebra is set (that is, when compartment doors are closed). To quantify the distribution of energy from an electromagnetic (EM) source inside a ship's compartments, data were sampled and received power levels were collected for various open/closed door configurations, for selected locations of the transmitter and receiver on three levels of the ex-USS *Shadwell*, and for different signal polarizations. Each data set consisted of 23 values of received power at frequencies running from between 800 MHz to 3 GHz in 100 MHz increments.

The second section discusses some of the problems and issues associated with RF communication that have been experienced on Navy ships and provides some historical background on RF propagation in confined ship spaces. The next two sections describe the broadband bistatic measurement system that was used to take the *Shadwell* data and the measurement methodology. The data analysis and associated theory are addressed in the fifth section. Some of the relevant EM theory is discussed, and an algorithm is provided for calculating the effective propagation loss from the measured received power at each

frequency. The propagation-loss parameter is chosen because it is independent of the measurement system. Consequently, the results should be applicable for arbitrary measurement systems. In the final section, the observations of test results are summarized.

HISTORICAL PERSPECTIVE AND BACKGROUND ON SHIPBOARD RF PROPAGATION

Ships of the future will require extensive, state-of-the-art, communication networks that are capable of integrating a multitude of communication architectures with numerous communication sources and technologies to ensure communication capabilities at any time throughout a ship. These systems must have the ability to transfer vast amounts of sensor data related to a ship's condition, damage-control operation, and C^3 functions. In addition, the systems must survive in the event of damage from casualty or conflict, must be resistant to hostile electronic attack (EA) and to electromagnetic interference (EMI) from other ownship RF sources, and must not cause EMI problems for other devices on the ship. A communication system can be programmed to perform operational testing to determine current coverage, to reroute data as necessary to reestablish coverage, and to reprogram or reconfigure itself to continue operation by shedding nonfunctional and/or destroyed segments to recover communication capabilities. Wireless RF communications can provide a flexibility not offered by wired and cabled systems when interruptions occur from damage to wire and fiber-optic conductors. With the implementation of spread-spectrum direct-sequence and frequency-hopping systems, wireless RF LANs have become leading candidates for use in the highly multipath environment of confined shipboard spaces. Although these RF communication systems cannot match the data throughput available in wired systems, they currently can achieve rates in excess of 10 Mb/s, with large throughput improvements on the horizon. However, the commercial-off-the-shelf (COTS) wireless LANs that are currently being deployed on Navy ships are susceptible to eavesdropping, EA, and ownship EMI. The impact of these vulnerabilities can be substantial. ·

This propagation problem has ramifications for a variety of competing shipboard interests: communications, radar, jamming, and EMI. In designing future ships, the trade-offs among these competing interests are important and require in-depth knowledge of RF propagation within the confines of Navy ships. Unfortunately, after undertaking an extensive search of the literature, very little characterization and documentation was found on the propagation of RF signals in confined ship spaces. Although current communication systems work well in confined ship spaces under ideal condtions for a broad range of frequencies, it is not known exactly how or why this is true. In fact, it is not clear whether signals from different sources in this environment can be discriminated. Since communication systems will share the RF spectrum with devices like radars and electrically driven machinery, one must know when a communication system will work and when problems can be expected.

In a related area, much speculation exists on whether ion-producing fires affect RF signals. It is well known that ion production in fires is a function of fuel type.[3-5] For instance, no ionization occurs with alcohol-based fuels; whereas heptane and diesel fuels induce ionization near the flame. Data support the contention that the magnitude of an RF signal can be increased by multiple-scatter induced focusing when the signal travels through an ionized medium. Specifically, trans-ionospheric data show that an RF signal is enhanced on the line-of-sight path through the ionosphere.[6] It is not clear whether this phenomenon is relevant to shipboard fires, because the ionization levels and the thickness of the ionized medium are much less than that of the ionosphere. In fact, one might well argue that the signal attenuation from soot, smoke, steam, and water mist is more important than the flame ionization. Questions regarding possible interruptions or enhancements caused by ion production, smoke, soot, steam, and water mist from large-scale and extremely hot fires to RF communications need to be answered, especially if these systems are to be used in support of damage control operations.

The propagation of electromagnetic (EM) waves below deck aboard Navy vessels has been a concern of shipboard personnel and test teams for many years. The most common example is the use of walkie talkies. The cables and piping that pass through a ship's space provide excellent conduits for RF energy to

pass from one location to another. These propagation channels have apparently led to EMI problems on ships. For example, the USS *Oak Hill* (LSD 51)[7] was surveyed for below-decks EMI from 23 September through 4 October 1996 as part of a Shipboard-Electromagnetic-Compatibility-Improvement-Program (SEMCIP) event. Mild-to-severe EMI was experienced by COTS PC monitors and televisions from portable VHF and UHF transceivers, and the AN/SPS-49 radar (851 - 942 MHz) caused severe EMI to a weather-deck phone and mild EMI to pilot-house phones.[8] These occurrences certainly illustrate the problems that arise from EM interactions between communication systems and high-powered radars on Navy ships.

EMI from shipboard portable transceivers are known to cause degradations in the performance of other shipboard systems. A case in point is the measured EMI (27-28 August 1997) from the AN/SRC-55 (XN-1) HYDRA UHF communication system on the USS *Ponce* (LPD 15)[7] to the SPS-40E, a two-dimensional air-search radar aboard amphibious ships. HYDRA operates from 406 to 420 MHz, with channels separated by 25 kHz. NRL's Radar Division (Code 5300) was tasked by SPAWAR Systems Center, Charleston Detachment (Code 514), to determine the severity of the EMI on the SPS-40E and to recommend appropriate filters to remedy the EMI effects. The levels of EMI were quantified for each channel, and a design for a bandpass filter was developed to correct the problem.[9] Testing the filter is scheduled for the spring of 2000. Moreover, to estimate the degradation of the performance of an electronic system by EMI, the Radar Division has developed the Advanced Technology Chamber (ATC) to simulate RF modes of propagation both on a ship's topside and in a shipboard compartment.

The ATC is a completely enclosed, welded, aluminum chamber (2.73 × 4.64 × 5.33 m) with access panels on its bulkheads that can be modified to feed cables or other objects into its interior. This chamber provides an accurate model of a tightly sealed ship compartment in a controlled laboratory setting. In fact, it is capable of providing 110 dB of effective shielding, whereas typical compartments on ships attain only 20 dB of shielding effectiveness. The chamber is equipped with its own measurement system consisting of a LabVIEW interface, a scalar network analyzer, electric-field intensity probes, a frequency synthesizer, and power amplifiers. The ATC is capable of modeling the effects of wireless communications inside the hull of a ship for frequencies between 200 MHz and 40 GHz.[10]

Recently (January 1999), the Office of Naval Research began funding The Charles Stark Draper Laboratory, Inc., to manage an Advanced Technology Demonstration (ATD) on Reduced Ship Crew by Virtual Presence (RSVP). This program is scheduled to run until October 2001, and three demonstrations are to be performed in the last year. The goal of the RSVP ATD is to develop a system that provides reliable near real-time monitoring and assessment of a ship's state at the compartment level to enable crew reduction under normal ship conditions.[11] RSVP is supposed to provide information on the state of a compartment in four functional areas: status of personnel (location, pulse, skin temperature, etc.), status of machinery (operational, configuration, health), the structural integrity of the space (hull girder stress, hull acceleration, corrosivity, etc.), and the environment (temperature, humidity, fire, flood, etc.). The ISM band (2.4 – 2.4835 GHz) has been selected for communication between access points, sensor clusters, personnel status monitors, and machinery monitors. Because the RSVP system is being developed for naval combatants, it must be able to run reliably in the electromagnetically dense and hostile environment of such vessels. Consequently, RSVP should work when competing with EA, ownship radars, and other ownship RF devices. To do so requires a good understanding of this complex propagation environment that currently does not exist.

Over the last four years, the NTCSS has sponsored a number of tests of wireless, spread-spectrum, RF LANs on the ex-USS *Shadwell* to determine the capabilities and limitations of such systems when they are operated in the highly multipath environment of confined ship spaces.[12-14] During one of these tests with a 915 MHz direct-sequence, spread-spectrum LAN, the expected major interruption of RF communications by the ship's steel structure (bulkheads, overheads, and decks), closed watertight doors, and compartment penetrations/obstructions did not occur. Instead, the dominant effect appeared to be an approximate 10 dB signal loss for each closed watertight door and/or bulkhead. It was therefore

determined that an understanding of the basic propagation characteristics of signals onboard ships is necessary to understand signal transmission in this environment, which led to the work that is discussed in this report.

Figure 1 shows examples of confined ship spaces in the starboard passageway of the *Shadwell's* main deck. In the left frame, the open watertight door is highlighted. Additionally, one can see two pipes running from the deck through the overhead in the left portion of the background. This is but one example of the clutter and compartment penetrations that abound on a ship. In the right frame, the MCT is shown above another watertight door. Although you can't see it, the distributed cable network passes through the top of the MCT. One of many cables in the bundle that passes through the MCT is the leaky-wave communication cable of Fig. 2. This cable runs the full length of the starboard and port passageways, with segments branching to other levels and connecting the two passageways at selected locations. In the figure, the top piece shows a cross sectional view of the cable, and the bottom piece shows the cable after the protective outer layer has been stripped to the corrugated copper layer. The copper is shaved along the full length of the cable on opposite sides to permit the communication signal to leak out of the cable as it propagates along the core. This is one of the many possible modes of signal propagation in confined ship spaces.
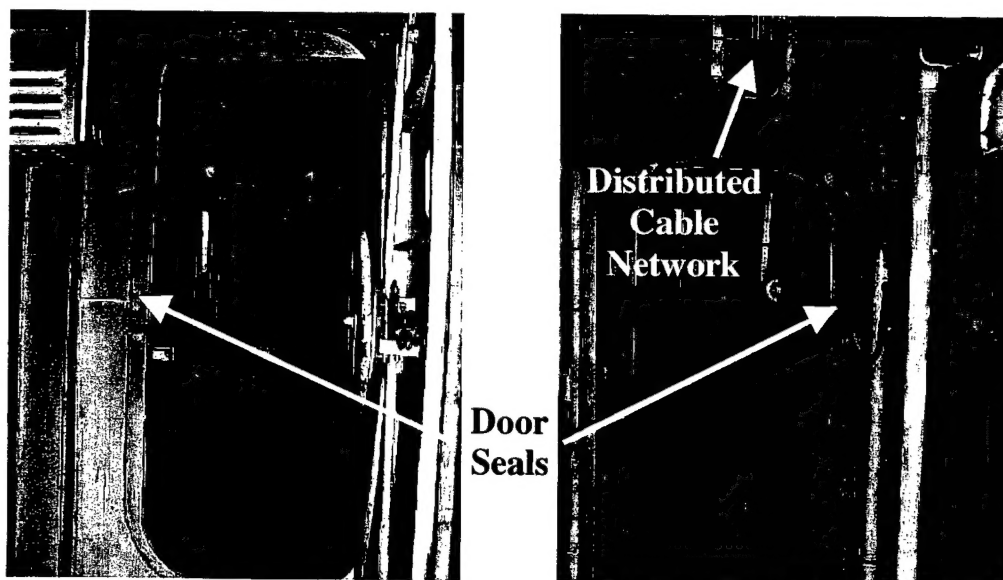
Fig. 1 — Distributed cable network, watertight door seals, pipes, and other penetrating objects on the main deck of the ex-USS *Shadwell*.

As noted in the introduction, preliminary investigations were conducted on the ex-USS *Shadwell* (23-25 February 1998) to investigate the contributions from the various modes of transfer of RF signals in a shipboard environment: distributed cable networks, watertight door seals, compartment penetrations/obstructions (MCTs, ducts, gratings, vents, etc.), the waveguide-like nature of ship compartments and passageways, the coaxial transmission behavior of shielded cable in compartments and passageways, and the effects of multipath. These tests determined the necessary measurement equipment and verified the ship-compartment geometries and types of tests that are required to investigate the modes of transfer of RF signals in confined ship spaces properly. The preliminary findings are presented in this report and are documented in an NRL Letter Report[15] and a conference paper.[16]
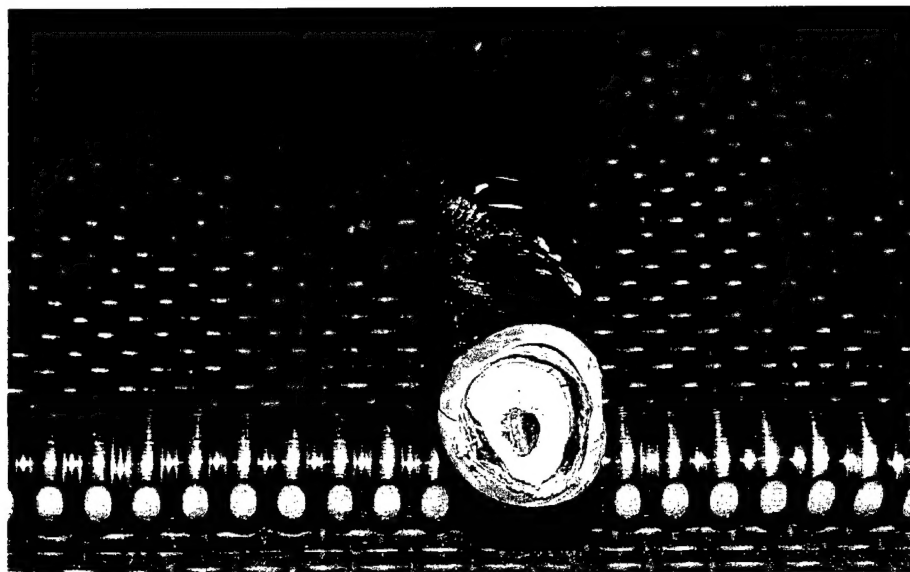
Fig. 2 — Leaky-wave communication cable.

Concurrent with the RF propagation testing on the ex-USS *Shadwell*, two other measurement campaigns were conducted. Under contract N00014-97C-2064, Lucent Technologies took CW measurements at 2.48 GHz to determine the performance of their modulated backscatter radios (MBS) for ambient and fire environments, and the results were excellent. The other group (Penn State University Applied Physics Laboratory), under the sponsorship of the RSVP program, tested the effects of a compartment fire on four RF spread-spectrum communications systems: two from 902 to 928 MHz, one at 2.4 GHz, and one at 5.6 GHz.

BISTATIC MEASUREMENT SYSTEM

The bistatic measurement system used in this study consists of a Hewlett Packard (HP) 8592L spectrum analyzer, an HP 83752A synthesized signal source (10 MHz to 20 GHz), an HP 8347A RF amplifier (100 kHz to 3 GHz), a broadband disc-cone transmitting antenna, a laptop computer, a broadband batwing receiving dipole, and a small coaxially tipped receiving probe. Figure 3 shows the system. Both the disc-cone (Fig. 4) and the batwing dipole (Fig. 5) can be repositioned to have a dual-polarization capability. The signal source is stepped (open-loop) in 100 MHz frequency increments from 800 MHz through 3 GHz, inclusive, so that the transmitting antenna emits a stepped CW signal at the indicated 23 frequencies. The broadband disc-cone, which also covers 800 MHz to 3 GHz, is attached to the signal source to form the transmitter, and the receiving antennas are connected to the spectrum analyzer to form the receiving system. The batwing dipole is the receiving antenna for most measurements; the smaller coaxial probe (Fig. 5) is used to measure the electric field intensities very close to an object's surface and near hard-to-reach places. The spectrum analyzer is controlled through an HPIB interface that is connected to the laptop computer and measures the absolute signal-amplitude levels. The computer then transfers the data from the spectrum analyzer to a file. Measurement software was developed and was integrated with the receiving system through the LabVIEW interface.
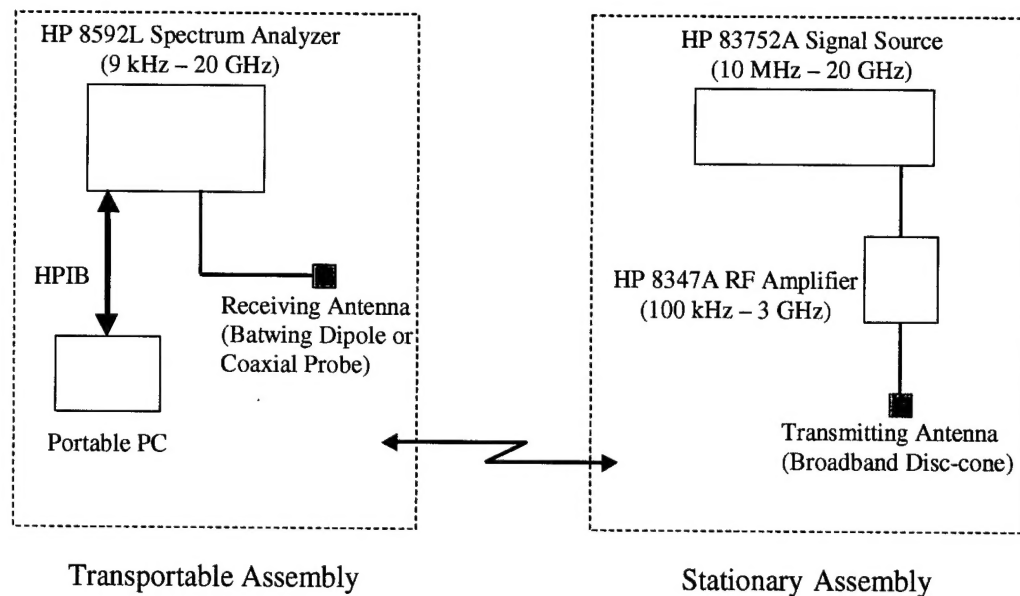
Fig. 3 — The bistatic measurement system
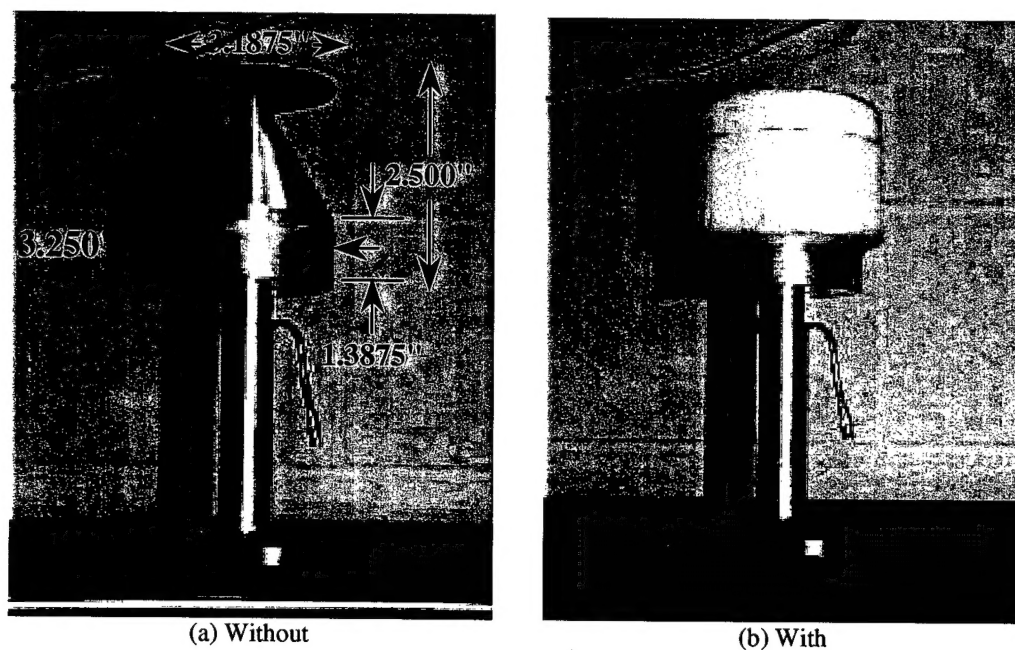
(a) Without   (b) With

Fig. 4 — Broadband disc-cone transmitting antenna without and with a protective styrofoam cover

The transmitting antenna is mounted on a tripod so that the center of the radiator is 5 ft above the ground. For this system, the disc-cone is a structure that consists of a truncated half-cone, a cylinder, and a disk (Fig. 4.). The disk has a 3.1875-in. diameter and sits atop the apex of the half cone. The height and diameter of the half-cone are 1.1125 in. and 3.250 in., respectively. The cylindrical portion has height and diameter of 1.3875 in. and 3.250 in., respectively, and lies below the half-cone. As Fig. 4 indicates, most of the antenna is protected by an outer layer of styrofoam. Reference 17 describes general properties of the disc-cone antenna.

(a) Broadband Batwing Dipole   (b) Coaxially Tipped Probe
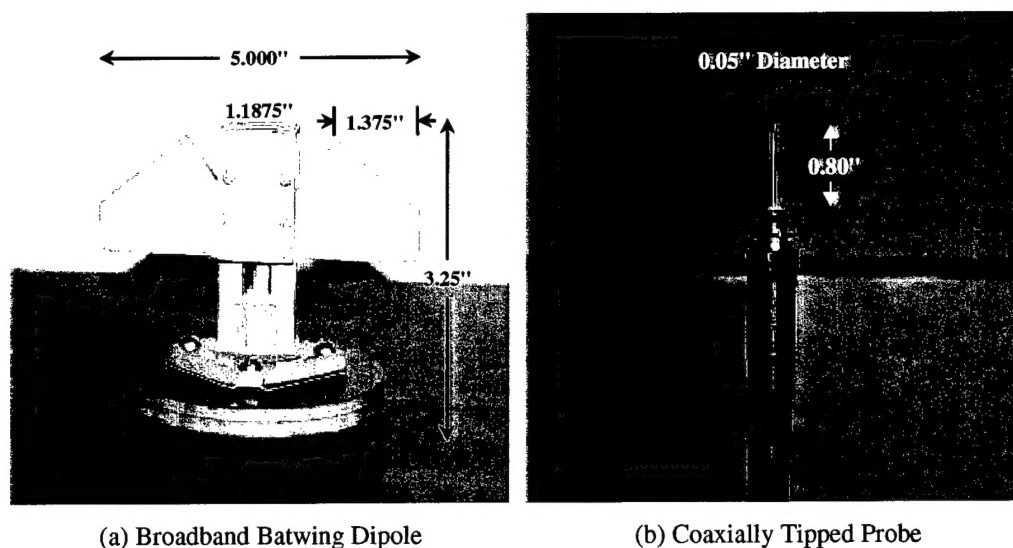
Fig. 5 — Receiving antennas

Figure 5 shows the batwing-dipole[18] receiving antenna. This antenna is mounted on a 7.5-ft rectangular post, with notches at 1-in. intervals on the post for different placements of the antenna. Predictably, this antenna has a favored polarization. To receive vertically (horizontally), the straight edge of the dipole is vertical (horizontal) as shown in Fig. 6. Figure 6 also displays the laptop computer and spectrum analyzer, which are mounted on a two-wheel dolly for portability. The watertight door, situated in the background between the dolly-mounted computer and the 7.5-ft post with the batwing dipole, is designated 1-28-1 and opens into compartment $D_{1,3}$. The dolly is placed just in front of an outside corner of $D_{1,3}$, and the view is from compartment $D_{1,2}$. This door figures prominently in subsequent discussion of the data. For places that are not accessible to the batwing dipole, a probe is used instead. The probe is 1-ft long, with a 0.8-in. tip and a 0.05-in. diameter.

Laptop Computer

Broadband Dipole Receiving Antenna

Spectrum Analyzer
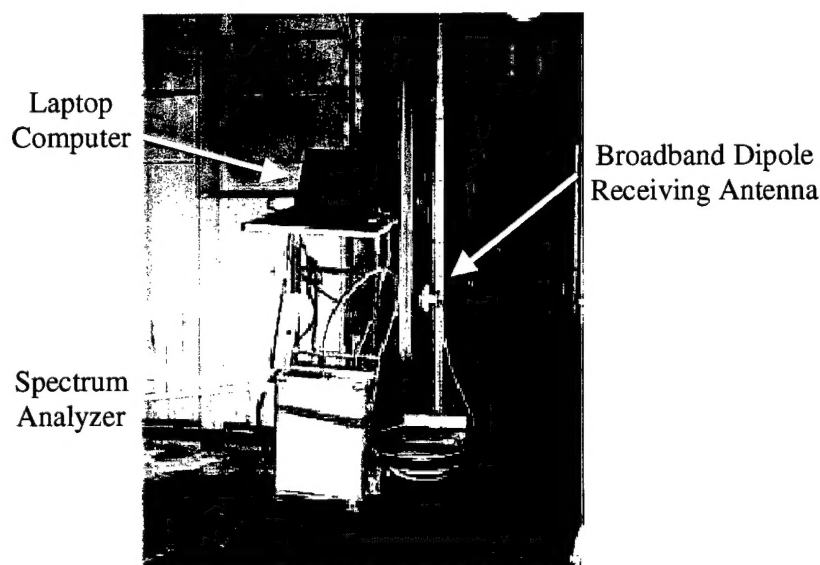
Fig. 6 — Integrated bistatic measurement system
on the main deck of the ex-USS *Shadwell*

Because the transmitter and receiver are not locked to a reference, the measurement is not coherent. The signal source in the transmitter executes a fast sweep through the designated frequency interval (800 MHz to 3 GHz), about 5 times in 7 seconds. Simultaneously, the spectrum analyzer samples the received signal spectrum by sweeping frequency. To register a received signal at a given frequency, the sweep windows for both devices must overlap, which takes approximately 7 seconds. The total time for acquiring the received signals at a specified number of frequencies exceeds seven times the number of frequencies. This lack of synchronization required a tradeoff between the number of frequencies and the total acquisition time for a given measurement configuration. As a consequence of the lengthy acquisition time, the number of frequencies was restricted to 23. Collecting the received signals at the 23 specified frequencies took approximately 3 minutes.

SHADWELL GEOMETRY AND TEST CONFIGURATIONS

For the *Shadwell* measurements of 23-25 February 1998, 113 sets of data were collected. All except two of the data sets correspond to specific placements of the receiving and transmitting antennas, and each data set consists of 23 values of the received power in dBm, one for each frequency. The measurements were taken in the forward test area of the 01 level, the main deck, and the 2nd deck of the *Shadwell* between frame 13 and frame 29. Each frame is 4-ft long (frame numbers appear at the bottom of Fig. 7). In Navy nomenclature, the 01 level is the deck above the main deck, and the 2nd deck is the deck below the main deck. To keep track of the data, compartment number n on the main deck, the 2nd deck, and the 01 level are designated $D_{1,n}$, $D_{2,n}$, and $D_{3,n}$, respectively.
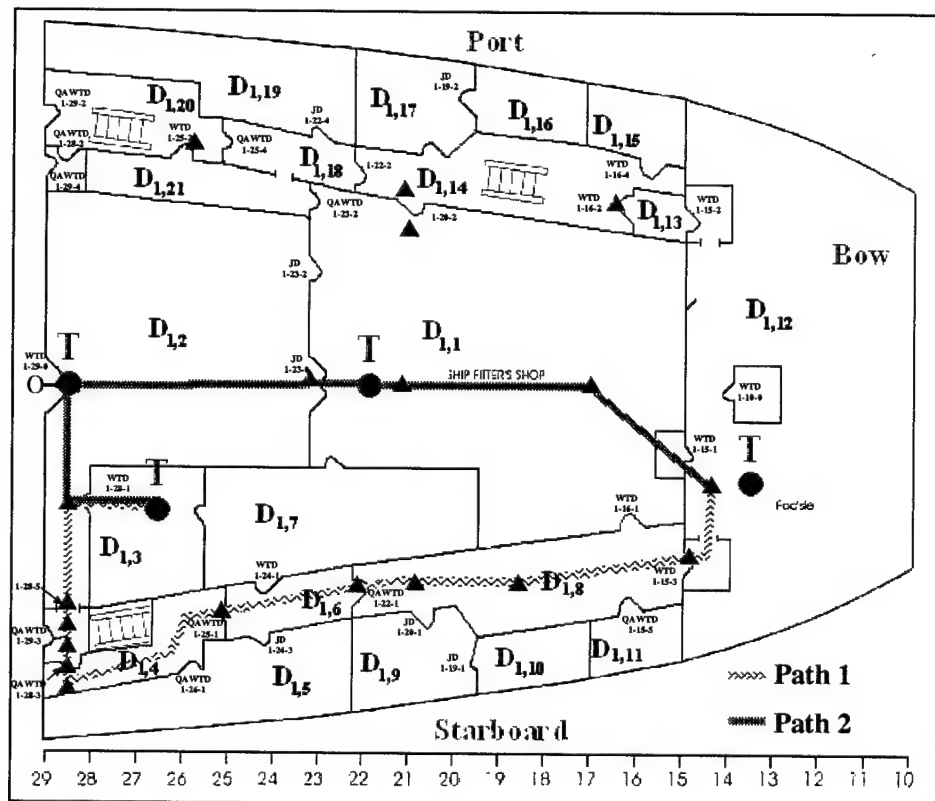
Fig. 7 — Locations of receiver (triangles) and transmitter (dots) positions in compartments ($D_{1,n}$) on the main deck of the ex-USS *Shadwell*

For most of the measurements, the transmitter was placed at one location (compartment $D_{1,3}$ of Fig. 7) on the main deck, and the receiver was moved about the three levels, but it was predominantly on the main deck. However, for seven of the measurements, the receiver was placed near the starboard ladderway halfway between frames 28 and 29 of the main deck, and the transmitter was moved aft along the *Shadwell's* centerline from the forecastle area toward the receiving antenna. The locations of all measurements on the main deck are indicated by the large solid dots and triangles in Fig. 7. The triangles denote the locations of the receiving dipole and probe positions, and the solid circles with 'T' above them correspond to transmitter positions. To note the precise positions of each transmitter-receiver placement, the origin of the *xyz*-coordinate frame, indicated by "O" at the left center of Fig. 7, is taken to be the point on the deck of the main deck at the juncture of the centerline and the back bulkhead of $D_{1,2}$. The positive *x*-axis lies in the plane of the paper and points to the starboard side, the positive *y*-axis lies in the plane of the paper and is directed along the centerline toward the bow, and the positive *z*-axis points out of the paper toward the overhead.

The measurements are indexed by the positive integer *n*, which ranges from 1 to 113. Measurement 101 is the background noise power, and measurement 113 is the power when the transmitter and receiver are connected directly. The remaining 111 measurements are the received powers at the different locations for various open/closed door configurations and antenna polarizations. The transmitter-receiver coordinates, the corresponding free-space propagation loss, the compartments where the transmitter and receiver are located, the antenna polarizations, and the open-closed door configuration for each measurement (except measurements 101 and 113) are tabulated in Appendix A.

Seven classes of data were collected: (A) five classes with the transmitter at the indicated fixed position in $D_{1,3}$; and (B) two classes with the receiver at a fixed position in the foyer of $D_{1,2}$ at the head of the starboard stairwell to the 2 Level (Fig.7). The various classes of A and B are:

A1. Fifty-five measurements ($n \varepsilon \{1,\dots,40\} \cup \{76,\dots,90\}$) at receiver points just outside $D_{1,3}$ around door 1-28-1 in the corridor of $D_{1,2}$ to determine if energy escapes through the door seal;

A2. Thirty measurements ($n \varepsilon \{41,\dots,70\}$) in the corridor consisting of $D_{1,2}$, $D_{1,4}$, $D_{1,6}$, and $D_{1,8}$ to determine if energy propagates along the aftward passageway of $D_{1,2}$ outside $D_{1,3}$ and through the starboard passageway. These measurements are also intended to determine whether energy propagates along the cables that pass through the MCTs in the starboard passageway;

A3. Five measurements ($n \varepsilon \{71,\dots,75\}$) in the forecastle ($D_{1,12}$) with doors 1-15-1 and 1-15-3 in appropriate open/closed configurations to determine if the transmitted signal propagates through the large central area en route to the forecastle ($D_{1,3} \to D_{1,2} \to D_{1,1} \to D_{1,12}$) or through the slanted L-shaped passageway ($D_{1,3} \to D_{1,2} \to D_{1,4} \to D_{1,6} \to D_{1,8} \to D_{1,12}$) to the forecastle;

A4. Ten measurements ($n \varepsilon \{91,\dots,100\}$) in the large central area and the port passageway to determine signal levels in the port passageway;

A5. Four measurements ($n \varepsilon \{102,\dots,105\}$) on the 01 and 2 levels near the starboard ladderways to test inter-deck propagation;

B1. Five measurements ($n \varepsilon \{106,\dots,110\}$) with the transmitter in the forecastle to test propagation along different paths;

B2. Two measurements ($n \varepsilon \{111,112\}$) with the transmitter moving along the centerline of $D_{1,1}$ and $D_{1,2}$ toward the receiver in the starboard foyer of $D_{1,2}$.

THEORY AND RESULTS

Analysis

Instead of directly analyzing the raw data, which are received power readings in dBm at the 23 frequencies for the 111 locations of interest, the effective propagation loss L_{sp} is studied because it is independent of the measurement system, which follows from Eq. (1). Therefore, the results should be applicable to any radar, communication, or surveillance system on the *Shadwell*. The effective

propagation loss embodies the losses from all modes of propagation that are generated in this complex environment. These propagation mechanisms include multipath scattering from the bulkheads, scattering from compartment penetrations and obstructions, surface waves along cables, waveguide effects from the nature of the ship spaces like the passageways, free-space propagation, and coaxial-cable effects. The last mechanism arises from a cable within a passageway behaving like the inner conductor of a coaxial cable with the steel bulkheads of the passageway forming the outer conductor. Energy is propagated along this "coax" between the two conductors.

The propagation loss L_{SP} is calculated from the *Shadwell* data and the system calibration measurements by applying a variation of the Friis transmission equation that incorporates system losses and by solving for L_{SP}. For a different system of interest, the derived values of L_{SP} and the pertinent parameters of the different system can then be substituted into the appropriate transmission equation to predict values of the received power for the transmitter-receiver locations of the *Shadwell* measurements. The governing equation is (see Appendix B for its derivation)

$$L_{SP} = \frac{P_{S1}}{P_{S2}} \left(\frac{\lambda}{4\pi R_{C1}} \right)^2 \left(\frac{P_{C1}}{P_{C2}} \right)^{-1} , \tag{1}$$

where

P_{C1} is the measured received power in the Radar Division's Compact Range when the transmitting and receiving antennas are separated by R_{C1} (5.6388 m for the batwing dipole and 4.699 m for the probe),

P_{C2} is the measured received power in the Compact Range when the transmitting port is connected directly to the receiving port,

λ is the wavelength corresponding to the specified frequency f,

P_{S1} is the measured received power on the *Shadwell*, and

P_{S2} is the measured received power on the *Shadwell* when the transmitting port is connected directly to the receiving port.

Although P_{C2} and P_{S2} are equal, both are included in Eq. (1) because P_{C1}/P_{C2} is the quantity that was measured in the Compact Range, and it contains the effect of the transmitting and receiving antennas. The squared quantity is the free-space propagation loss for the Compact-Range measurement, denoted L_{0C}. Let P_{C12} be the ratio P_{C1}/P_{C2} and define p_{C12} as $10\log_{10}(P_{C12})$. Similarly, let lower-case letters represent 10log10 of the remaining quantities in Eq. (1); that is, $p_{S1} = 10\log_{10}(P_{S1})$, $p_{S2} = 10\log_{10}(P_{S2})$, $l_{SP} = 10\log_{10}(L_{SP})$, and $l_{0C} = 10\log_{10}(L_{0C})$. Take $10\log_{10}$ of Eq. (1) to obtain

$$l_{SP} = p_{S1} + l_{0C}(f) - p_{S2} - p_{C12}. \tag{2}$$

Equation (2) expresses the effective propagation loss in terms of four measured or derived quantities, which are briefly discussed before scrutinizing the behavior of l_{SP}. The received power p_{S2}, when the transmitter and receiver are connected directly, is the response of the bistatic measurement system without the antennas. As Fig. 8 indicates, p_{S2} decreases monotonically across the frequency band, with a maximum of 13.17 dBm (20.75 mW) at 800 MHz and a minimum of 8.67 dBm (7.36 mW) at 3 GHz.
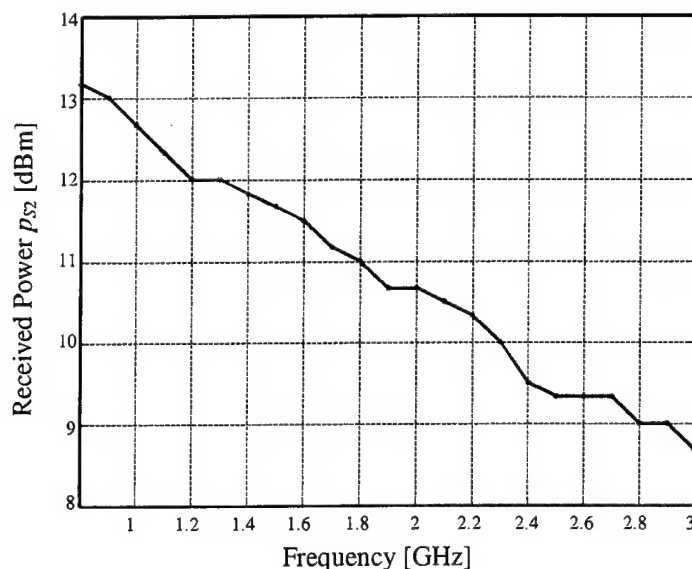
Fig. 8 — Measured received power p_{S2} vs frequency f when the transmitting port and
the receiving port are connected directly without the antennas

Figure 9 plots the Compact-Range measurements of the combined effective gain p_{C12} of the transmitting and receiving antennas vs frequency for the two receiving antennas. The measurements were made at 801 equally spaced frequencies between 800 MHz and 3 GHz, inclusive. From the figure, p_{C12} depends on the type of receiving antenna. The values of p_{C12} for the probe oscillate between −56 and −74 dB. The performance of the probe is substantially less than the performance of the batwing dipole. In particular, the values of p_{C12} for the batwing exceed those for the probe by as little as 3.54 dB at 2.7 GHz to as much as 30.03 dB at 1 GHz. The difference in the behavior of the two receiving antennas is much smaller at the upper end of the band ($f \geq 2.5$ GHz), which is attributable to the poor performance of the batwing dipole for frequencies above 2.1 GHz and to the roughly flat average response (−65 ± 9 dB) of the probe. Basically, the batwing dipole has relatively good broadband performance (that is, p_{C12} has a fairly constant value of −46 ± 3 dB) only from 800 MHz to roughly 2.1 GHz.
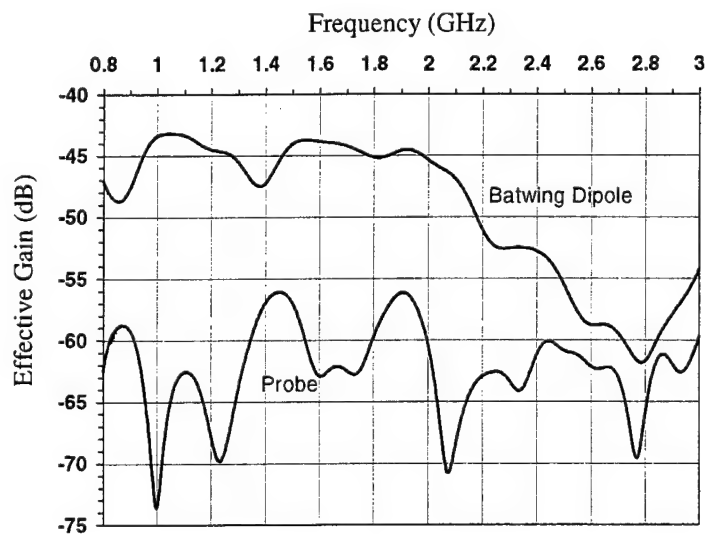
Fig. 9 — Compact-Range measurements of the effective combined gain
p_{C12} of the transmitting antenna (disc-cone) and receiving antennas
(coaxially tipped probe and batwing dipole)

In contrast to p_{C12}, the free-space propagation loss l_{0C} for the Compact-Range measurements is independent of antenna type. As noted earlier,

$$L_{0C}(f) = \left(\frac{\lambda}{4\pi R_{C1}}\right)^2,$$

(3)

where $\lambda f = c$, $c = 2.9979 \times 10^8$ m/s, and R_{C1} has different values for the probe (4.699 m) and the batwing dipole (5.6388 m). Equation (3) is used to compute l_{0C} for these antennas at the 23 frequencies, and the values are provided in Tables 1 and 2 for the probe and the batwing dipole, respectively. Note that the difference in the values of l_{0C} between the two antennas is the same (1.584 dB) at each frequency. This 1.584 dB differential corresponds to $20\log_{10}(5.6388/4.699)$.

In addition to providing values of l_{0C}, Tables 1 and 2 give values for p_{S2} and p_{C12}. In tabulating p_{C12}, the 23 frequencies of interest are not necessarily among the measured frequencies. For those frequencies not corresponding to one of the measured frequencies, the value of p_{C12} is linearly interpolated from the data that determines the plots in Fig. 9.

Table 1 — Parametric Values for the Effective Propagation
Loss when the Receiving Antenna is the Coaxial Probe

f [MHz]	$l_{0C}(f)$ [dB]	p_{S2} [dBm]	p_{C12} [dB]	$l_{0C}(f) - p_{S2} - p_{C12}$
800	- 43.950	13.17	-62.50	5.380
900	- 44.973	13.00	-59.21	1.237
1000	- 45.888	12.67	-73.47	14.907
1100	- 46.716	12.33	-62.63	3.581
1200	- 47.472	12.00	-67.87	8.395
1300	- 48.167	12.00	-63.94	3.774
1400	- 48.811	11.83	-56.96	- 3.677
1500	- 49.410	11.67	-56.99	- 4.090
1600	- 49.970	11.50	-62.91	1.437
1700	- 50.497	11.17	-62.47	0.804
1800	- 50.993	11.00	-59.74	- 2.255
1900	- 51.463	10.67	-56.19	- 5.943
2000	- 51.909	10.67	-60.40	- 2.181
2100	- 52.332	10.50	-68.67	5.833
2200	- 52.736	10.33	-62.94	- 0.130
2300	- 53.123	10.00	-63.32	0.198
2400	- 53.492	9.50	-61.22	- 1.771
2500	- 53.847	9.33	-60.84	- 2.339
2600	- 54.187	9.34	-62.16	- 1.367
2700	- 54.515	9.35	-62.98	- 0.882
2800	- 54.831	9.00	-66.01	2.181
2900	- 55.136	9.01	-61.92	- 2.225
3000	- 55.430	8.67	-59.71	- 4.386

Table 2 — Parametric Values for the Effective Propagation
Loss when the Receiving Antenna is the Batwing Dipole

f [MHz]	$l_{0C}(f)$ [dB]	p_{S2} [dBm]	p_{C12} [dB]	$l_{0C}(f) - p_{S2} - p_{C12}$
800	- 45.533	13.17	- 47.11	- 11.593
900	- 46.556	13.00	- 47.64	- 11.916
1000	- 47.472	12.67	- 43.39	- 16.752
1100	- 48.299	12.33	- 43.32	- 17.309
1200	- 49.055	12.00	- 44.52	- 16.535
1300	- 49.750	12.00	- 45.56	- 16.190
1400	- 50.394	11.83	- 47.25	- 14.974
1500	- 50.993	11.67	- 44.05	- 18.613
1600	- 51.554	11.50	- 43.85	- 19.204
1700	- 52.081	11.17	- 44.23	- 19.021
1800	- 52.577	11.00	- 45.15	- 18.427
1900	- 53.047	10.67	- 44.61	- 19.107
2000	- 53.492	10.67	- 45.39	- 18.772
2100	- 53.916	10.50	- 46.93	- 17.486
2200	- 54.320	10.33	- 51.09	- 13.560
2300	- 54.706	10.00	- 52.58	- 12.126
2400	- 55.076	9.50	- 52.86	- 11.716
2500	- 55.430	9.33	- 55.49	- 9.270
2600	- 55.771	9.34	- 58.78	- 6.331
2700	- 56.099	9.35	- 59.44	- 6.009
2800	- 56.415	9.00	- 61.72	- 3.695
2900	- 56.720	9.01	- 57.99	- 7.740
3000	- 57.014	8.67	- 54.26	- 11.424

The values in Tables 1 and 2 are then appropriately applied to each of the 111 data sets for p_{S1} to obtain the corresponding derived data sets and curves for l_{SP}. The curves for p_{S1} and l_{SP} are given in Appendix C and Appendix D, respectively. The curves for p_{S1} include error bars as estimates of the measurement accuracy; whereas the plots of l_{SP} contain a graph of the free-space propagation loss l_0 that would be associated with each measurement if the measurement had been taken in free space. For example, Fig. 10 displays $p_{S1}(98)$ and $l_{SP}(98)$. For this data set, the transmitter was located in $D_{1,3}$, and the receiver was placed in $D_{1,20}$ of the port passageway between the door 1-25-4 to $D_{1,18}$ and the ladderway in the top-left part of Fig. 6. The transmitter-receiver separation for this case is 9.38 m. The 98th data set is chosen because all of its 23 measurements are valid and because substantial measurement error is associated with this data set. At each frequency, the true received power lies along the error bar. The largest error occurs at 2.9 GHz, where p_{S1} is −85.8 dBm and the true signal must be within 11.1 dB above −85.8 dBm and within 4.7 dB below −85.8 dBm. The corresponding effective propagation loss $l_{SP}(98)$ has somewhat similar general behavior to $p_{S1}(98)$, but the drop-off at the higher frequencies ($f \geq 2$ GHz) is much less severe, because the data have been normalized to remove the poor performance of the batwing dipole. For comparison, the free-space propagation loss $l_0(98)$ is plotted. Except for 2.8 GHz, $l_{SP}(98) - l_0(98) \geq 25$ dB. Consequently, propagation mechanisms other than the free-space effect must be significantly impacting the signal propagation.
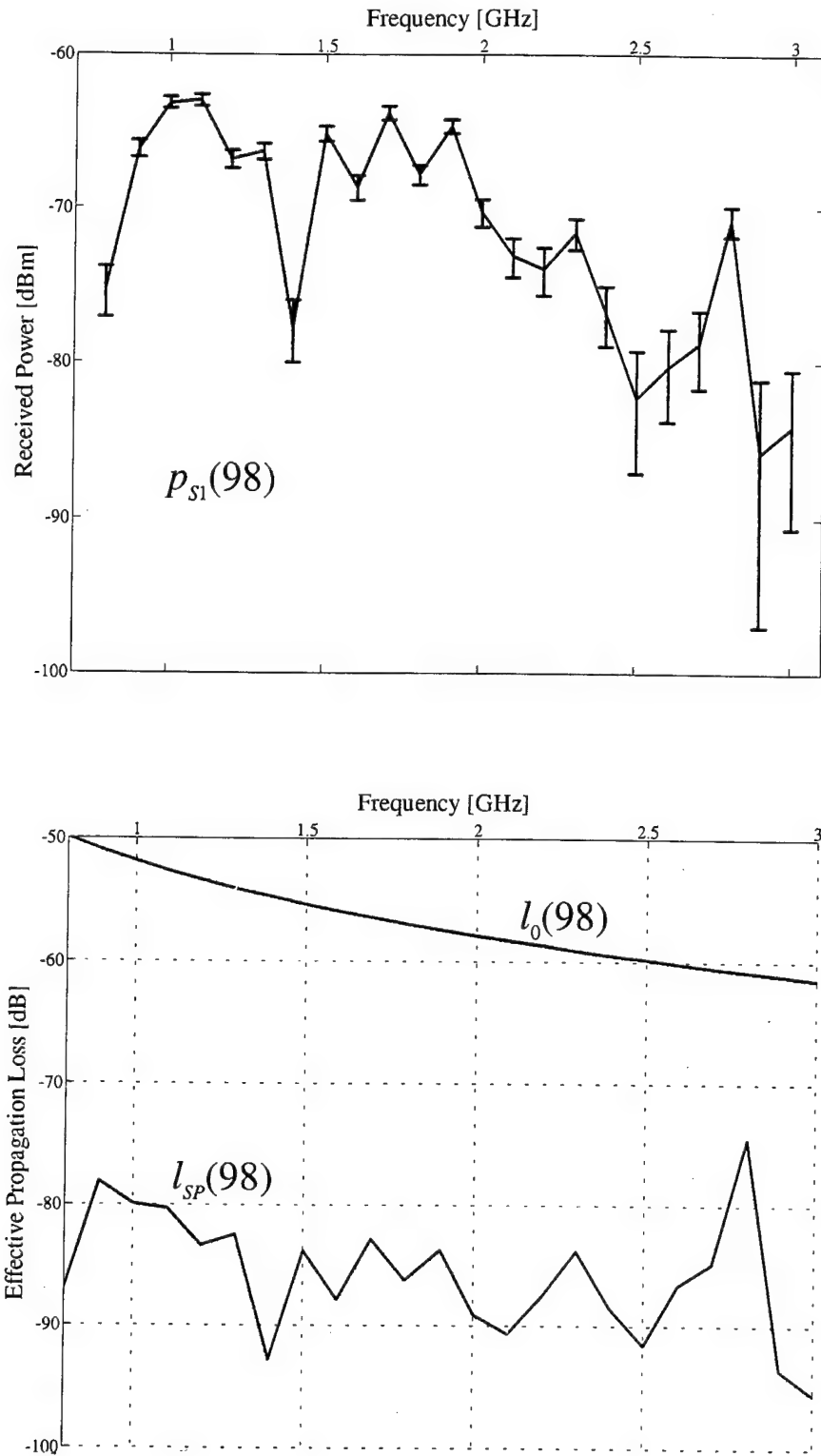
Fig. 10 — Received power $p_{s_1}(98)$ for the 98th *Shadwell* data set with error bars, the associated effective propagation loss $l_{sp}(98)$, and the associated free-space propagation loss $l_0(98)$ when the transmitter-receiver separation R_{98} is 9.38 m

The measurement accuracy of p_{S1} is a function of how close p_{S1} is to the background noise floor p_N on the *Shadwell*. Generally, the measurement accuracy decreases as p_{S1} approaches p_N; that is, the accuracy increases as the signal-to-noise ratio P_{S1}/P_N increases, which is argued in Appendix E. For the *Shadwell* measurements, p_N is roughly −90 dBm with a minimum of −90.67 dBm and a maximum of −88.67 dBm (Fig. 11). For p_{S1} to be considered a good measurement, the logarithmic signal-to-noise ratio $\alpha (=p_{S1} - p_N)$ should exceed 20 dB. To summarize the results of Appendix E, the true signal power lies in the interval $[p_L, p_U]$, where

$$p_L = p_{S1} - \varepsilon_L, \qquad p_U = p_{S1} + \varepsilon_U, \qquad \alpha = 10\log_{10}\left(\frac{P_{S1}}{P_N}\right),$$

$$\varepsilon_L = -20\log_{10}\left(1 - \sqrt{\frac{P_N}{P_{S1}}}\right), \qquad \varepsilon_U = 20\log_{10}\left(1 + \sqrt{\frac{P_N}{P_{S1}}}\right).$$

(4)

Note that P_{S1} replaces P_M in Appendix E, where $P_N < P_{S1}$ for the measurements of interest. In the top frame of Fig. 10, ε_U and ε_L correspond to the upper and lower horizontal segments, respectively, of the error bars.
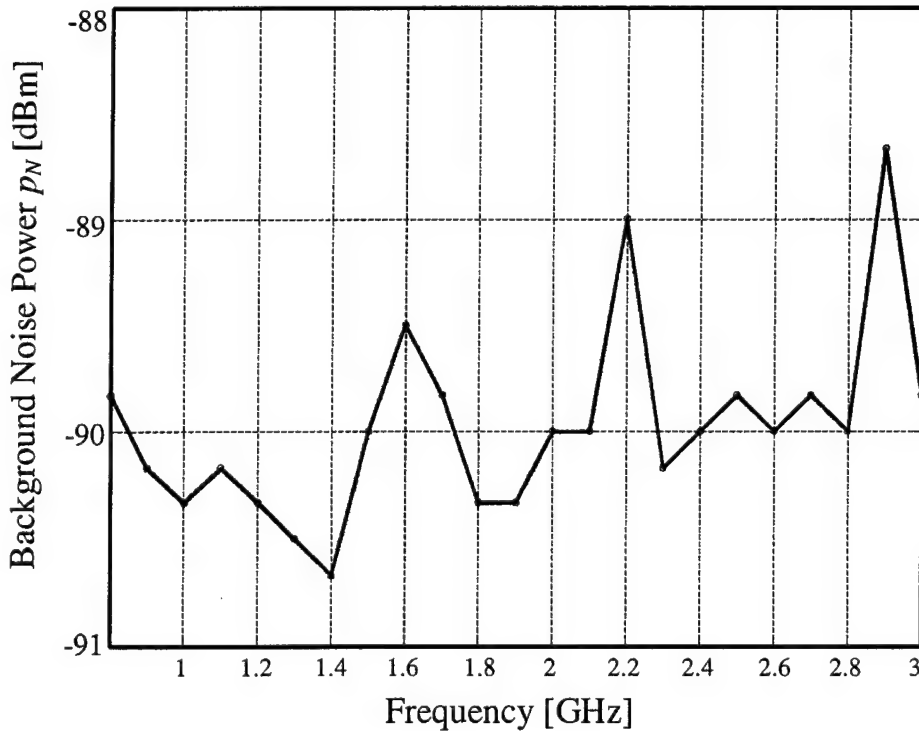
Fig. 11 — Background noise power p_N vs frequency on the *Shadwell*

Effective Propagation Losses for *Shadwell* Data Sets

In the next several subsections, the effective propagation loss is plotted for selected data sets within each of the classes listed earlier. Instead of the individual plots of Appendix D, several curves are compared in each figure to establish general behavioral trends.

Class A1

The 40 data sets of this class correspond to a fixed transmitter location in $D_{1,3}$ and to receiver locations in $D_{1,2}$ on a grid about 9 in. from door 1-28-1, which connects $D_{1,2}$ and $D_{1,3}$. The grid points are spaced every 12 in. in the vertical and horizontal directions (Fig.12), so that the grid structure consists of five columns and seven rows of points, with the middle column along the door's vertical centerline. Each column has seven grid points, ranging from 12 in. to 84 in., and each row has five grid points. The extra five data sets ($n \in \{1,3,11,12,29\}$) are bad data and are indicated by the B in Table A1 of Appendix A. The purpose of these measurements was to determine whether the readings by the door seals were higher, indicating energy leakage through the seals.
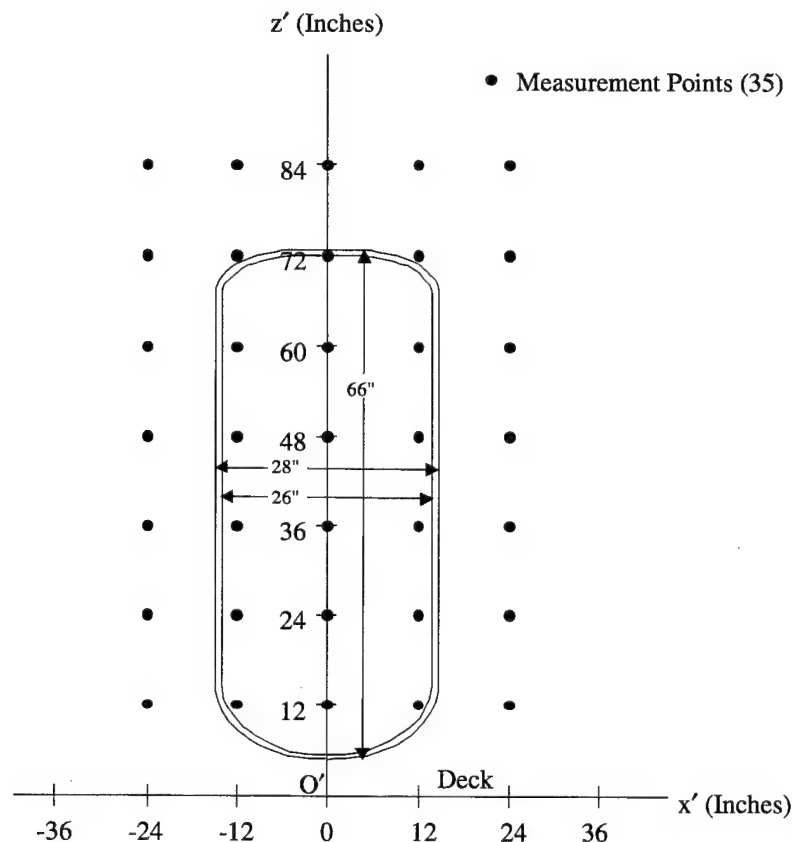
Fig. 12 — Grid of 35 measurement locations of effective propagation loss l_{sp} when the receiver was 9 in. from the closed door 1-28-1 in the passageway of compartment of $D_{1,2}$ and the transmitter was in compartment $D_{1,3}$ (5-ft high and 4 ft from 1-28-1). The local origin O′ was located on the deck along the door's centerline.

The propagation loss is plotted in Fig.13 for the 5 grid points in the row that is 36 in. above the deck (corresponds to $n = 5, 14, 22, 29, 36$). These five curves are associated with grid points at the door's vertical centerline and at 12 in. and 24 in. to the left and right of the centerline. The effective propagation losses vary with position and frequency and appear to follow a general trend within a 10 dB to 20 dB band, which decreases as the frequency increases to 2 GHz and then rises slightly. Except for one data point at 3 GHz along the centerline, $\alpha > 20$ dB, which implies a measurement error that is less than 0.915 dB by Table E1. Even the value of p_{s_1} for the 3 GHz point is 5.5 dB above the noise floor. Therefore, the measurement error causes only a small part of the 10 dB to 20 dB fluctuations in the effective propagation loss.
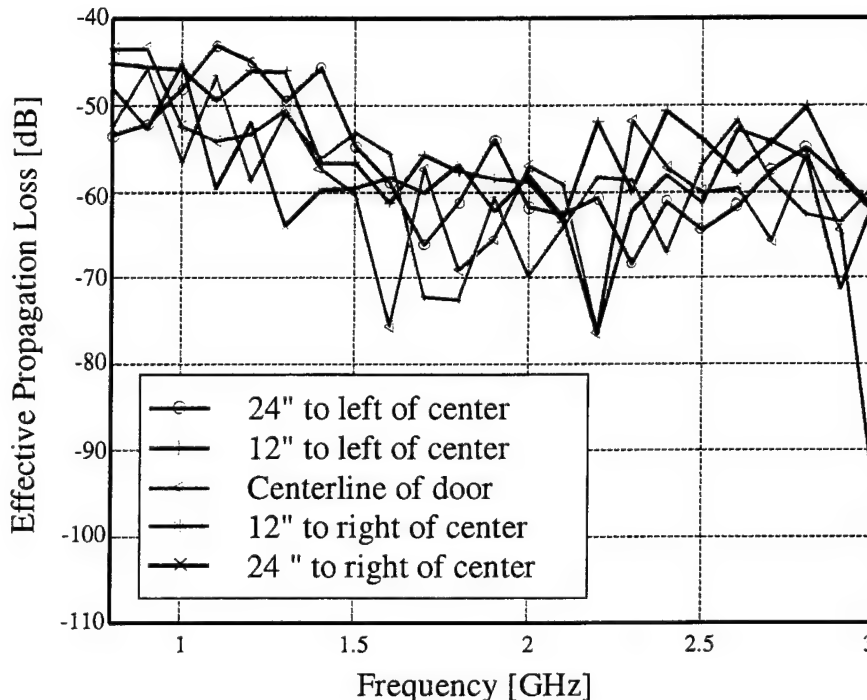
Fig. 13 — Five measurements of effective propagation loss when the receiver is 9 in. from closed door 1-28-1 in the passageway of compartment $D_{1,2}$ at a height of 3 ft and the transmitter is in compartment $D_{1,3}$ at a height of 5 ft and a distance of 4 ft from 1-28-1

Since RF spread spectrum communication systems over 902 to 928 MHz are being tested for use during shipboard fires, consider the values at 900 MHz in Fig. 13. The effective propagation loss is the same (approximately −45 dB) for the points closest to the door seal, the two points that are 12 in. on either side of the centerline. Since these two locations do not correspond to the smallest effective propagation loss for the five locations, one cannot argue that the transmitted energy is leaving $D_{1,3}$ through the door seals. It is not clear why such variations in the door readings were measured. A likely cause is the multipath from the energy bouncing off the metallic surfaces, which bound the passageway outside 1-28-1. In any event, the results are inconclusive.

Eleven of the remaining fifteen measurements of Class A1, corresponding to $n \, \varepsilon \, \{76\text{-}81, 86\text{-}90\}$, were an attempt to isolate the different ways the energy could leave $D_{1,3}$ when both doors to it are closed. In all cases, the receiver was placed 29 in. from 1-28-1 in $D_{1,2}$ along the door's center at a height of 48 in. Since the door's watertight seal was a worn rubber gasket, various attempts were made to improve the seal, such as removing the gasket, sanding the seal-door interface, and tightly packing the region at the

door seal with steel wool. These efforts yielded little or no change in the received power. In addition, wires, holes, meshes, and nonmetallic sections penetrated the bulkheads of $D_{1,3}$. Attempts to make the exterior of this compartment electrically quiet were made by covering these locations with aluminum foil, steel wool, and metallic plates. Again, the results are inconclusive, perhaps because measurements were taken at only one location.

The remaining four measurements (n = 82, 83, 84, 85) of Class A1 provide a very limited look at the impact of the propagation environment on the polarizations of the transmitting and receiving antennas. The transmitter-receiver placement is the same as the preceding 11 measurements. The designations V and H in Fig. 14 represent the polarizations of the antennas; the first letter and the second letter denote the polarizations of the transmitting antenna and the receiving antenna, respectively. For example, HV means that the transmitting antenna is horizontally polarized and the receiving antenna is vertically polarized. Figure 14 shows a general downward trend until 2 GHz, then a milder upward trend.
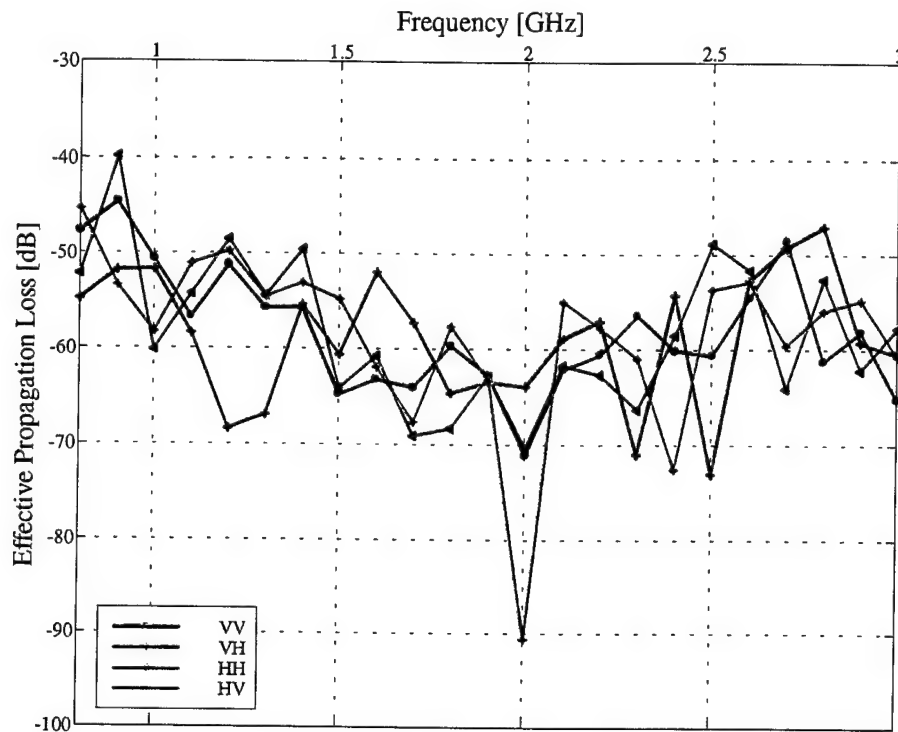
Fig. 14 Effective propagation losses for different polarizations when the receiver is 29 in. from closed door 1-28-1 in the passageway of compartment of $D_{1,2}$ at a height of 4 ft and the transmitter is in compartment $D_{1,3}$ at a height of 5 ft and a distance of 4 ft from 1-28-1

Class A2

For the measurements along the slanted L-shaped passageway that is formed by the starboard passageway and the back passageway-like part of the starboard half of $D_{1,2}$, the received power exceeds the background noise level by 10 to 30 dBm over the entire frequency band for most of the data. This variation in the power measurements depends on which doors were closed. In any case, significant energy is propagated along this passageway. The authors suspect that the waveguide-like nature of the passageway directs the energy. However, since a distributed cable network that contains a leaky-wave communication line (Fig. 2) also runs overhead along the starboard passageway, surface-wave and

coaxial-cable modes may be other means of propagation. For the cable network to run between adjacent compartments that comprise the passageway, it passes through the nonmetallic MCT, a cutout portion of the bulkhead over the connecting door that adjoins the compartments. Since it is possible that surface waves are induced on this cable, the MCT is a likely propagation conduit.

As the solid triangles in Fig. 7 indicate, measurements were taken at several locations in $D_{1,2}$, $D_{1,4}$, and $D_{1,8}$. In particular, Fig. 15 displays l_{SP} for the source in $D_{1,3}$ and for the receiving probe at the two locations of the MCT in $D_{1,4}$: one above door 1-28-3 that connects $D_{1,2}$ and $D_{1,4}$ (denoted $l_{SP}(56)$), and the other above door 1-25-1 that connects $D_{1,4}$ and $D_{1,6}$ ($l_{SP}(57)$). The distances between the source and the two receiver locations above doors 1-28-3 and 1-25-1 are 4.376 m and 3.974 m, which are respectively designated R_{56} and R_{57}. The MCT above door 1-25-1 is closer to the source because an adjacent bulkhead of $D_{1,4}$ is shared with $D_{1,4}$. In both instances, the door (1-28-1) between the source compartment $D_{1,3}$ and $D_{1,2}$ and the door (1-28-5) between $D_{1,2}$ and its foyer are open, and the door between the $D_{1,2}$ foyer and $D_{1,4}$ (1-28-3) is closed.
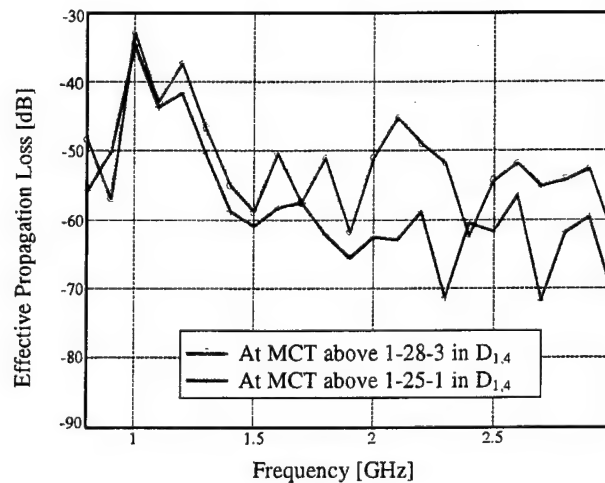
Fig. 15 — Effective propagation losses with the probe at the mast cable transits (MCTs) in $D_{1,4}$, one above door 1-28-3 and one above door 1-25-1. Both measurements are taken at a height of 7 ft.

From Fig. 15, $l_{SP}(56) > l_{SP}(57)$ for all frequencies except 900 MHz and 2.5 GHz. Hence for the majority of frequencies, the energy appears to follow the corridor of $D_{1,2}$ through 1-28-5 into $D_{1,4}$, through 1-28-3, and finally through $D_{1,4}$ to 1-25-1. Even though $R_{56} > R_{57}$, the path to 1-25-1 through $D_{1,4}$ is a good 5 m longer than the path to 1-28-3, which accounts for the fact that the signal to 1-25-1 incurs more attenuation for most frequencies. On the other hand, since $l_{SP}(56) < l_{SP}(57)$ when f is 900 MHz or 2.5 GHz, it is inferred that some energy must have followed another path, perhaps via $D_{1,7}$ to $D_{1,6}$ to $D_{1,4}$, via a venting structure from $D_{1,3}$, or via some kind of surface wave between the common boundaries of $D_{1,3}$ and $D_{1,4}$ for these two frequencies. The last possibility seems least likely since the thick metallic bulkheads that comprise the boundary should reflect signals. Further measurements are required to determine why different results are obtained for 900 MHz and 2.5 GHz. From a practical standpoint, any special behavior at these two frequencies is of particular interest, since they are near the frequencies of existing wireless LANs that use two of the ISM bands (902 to 928 MHz, 2.4 to 2.4835 GHz): the RSVP LAN which operates from 2.4 to 2.485 GHz; and personal-computer based LANs that use the WaveLAN®/PCMCIA card by Lucent Technologies (915 MHz and 2.4 GHz).[19]

Class A3

This subsection discusses three examples. First, two measurements from Class A3 are presented to compare propagation in the central area of the main deck to propagation along the starboard passageway of that level. In the remaining two examples, data sets from Classes A1, A2, and A3 are grouped to discuss propagation along the starboard passageway of the main deck.

In the first example, two propagation paths between the transmitter in $D_{1,3}$ and the receiver in the forecastle $D_{1,12}$ near doors 1-15-1 and 1-15-3 are considered. The paths (Fig. 7), one traversing along the starboard passageway and the other passing through the large central room, are given by

$$\text{Path 1: } D_{1,3} \rightarrow D_{1,2} \rightarrow D_{1,4} \rightarrow D_{1,6} \rightarrow D_{1,8} \rightarrow D_{1,12} \text{ [Starboard Passageway]};$$
$$\text{Path 2: } D_{1,3} \rightarrow D_{1,2} \rightarrow D_{1,1} \rightarrow D_{1,12} \text{ [Central Room]}.$$

Since all the doors in $D_{1,3}$ and $D_{1,7}$ are closed except 1-28-1, the authors assumed that a significant amount of the energy leaving $D_{1,3}$ does so through 1-28-1. Moreover, the door (1-20-2) from $D_{1,1}$ to $D_{1,14}$ is closed, and all doors along the starboard passageway (1-28-5, 1-28-3, 1-25-1, 1-22-1) are open to guide most of the energy along these two paths. When 1-15-1 is closed and 1-15-3 is open ($l_{sp}(72)$), the authors consider Path 1 to be open and Path 2 to be closed. Similarly, when 1-15-1 is open and 1-15-3 is closed ($l_{sp}(75)$), Path 2 is open and Path 1 is closed.

According to Fig. 16, the path through the large central room (Path 2 open) permits better propagation than the path along the starboard passageway (Path 1 open) at all frequencies, probably because Path 1 has more length as a result of its slanted-L shape and because the large central room acts more like free space. The received signal power for the starboard path is attenuated between 3 and 28 dB more than the received signal for the central-room path. The propagation losses are highly variable across the frequency band. For example, at 900 MHz, 1 GHz, 1.6 GHz, 2 GHz, and 2.9 GHz, the signal corresponding to the starboard path is further attenuated by 18 dB, 6 dB, 3 dB, 29 dB, and 3 dB, respectively. However, the received power level for the starboard path is significant, which is probably a result of the waveguide-like nature of the passageway, coupling to the leaky-wave communication cable that runs along the passageway, and surface/TEM waves from the many other cables along the passageway.
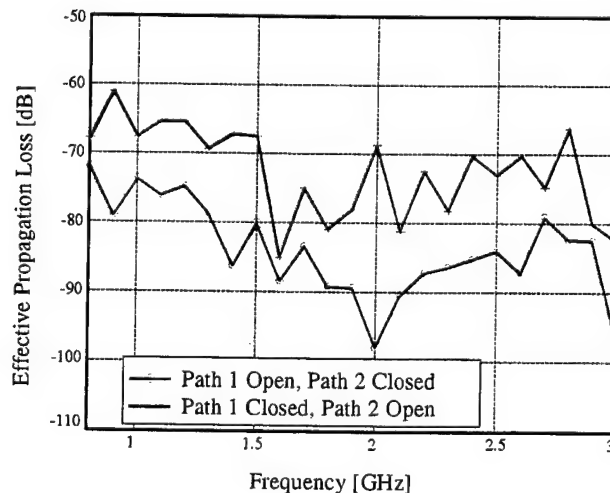
Fig. 16 — Comparison of effective propagation losses for path along starboard passageway (Path 1) and for path through central-room (Path 2). The receiver is in the forecastle $D_{1,12}$ near door 1-15-1, and the transmitter is in $D_{1,3}$.

In the second example, signal propagation is compared at four successively more distant points along the starboard passageway (Path 1), when every door along this path is open. As one traverses Path 1 from $D_{1,3}$ to $D_{1,12}$, the doors in succession are 1-28-1, 1-28-5, 1-28-3, 1-25-1, 1-22-1, and 1-15-3. In order of increasing distance from the transmitter along Path 1, the four placements of the receiving antenna were in $D_{1,2}$ just outside $D_{1,3}$ ($l_{SP}(41)$), in $D_{1,4}$ near the door 1-28-3 to the foyer of $D_{1,2}$ ($l_{SP}(48)$), in $D_{1,8}$ about 5 ft from door 1-22-1 ($l_{SP}(68)$), and in the forecastle $D_{1,12}$ ($l_{SP}(71)$). As one would expect, the inequality, $l_{SP}(41) > l_{SP}(48) > l_{SP}(68) > l_{SP}(71)$, is generally true (Fig. 17). The few frequencies where the inequality does not hold are most likely the result of multipath interference.

In the third example, the effective propagation losses for three locations along the starboard passageway when the doors were open (Fig. 18(a)) are compared to the losses when the doors were closed (Fig. 18(b)) at the same locations. The transmitter was in $D_{1,3}$, and the open doors are listed in the preceding example. In order of increasing distance from the transmitter along Path 1, two measurements were taken at each of the following three locations: (1) $l_{SP}(41)$ for open doors and $l_{SP}(6)$ for closed doors in $D_{1,2}$ just outside $D_{1,3}$; (2) $l_{SP}(48)$ for open doors and $l_{SP}(51)$ for closed doors in $D_{1,4}$ near the door 1-28-3 to the foyer of $D_{1,2}$; and (3) $l_{SP}(71)$ for open doors and $l_{SP}(73)$ for closed doors in the forecastle $D_{1,12}$. At each location, the effective propagation loss for the open-door configuration exceeds the effective propagation loss for the closed-door configuration by 5 dB to 25 dB, with few exceptions. In addition, whether the doors were open or closed, the effective propagation loss decreases as the distance along Path 1 increases. Exceptions occur at 900 MHz for both door configurations and at the higher frequencies of the band ($f \geq$ 2.3 GHz) when the doors were closed.
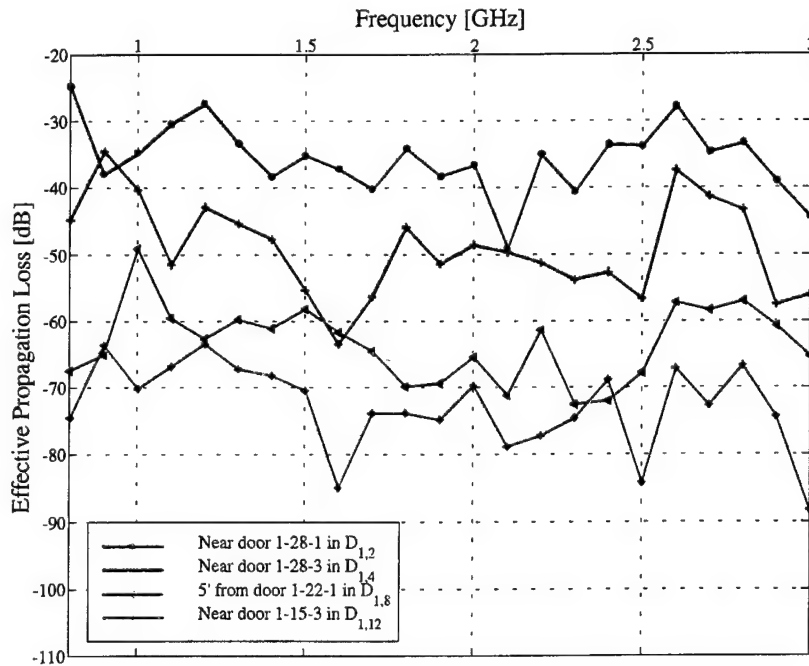
Fig. 17 — Impact on effective propagation loss as the receiver is moved further away from the transmitter in $D_{1,3}$ along Path 1. All watertight doors along Path 1 are open. Four measurements of increasing pathway distance are plotted: $l_{SP}(41)$ is dark blue, $l_{SP}(48)$ is green, $l_{SP}(68)$ is red, and $l_{SP}(71)$ is light blue.
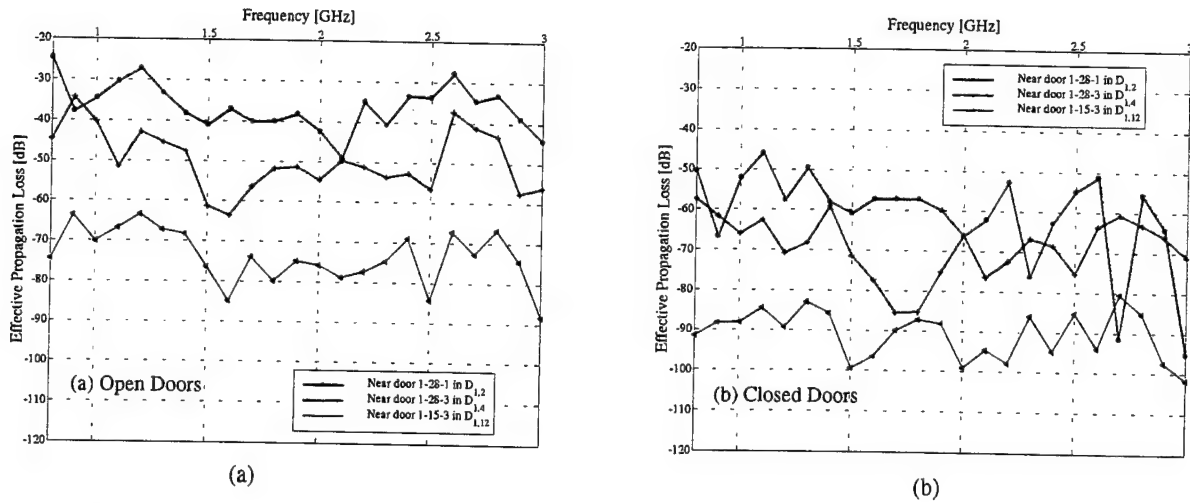
Fig. 18 — Impact of door configuration on effective propagation loss along Path 1: (a) All doors are open; $l_{SP}(41)$ is dark blue, $l_{SP}(48)$ is green, and $l_{SP}(71)$ is red. (b) All doors are closed; $l_{SP}(6)$ is dark blue, $l_{SP}(51)$ is green, and $l_{SP}(73)$ is red.

Class A4

For every data set in Class A4, the transmitter was located in $D_{1,3}$, and the connecting door (1-28-1) between $D_{1,3}$ and $D_{1,2}$ was closed. Seven of the 10 data sets in Class A4 were collected in the port passageway ($D_{1,14}$ and $D_{1,20}$). As a result of the large transmitter-receiver separations, the intervening structure of the ship, and the closure of 1-28-1, three of the data sets ($n = 94, 99, 100$) have no value because the received powers were in the noise for several frequencies.

Of the 10 data sets in this class, four of them ($n = 91, 92, 93, 95$) and data set 9 of Class A1 are now discussed in the context of comparing propagation in the central area and the port passageway (Fig. 19). For the central-room path, the receiver was placed in succession near 1-28-1 in $D_{1,2}$ ($l_{SP}(9)$), near $D_{1,2}$ along the centerline of $D_{1,1}$ ($l_{SP}(91)$), and near the door 1-15-1 to the forecastle along the centerline of $D_{1,1}$ ($l_{SP}(92)$). The path to the port passageway follows the central-room path for the first two data sets; then the receiver was placed in $D_{1,1}$ near door 1-20-2 to the port passageway ($l_{SP}(93)$) and in $D_{1,14}$ near the door 1-16-2 to the forecastle ($l_{SP}(95)$).

Generally, the effective propagation loss is worse (decreases) as the transmitter-receiver separation increases. For example, with the exception of three frequencies (1.7, 2.5, and 3 GHz), $l_{SP}(9) > l_{SP}(91)$, which is consistent with $R_9 = 1.61$ m < 6.30 m $= R_{91}$ (Table A1). However, the three exceptions indicate that at least one other propagation mode exists so that the transmitted energy follows a path other than exiting $D_{1,3}$ through 1-28-1 and proceeding up the centerline of $D_{1,2}$ and $D_{1,1}$. Since 1-28-1 is closed, perhaps comparable energy is leaving $D_{1,3}$ through the closed connecting door to $D_{1,7}$ and out the other door of $D_{1,7}$ to $D_{1,1}$. Other possible propagation mechanisms are the wire holes, plain holes, MCTs, and stuffing tubes leaving $D_{1,3}$. Except for fire barriers and chemical-warfare zones, these compartment intrusions are permitted and, consequently, are common above the ship's V line, the height to which the hull must be watertight. Unfortunately, measurements were taken at an insufficient number of locations to test whether these inferences have validity. With respect to propagation along the centerline of $D_{1,2}$ and $D_{1,1}$ vs propagation to the port passageway, inspect the bottom curves of Fig . 19(a) and Fig. 19(b), respectively. Except at 2 GHz and 3 GHz, $l_{SP}(92) > l_{SP}(95)$, which is consistent with $R_{92} = 12.29$ m < 15.48 m $= R_{95}$.
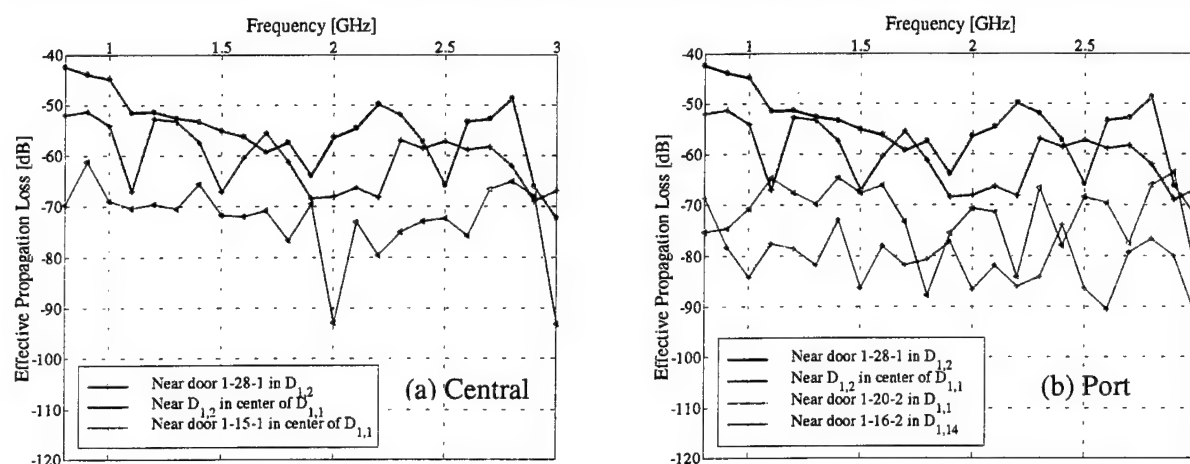
Fig. 19 — Comparison of propagation to the port passageway and propagation through the central room when 1-28-1 is closed. (a) Central Path: $l_{sp}(9)$ is the dark blue curve, $l_{sp}(91)$ is the green curve, and $l_{sp}(92)$ is the red curve. (b) Port Path: $l_{sp}(9)$ is the dark blue curve, $l_{sp}(91)$ is the green curve, $l_{sp}(93)$ is the red, and $l_{sp}(95)$ is the light blue curve.

Class A5

For Class A5, four measurements were taken to test inter-deck propagation. The transmitter was placed in compartment $D_{1,3}$ with door 1-28-1 closed and doors 1-28-3 and 1-28-5 open. The receiver was placed on the 01 level above the foyer of $D_{1,2}$ at frame 28 and on the 2nd deck below door 1-25-1 and on the forward side of door 2-25-1 at frame 25. The stairwell down to the 2nd deck is accessed from an opening in the foyer of $D_{1,2}$. The ladderway to the 01 level is reached by passing from the foyer of $D_{1,2}$ into $D_{1,4}$, by following the passageway until door 1-25-1, and then by turning aft to face the ladderway. A hatch at the top of this ladderway seals the 01 level from the main deck.

Plots for the effective propagation losses when the receiver is placed near the hatch on the 01 Level are displayed in Fig. 20(a). The blue curve ($l_{sp}(102)$) and the green curve ($l_{sp}(103)$) indicate that the hatch is open and closed, respectively. Except at 900 MHz and 2.6 GHz where the losses are equal, $l_{sp}(102) > l_{sp}(103)$. For most frequencies, the closed hatch yields at least 5 dB of additional loss, which is expected. Apparently, the status (open vs closed) of the hatch does not affect the propagated signal at the excepted frequencies, and the reason for this is not known. Figure 20(b) shows similar plots when the receiver is placed one deck down on the 2nd deck by watertight door 2-25-1. In this case, the open door corresponds to $l_{sp}(104)$, the closed door corresponds to $l_{sp}(105)$, and $l_{sp}(104) > l_{sp}(105)$ for all frequencies. Figures 20(a) and 20(b) are placed side by side to compare the blue curves or the green curves; however, no obvious pattern is discernible.

With door 2-25-1 and the hatch on the 01 level open, the 01-level measurement ($l_{sp}(102)$) and the 2nd-deck measurement ($l_{sp}(104)$) are compared to a Class-A1 measurement ($l_{sp}(44)$) made in the foyer of $D_{1,2}$ in Fig. 20(c). For 800 MHz $\leq f \leq$ 1300 MHz, $l_{sp}(44) > l_{sp}(104) > l_{sp}(102)$. Hence propagation to the foyer of $D_{1,2}$ is better than propagation to 2nd deck, which is better than propagation to the 01 level. This makes sense because the path to the foyer is shorter than the path to the 2nd deck, which itself is shorter than the path to the 01 level. In particular, the differences in effective propagation loss at 900 MHz between the main deck and the 2nd deck and the 01 level are 15 dB and 20 dB, respectively, which are significant. However, this pattern does not hold for the higher frequencies, where the relative positions of the three curves change. The reasons for the different behaviors are unclear. The most that can be said is that these measurements easily exceed the background noise level, which strongly suggests good inter-deck propagation. This good propagation is consistent with demonstrations of notebook-computer LANs on the ex-USS *Shadwell* in September 1998 and April 1999, where excellent voice and video communications were achieved between different levels of the *Shadwell*.[20,21]
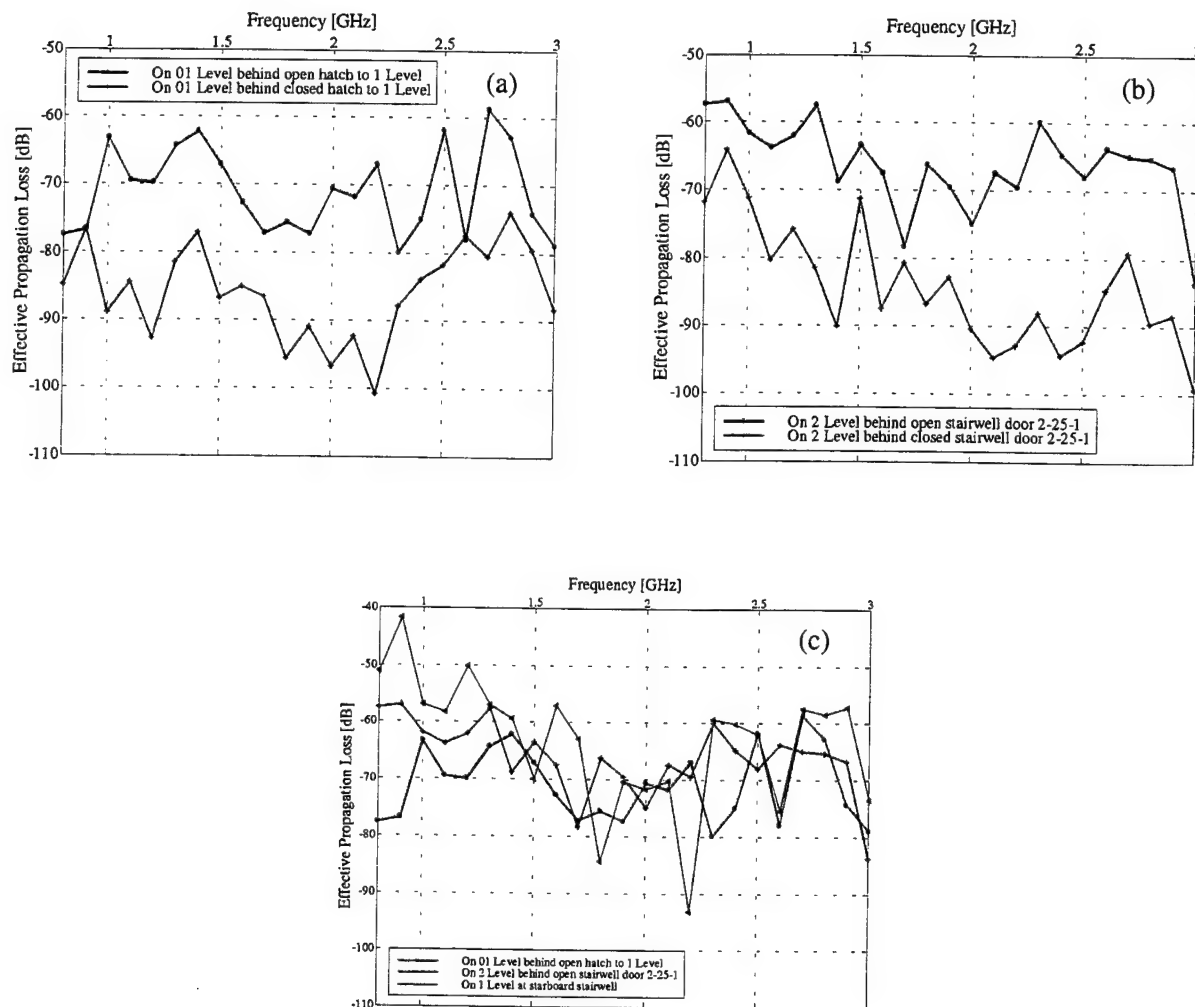
Fig. 20 — Comparison of the effect of inter-deck propagation. The transmitter is in $D_{1,3}$, and the receiver is placed at three positions (one on each of the 01 level, the main deck, and 2nd deck) by the starboard ladderway at frame 28. (a) The receiver is one deck above the main deck on the 01 level at the hatch that connects the two decks: open hatch for blue curve and closed hatch for green curve. (b) The receiver is one deck below the main deck on the 2nd deck by door 2-25-1: open door for blue curve and closed door for green curve. (c) The receiver is also on the 1 level at the ladderway down to the 2nd deck, and the three data sets are plotted when the hatch and door are open.

Class B1

In these five data sets, the transmitting antenna was placed in the open air on the forecastle $(D_{1,12})$ about 4 to 6 ft from doors 1-15-1 and 1-15-3, and the receiving antenna was placed in the foyer of $D_{1,2}$ at the starboard stairwell leading down to the 2nd deck. For the four data sets of Fig. 21, the door 1-20-2 connecting the port passageway $(D_{1,14})$ to the central area $(D_{1,1})$ is open. In Fig. 21(a), $l_{SP}(106)$ is compared to $l_{SP}(108)$. For $l_{SP}(106)$, door 1-15-1 is closed, door 1-15-3 is open, and the receiving antenna (batwing dipole of Fig. 6) is facing starboard; that is, the path along the starboard passageway is open and the path through the central area is closed. For $l_{SP}(108)$, door 1-15-1 is open, door 1-15-3 is closed, and the batwing dipole is facing port (central area); that is, the path along the starboard passageway is closed and the path through the central area is open. The two curves tend to switch positions as the frequency varies, except from 2 to 2.8 GHz, where propagation along the starboard path seems to be slightly better. Also note that the starboard path has pronounced losses at 1 GHz and 1.8 GHz $(l_{SP}(106) \leq -93$ dB). Aside from these minor features, no general pattern is observable, which is probably caused in part by the open port-propagation path resulting from open door 1-20-2.

The plots in Fig. 21(b) differ from those in Fig. 21(a) in that both doors, 1-15-1 and 1-15-3, are closed, that is, both the starboard and central propagation paths are closed insofar as the watertight doors are concerned. For these two data sets, the batwing dipole was facing starboard for $l_{SP}(107)$ and port (central area) for $l_{SP}(109)$. As in Fig. 21(a), $l_{SP}(107)$ and $l_{SP}(109)$ generally switch positions as the frequency varies; however, at the lower frequencies (800 MHz to 1.3 GHz), propagation along the starboard path was slightly better. Since port door 1-20-2 was also open for these two data sets, it is reasonable to expect less loss when the receiving antenna was pointed toward the central path. Although this may have been true, it is not readily apparent from the figure, because the experiment was not controlled enough to isolate such effects. When comparing the general behavior of the plots in Fig. 21(b) to those in Fig. 21(a), the losses in the right frame appear to be 5 to 10 dB greater, which was the result of having both 1-15-1 and 1-15-3 closed. As a final comment, the measurements represented by Fig. 21 differ from the earlier ones of Fig. 19 in that the transmitter-receiver positions are essentially reversed. Because the transmitter was not in the confined metallic spaces of the ship in Fig. 21, much less energy is transmitted into the ship. The switching of the receiving and transmitting antennas and the associated reciprocity issues are not addressed in this report.
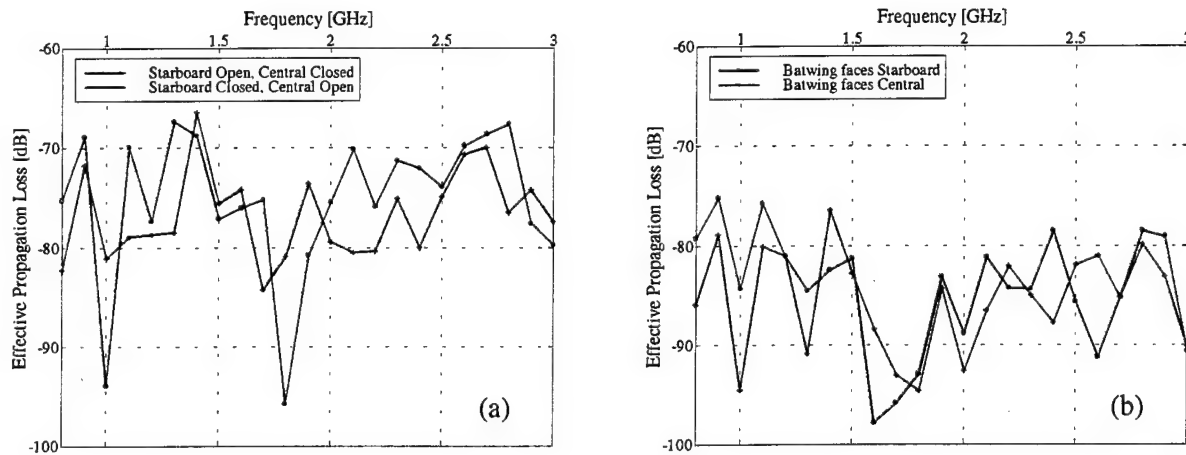
Fig. 21 — The transmitter is in the forecastle $D_{1,12}$, and the receiver is in the foyer of $D_{1,2}$ at down starboard ladderway to the 2nd deck. (a) Compares the propagation along the open central path ($l_{SP}(108)$) to propagation along the open starboard path ($l_{SP}(106)$). (b) Compares the propagation along the closed central path ($l_{SP}(109)$) to propagation along the closed starboard path ($l_{SP}(107)$).

Class B2

In the two data sets of this class, the location of the receiving antenna is fixed in the foyer of $D_{1,2}$ at (285 in., 24 in., 48 in.), the head of the starboard ladderway that leads down to the 2nd deck, and the transmitting antenna was moved aft along the centerline of $D_{1,1}$ and $D_{1,2}$ toward the receiving antenna. For data set 111, the transmitting antenna was placed in $D_{1,1}$ at (0 in., 292 in., 60 in.) about 0.25 m from the boundary of $D_{1,2}$. For data set 112, the transmitting antenna was placed at (0 in., 20 in., 60 in.), 6.91 m away from the location of data set 111 and 0.51 m from the aft bulkhead of $D_{1,2}$, with a line-of-sight (LOS) view of the receiving antenna. For 4 ft on both sides of the ship's centerline at the border of $D_{1,1}$ and $D_{1,2}$, no physical boundary separates the compartments.

The effective propagation losses for these data sets are plotted in Fig. 22(a), where the blue curve and the green curve correspond to $l_{SP}(111)$ and $l_{SP}(112)$, respectively. Both curves have roughly the same general behavior, but $l_{SP}(111) < l_{SP}(112)$ for all frequencies and suffers at least 10 dB more loss at 20 of the 23 frequencies. Since the transmitter-receiver distance R_{111} is greater than R_{112}, this inequality is expected just on the basis of the free-space propagation loss L_0. To get a sense of how much the free-space loss L_0 contributes to the effective propagation loss L_{SP} in this example, $10\log_{10}[L_0(f,111)/L_0(f,112)]$ and $l_{SP}(111) - l_{SP}(112)$ are plotted as the green curve and the blue curve, respectively, in Fig. 22(b). Recall from Eq. (3) that

$$L_0(f,n) = \left(\frac{\lambda}{4\pi R_n}\right)^2,$$ (5)

which implies that

$$l_0(f,111) - l_0(f,112) = 10\log_{10}\left(\frac{L_0(f,111)}{L_0(f,112)}\right) = 20\log_{10}\left(\frac{R_{112}}{R_{111}}\right) = 20\log_{10}\left(\frac{7.25\text{ m}}{9.94\text{ m}}\right) = -2.74\text{ dB.}$$ (6)

The index n is included for l_0 and L_0 to indicate the measurement number. Note that the ratio $L_0(f,111)/L_0(f,112)$ is independent of frequency, hence the constant value of −2.74 dB in Eq. (6) and for the ordinate of the green curve in Fig. 22(b). Except at 1.4 GHz, the differential effective propagation loss, $l_{SP}(111) - l_{SP}(112)$, is well below the corresponding differential free-space propagation loss, $l_0(f,111) - l_0(f,112)$, which clearly implies the presence of other propagation modes.
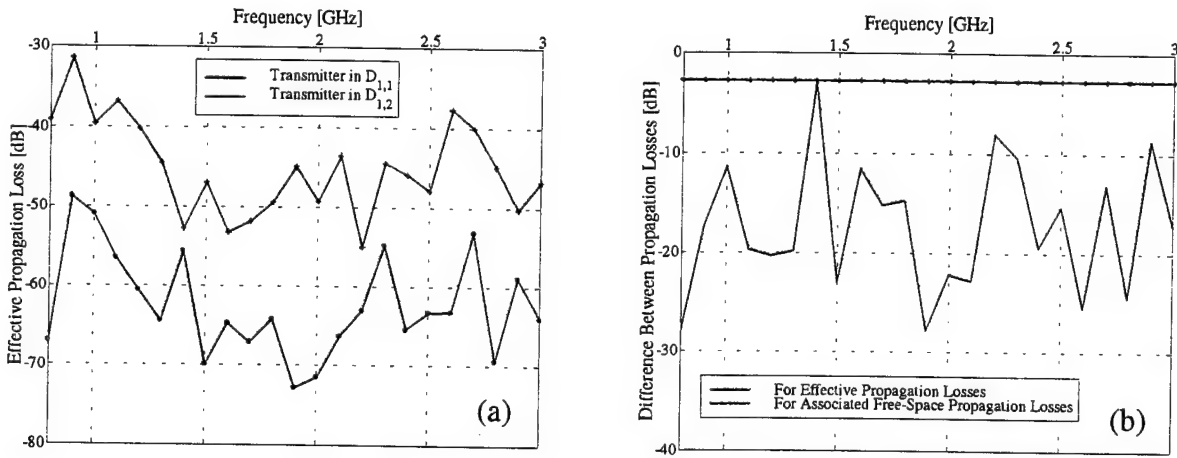
Fig. 22 — The transmitter was placed at two locations along the centerline of the main deck, one in $D_{1,1}$ near its border with $D_{1,2}$ (data set 111) and one in $D_{1,2}$ near its aft bulkhead (data set 112). The receiver was in the foyer of $D_{1,2}$ at down starboard stairwell to the 2nd deck. (a) Compares l_{SP} for both transmitter locations: $l_{SP}(111)$ is the blue curve; and $l_{SP}(112)$ is the green curve. (b) Compares the differences in l_{SP} (blue curve) and l_0 (green curve) between the two locations.

Other Comparisons

Repeatability is an important issue with respect to the stability of a measurement system. As a consequence of the limited time frame for collecting data on the *Shadwell*, only two sets of measurements (data sets 87 and 88) were directed to establishing the repeatability of the bistatic system. These data sets were collected with the receiving antenna in $D_{1,2}$ just outside closed door 1-28-1 and the transmitting antenna in closed compartment $D_{1,3}$. As Fig. 23(a) indicates, agreement between the measurements of received power for the data sets, $p_{S1}(87)$ and $p_{S1}(88)$, is very good. The curves nearly coincide for the lower frequencies (800 MHz $\leq f \leq$ 1.8 GHz), but the agreement is not as good for the higher frequencies (1.8 GHz $< f \leq$ 3 GHz), where p_{S1} was 10 to 20 dBm lower for both data sets. To display the closeness of the curves in Fig 23(a), the difference $p_{S1}(87) - p_{S1}(88)$ is graphed in Fig. 23(b). The greater differences between the data sets at the higher frequencies may be partially attributable to measurement error, because they certainly are closer to the background noise. However, since all measurements exceed the background noise level by at least 20 dBm, any lack of agreement is not solely attributable to measurement error.
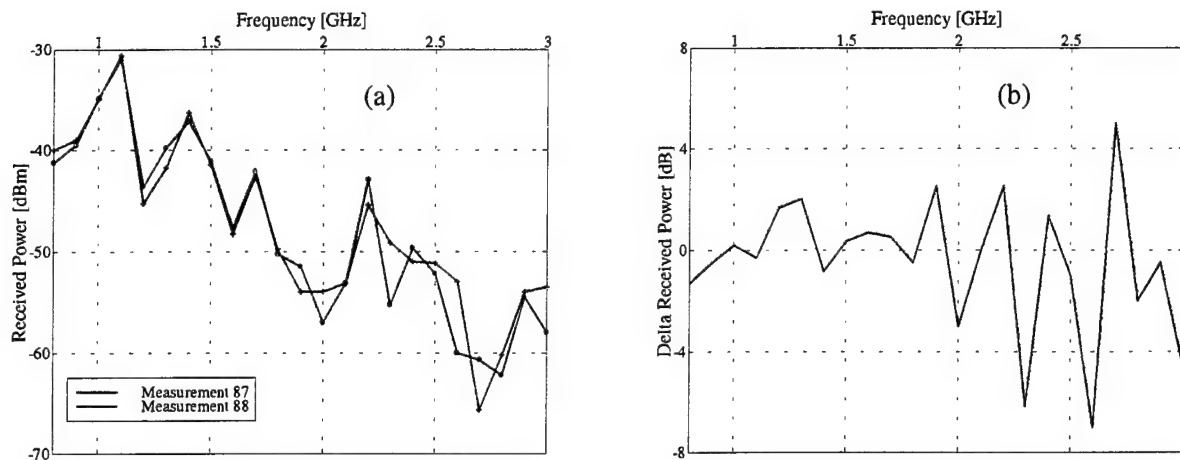
Fig. 23 — Repeatability of the bistatic measurement system: (a) Compares $p_{S_1}(87)$
and $p_{S_1}(88)$; (b) Difference $p_{S_1}(87) - p_{S_1}(88)$

In the next example, the effect of closing the watertight doors is examined by comparing the received powers when the transmitter was in $D_{1,3}$ and when each of three doors (1-28-1, 1-20-2, 1-15-1) was open and closed. Door 1-28-1 connects $D_{1,2}$ and $D_{1,3}$, 1-20-2 connects $D_{1,1}$ and $D_{1,14}$, and 1-15-1 connects $D_{1,1}$ and $D_{1,12}$. The receiving antenna was located in $D_{1,2}$ for 1-28-1, in $D_{1,14}$ for 1-20-2, and in $D_{1,12}$ for 1-15-1. The corresponding transmitter-receiver separations were 1.52 m, 12.04 m, and 18.86 m.

The received power when 1-28-1 was open (green curve: $p_{S_1}(41)$) is compared to the received power when it was closed (blue curve: $p_{S_1}(6)$) in Fig. 24(a). Clearly, $p_{S_1}(41)$ significantly exceeds $p_{S_1}(6)$, and the difference $p_{S_1}(41) - p_{S_1}(6)$ is plotted as the blue curve in Fig. 24(d). This difference usually is greater than 20 dB and exceeds 13 dB across the entire frequency band. For door 1-20-2, data set 96 (green curve: open door) and data set 97 (blue curve: closed door) are compared in Fig. 24(b). Again, the open-door power $p_{S_1}(96)$ is larger than the closed-door power $p_{S_1}(97)$ for all frequencies, but the differential $p_{S_1}(96) - p_{S_1}(97)$ between them (red curve in Fig. 24(d)) is on average less than $p_{S_1}(41) - p_{S_1}(6)$. The powers associated with door 1-15-1, corresponding to the most distant receiver location, are even closer (Fig. 24(c)). The general pattern that the received power for the open door ($p_{S_1}(108)$) exceeds that for the closed door ($p_{S_1}(109)$) is still maintained. According to the green curve in Fig. 24(d), $p_{S_1}(108) - p_{S_1}(109)$ varies between 2 dB and 16 dB, with an average of roughly 8 dB. It is interesting that $p_{S_1}(109)$ has the same order as $p_{S_1}(97)$, even though the transmitter-receiver distance for data set 109 is more than 1.5 times the distance for data set 97. In fact, $p_{S_1}(109) > p_{S_1}(97)$ for most frequencies.

The effect of closing a watertight door on the received power seems to be a loss between 5 dB and 30 dB, depending on the transmitter-receiver distance and the layout of the compartments. Moreover, that loss decreases as the door-transmitter distance increases. Even though closed doors result in substantial signal loss, the attenuated signal still has sufficient power to ensure good propagation (and possibly good communication) in the absence of other competing signals.
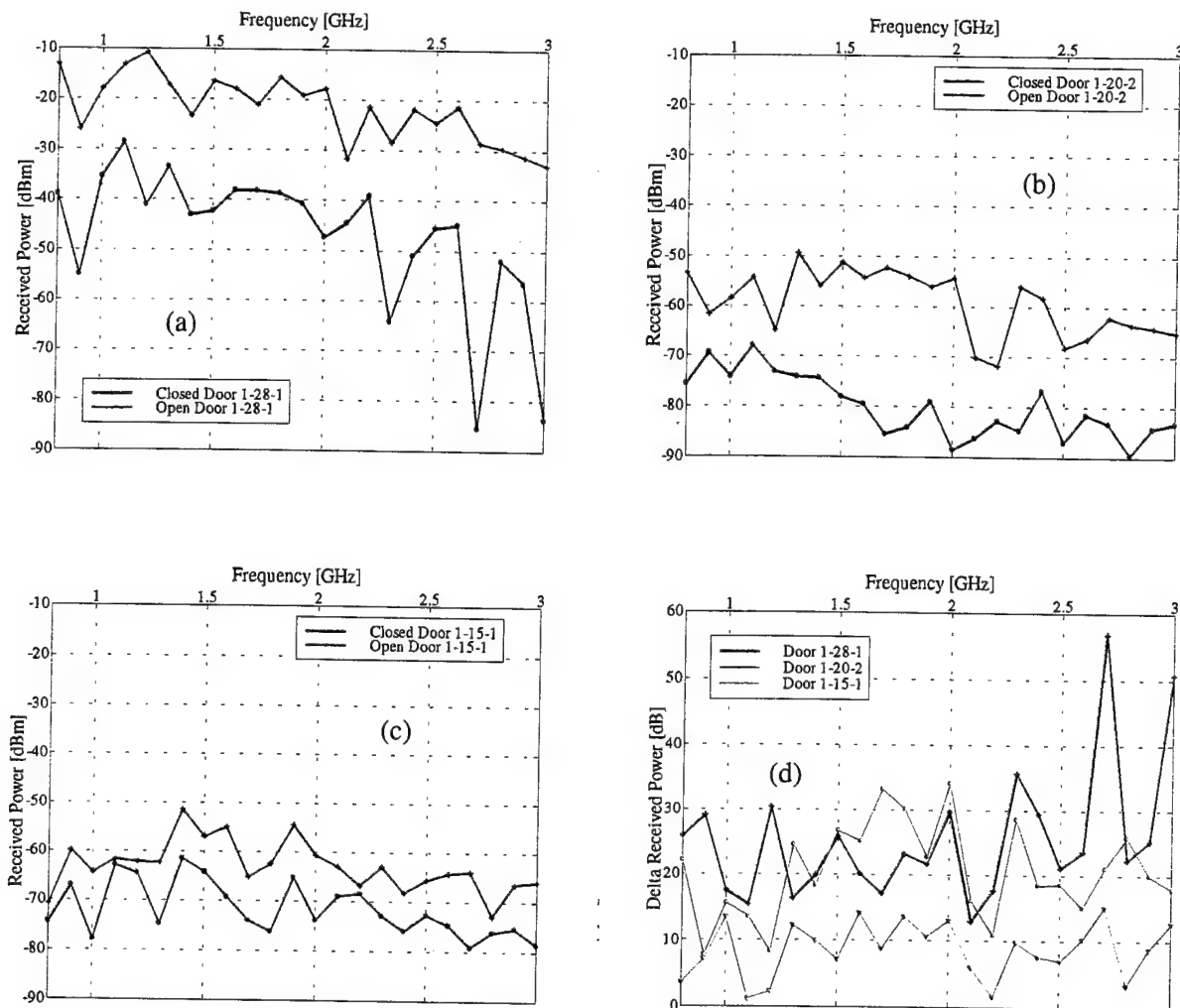
Fig. 24 — Closed-door open-door measurements of received power p_{s_1} with the transmitter in $D_{1,3}$. (a) Receiver in $D_{1,2}$ at door 1-28-1: door closed for blue curve ($p_{s_1}(6)$); door open for green curve ($p_{s_1}(41)$). (b) Receiver in $D_{1,14}$ at door 1-20-2: door closed for blue curve ($p_{s_1}(97)$); door open for green curve ($p_{s_1}(96)$). (c) Receiver in $D_{1,12}$ at door 1-15-1: door closed for blue curve ($p_{s_1}(109)$); door open for green curve ($p_{s_1}(108)$). (d) Delta received power: $p_{s_1}(41) - p_{s_1}(6)$ is the blue curve; $p_{s_1}(96) - p_{s_1}(97)$ is the red curve; and $p_{s_1}(108) - p_{s_1}(109)$ is the green curve.

SUMMARY

The measurements taken on the ex-USS *Shadwell* (23-25 February 1998) have provided an initial glimpse into the complex electromagnetic environment of the confined ship spaces aboard a naval vessel. This collection effort was a first attempt at obtaining some insight into RF propagation in this environment. A site survey was conducted, data were collected, and the data were processed and analyzed. As a consequence of equipment limitations (including a spectrum analyzer instead of a network analyzer and an open-loop synthesizer that caused synchronization problems between the spectrum analyzer and the signal generator) and insufficient measurement locations, no major conclusions have been reached on how the electromagnetic energy was propagated in the confined spaces of the *Shadwell*. However a few inferences are drawn.

The fact that most measurements were well above the background noise level over the entire frequency interval (800 MHz to 3 GHz), even for many closed-door configurations, strongly suggests that power levels are sufficient to ensure inter-deck and intra-deck communication when doors are closed for many operational situations. In particular, only 5 to 10 dB losses in signal power were incurred for closed watertight doors at many frequencies. In addition, the measurements indicate that intra-deck propagation

occurred along different paths, such as through central-room compartments and along the starboard and port passageways. Data substantiate the observed good performance of wireless communication systems at 915 MHz and 2.4 GHz that are currently being tested on the *Shadwell* for use during anticipated emergency situations. Evidence of some of the suggested modes of propagation in confined ship spaces was observed, for example, the multipath effects caused by scatter from the steel structure of the *Shadwell*. However, these measurements were not controlled well enough to separate the propagation modes. For example, *Shadwell* personnel and individuals involved with other concurrent testing had to move through the test area. These unavoidable and unscheduled intrusions affected the measurements by altering the door configuration and by introducing people as scatterers.

Clearly, more rigidly controlled testing and substantially more measurements are needed to gain a better understanding of the propagation modes in this environment and their relative impact on RF signals. Specifically, carefully designed laboratory tests to separate the propagation modes and to assess their relative strengths should precede further ship tests. The authors recommend improving the measurement system by replacing the antennas with better broadband antennas and by using a network analyzer instead of a spectrum analyzer. Furthermore, a short-pulse ultrawideband system might be a good device for temporally isolating some of the different modes like multipath.

That confined ship spaces support good communication also means that they will support good propagation of other RF sources like high-power radars and enemy jammers. Good propagation is not the only issue for a wireless LAN communication system. A wireless LAN also must not adversely affect the running of other ship systems like electrically driven machinery (for example, RF coupling to a ship's engine that could cause the ship to shut down). Consequently, it is important to understand the transfer characteristics associated with the different RF signals that could be present on a ship and to determine whether wireless LANs can co-exist with other Navy systems. To date, no detailed studies have been conducted on the propagation and interaction of the possible RF signals on naval ships.

In summary, this preliminary effort has determined that more extensive, controlled measurements with an improved measurement system are required to separate and understand more fully the modes of propagation in confined ship spaces. The current rush to use wireless LANs in a number of Navy programs (DC-ARM, RSVP, DD 21, and CG 21) makes it critical that studies be undertaken to establish the modes of transfer of the various RF signals that will be present in shipboard environments. Understanding the interactions of the various competing RF signals is necessary for the smooth operation and control of the relevant electromagnetic signals for naval ships.

ACKNOWLEDGMENTS

REFERENCES

1. "Welcome Aboard NRL's Advanced Fire Research Vessel," Publication 0076-6180, Naval Research Laboratory, October 1996.

2. H.W. Carhart and F.W. Williams, "The Ex-Shadwell-Full Scale Fire Research and Test Facility," NRL Memorandum Report 6074, 6 October 1987.

3. T.M. Gilliland, "Radar Attenuation by Rocket Plumes," Report CPTR 81-7, Chemical Propulsion Information Agency, Naval Plant Representative Office, Laurel, MD, October 1981.

4. B.R. Choquette, F.W. Williams, and T.T. Street, "The Effects of a Fire on Radio Wave Transmissions," NRL/MR/6180--98-8156, Naval Research Laboratory, 15 April 1998.

5. J. Lawton and F.J. Weinberg, *Electrical Aspects of Combustion* (Clarendon Press, Oxford, 1969).

6. D.L. Knepp and H.L.F. Houpis, "VHF/UHF Radar Scintillation Effects Observed by ALTAIR," in *The Effect of the Ionosphere on Radiowave Signals and System Performance* (Proceedings of Ionospheric Effects Symposium), eds. J.M. Goodman et al., 1-3 May 1990.

7. R. Sharpe, ed., *Jane's Fighting Ships*, 99th ed. (Jane's Information Group Limited, Coulsdon, Surrey, United Kingdom, 1996), pp. 825-826.

8. "Below-Decks Survey as Part of SEMCIP of USS OAK HILL (LSD 51)," Executive Summary, Contract N00178-95-C-3024, Eldyne, Inc., Norfolk, VA, 1996.

9. L.S. Cohen and A.H. Light, "Investigation of AN/SRC-55 (XN-1) Hierarchical Yet Dynamically Reprogrammable Architecture (HYDRA) Electromagnetic Interference (EMI) to AN/SPS-40E," Letter Report 5332/002, Naval Research Laboratory, 14 January 1998.

10. J. Perini and L.S. Cohen, "An Alternative Way to Stir the Fields in a Mode Stirred Chamber," submitted for publication in *IEEE Trans. Electromag. Compat.*

11. G. Schwartz, "Systems Engineering Study for the Reduced Ships-Crew by Virtual Presence (RSVP) Advanced Technology Demonstration (ATD)," Doc. No. 389826, Rev. – April 1999, The Charles Stark Draper Laboratory, Inc., Cambridge, MA, April 1999.

12. T.T. Street, "Feasibility of Implementing a Network for Repair Locker #2 Area of Concern Using RF Communications: Emissions Testing," Letter Report 6180/0713.1, Naval Research Laboratory, 22 November 1995.

13. T.T. Street, "Wireless, Spread Spectrum, Low Level RF, DC Communications Network for Repair #2 and the Submarine Mockup Area on ex-USS *Shadwell*," Letter Report 6180/0724.1, Naval Research Laboratory, 22 November 1995.

14. T.T. Street and R.A. Robinson, "Wireless Communications Network RF Emission Survey," Letter Report 6180/0198, Naval Research Laboratory, 20 June 1997.

15. E.L. Mokole, M. Parent, S.N. Samaddar, J. Valenzi, and E. Tomas, "Preliminary Report on Electromagnetic Propagation in an Enclosed Ship Environment," Letter Report 5340/193, Naval Research Laboratory, 30 October 1998.

16. E.L. Mokole, M. Parent, S.N. Samaddar, E. Tomas, B.T. Gold, J. Valenzi, and T.T. Street, "Initial Bistatic Measurements of Electromagnetic Propagation in an Enclosed Ship Environment," *Proceedings of the 1999 Antenna Applications Symposium*, September 15-17, 1999, Allerton Park, IL, sponsored by the Air Force Research Laboratory Sensors Directorate, the Electrical and Computer Engineering Department of the University of Massachusetts Amherst, and the Electromagnetics Laboratory of the University of Illinois at Urbana-Champaign, pp. 1-29.

17. A.J. Poggio and E.K. Miller, "Techniques for Low-Frequency Problems," in *Antenna Handbook: Theory, Applications, and Design*, Y.T. Lo and S.W. Lee, eds., (Van Nostrand Reinhold, New York , 1988), Ch. 3, p. 3-30.

18. G.W. Collins, "TV and FM Broadcast Antennas," in *Antenna Handbook: Theory, Applications, and Design*, Y.T. Lo and S.W. Lee, eds., Ch. 27, p. 27-33, (Van Nostrand Reinhold, New York , 1988).

19. H. Davison and W. van der Moolen, *WaveLAN®/PCMCIA Card User's Guide* (Lucent Technologies, Nieuwegein, The Netherlands, 1996), p. A-1.

20. T.T. Street, "Wireless, On-Site Video Demonstration ISFE/DC-ARM ARM Test Exercise on September 24, 1998 on ex-USS *Shadwell*," Letter Report 6180/0499A, Naval Research Laboratory, 15 September 1998.

21. T.T. Street, "EM Emission Surveys and RF Transmission Testing On-Board ex-USS *Shadwell*," Letter Report 6180/0101, Naval Research Laboratory, 18 February 1999.

Appendix A

TRANSMITTER-RECEIVER LOCATIONS
AND OPEN-CLOSED DOOR CONFIGURATIONS

This appendix consists of two tables that permit the reader to associate each data set that was taken on the ex-USS *Shadwell* with the location and the open-closed door configuration of that data set. In particular, these tables should be used in conjunction with Fig. 7 to develop a good mental picture of the geometry of each measurement. Each data set is associated with the index n, which runs from 1 through 112 (except 101 – the background noise measurement). For each n (data set), Table A1 enumerates the compartments of the transmitting and receiving antennas, the positions relative to a selected coordinate frame of the transmitter and receiver, the polarizations of transmitting and receiving antennas, and the free-space distance between the antennas.

In column 1 of Table A1, the appearance of B, Q, N in parentheses denotes something very specific about that data set. The B means that the data set was bad for some reason and was discarded. The designation Q signifies that the measured power for at least one of the 23 frequencies is within 5 dBm of the noise power. Similarly, the designation N means that the measured power for at least one of the frequencies is in the noise. The second column and the sixth column list the compartments for the receiving antenna and the transmitting antenna, respectively. As stated in the body of the report, $D_{i,j}$ is compartment j on deck i, where i = 1,2,3 for these measurements. Decks 1, 2, and 3 correspond to the levels 1, 2, and 01, respectively. Furthermore, when P appears parenthetically in the second column, the receiving antenna was the coaxially tipped probe; otherwise, the receiving antenna was the batwing dipole. Columns three through five and columns seven through nine respectively are the xyz coordinates of the receiving antenna's position (x_R, y_R, z_R) and the transmitting antenna's position (x_T, y_T, z_T), both in inches, relative to the origin O on the 1 level in Fig. 7. The tenth column represents the distance in meters between the transmitting and receiving antennas. The last column indicates the polarizations of the transmitting antenna and the receiving antenna. For example, the first letter of VH means the transmitting antenna is vertically polarized (the axis of the disc-cone is along the z-axis), and the second letter means that the receiving antenna is horizontally polarized (the axis of the batwing dipole is in the xy-plane).

Table A2 provides a listing of the open and closed doors for 111 of the data sets. The doors are designated by three sets of arabic numbers that are separated by hyphens (A-B-C): A is the number of the level; B is the frame; and C indexes the doors. The number A takes values like 1, 2, 3, 01, 02, and 03. When 0 begins the number, the level is above the 1 level, and increasing the number following 0 means that the level is getting higher above the 1 level. Frame 0 is at the bow of the ship, and each frame is 4 ft long. The final number C counts the number of doors and indicates whether the door is along the centerline (0), is on the starboard side (odd positive integers), or is on the port side (even positive integers). For example, door 1-28-5 is one of at least three doors on the starboard side of the 1 level near frame 28, roughly 112 ft from the bow of the *Shadwell*.

33

Table A1 — Indexing, Coordinates, Polarizations, and Corresponding Free-Space
Propagation Losses for Transmitter-Receiver Locations on the ex-USS *Shadwell*

n	$D_{i,j}$	x_R (in)	y_R (in)	z_R (in)	$D_{i,j}$	x_T (in)	y_T (in)	z_T (in)	R_n (m)	Pol.
1 (B)	$D_{1,2}$	157	36	12	$D_{1,3}$	149	94	60	1.92	VV
2	$D_{1,2}$	157	36	12	$D_{1,3}$	149	94	60	1.92	VV
3 (B)	$D_{1,2}$	157	36	24	$D_{1,3}$	149	94	60	1.75	VV
4	$D_{1,2}$	157	36	24	$D_{1,3}$	149	94	60	1.75	VV
5	$D_{1,2}$	157	36	36	$D_{1,3}$	149	94	60	1.61	VV
6	$D_{1,2}$	157	36	48	$D_{1,3}$	149	94	60	1.52	VV
7	$D_{1,2}$	157	36	60	$D_{1,3}$	149	94	60	1.49	VV
8	$D_{1,2}$	157	36	72	$D_{1,3}$	149	94	60	1.52	VV
9	$D_{1,2}$	157	36	84	$D_{1,3}$	149	94	60	1.61	VV
10	$D_{1,2}$	145	36	12	$D_{1,3}$	149	94	60	1.91	VV
11 (B)	$D_{1,2}$	145	36	24	$D_{1,3}$	149	94	60	1.74	VV
12 (B)	$D_{1,2}$	145	36	24	$D_{1,3}$	149	94	60	1.74	VV
13	$D_{1,2}$	145	36	24	$D_{1,3}$	149	94	60	1.74	VV
14	$D_{1,2}$	145	36	36	$D_{1,3}$	149	94	60	1.60	VV
15	$D_{1,2}$	145	36	48	$D_{1,3}$	149	94	60	1.51	VV
16	$D_{1,2}$	145	36	60	$D_{1,3}$	149	94	60	1.48	VV
17	$D_{1,2}$	145	36	72	$D_{1,3}$	149	94	60	1.51	VV
18	$D_{1,2}$	145	36	84	$D_{1,3}$	149	94	60	1.60	VV
19	$D_{1,2}$	133	36	12	$D_{1,3}$	149	94	60	1.95	VV
20 (B)	$D_{1,2}$	133	36	24	$D_{1,3}$	149	94	60	1.78	VV
21	$D_{1,2}$	133	36	24	$D_{1,3}$	149	94	60	1.78	VV
22	$D_{1,2}$	133	36	36	$D_{1,3}$	149	94	60	1.65	VV
23	$D_{1,2}$	133	36	48	$D_{1,3}$	149	94	60	1.56	VV
24	$D_{1,2}$	133	36	60	$D_{1,3}$	149	94	60	1.53	VV
25	$D_{1,2}$	133	36	72	$D_{1,3}$	149	94	60	1.56	VV
26	$D_{1,2}$	133	36	84	$D_{1,3}$	149	94	60	1.65	VV
27	$D_{1,2}$	169	36	12	$D_{1,3}$	149	94	60	1.98	VV
28	$D_{1,2}$	169	36	24	$D_{1,3}$	149	94	60	1.81	VV
29	$D_{1,2}$	169	36	36	$D_{1,3}$	149	94	60	1.67	VV
30	$D_{1,2}$	169	36	48	$D_{1,3}$	149	94	60	1.59	VV
31	$D_{1,2}$	169	36	60	$D_{1,3}$	149	94	60	1.56	VV
32	$D_{1,2}$	169	36	72	$D_{1,3}$	149	94	60	1.59	VV
33	$D_{1,2}$	169	36	84	$D_{1,3}$	149	94	60	1.67	VV
34	$D_{1,2}$	181	36	12	$D_{1,3}$	149	94	60	2.08	VV
35	$D_{1,2}$	181	36	24	$D_{1,3}$	149	94	60	1.91	VV
36	$D_{1,2}$	181	36	36	$D_{1,3}$	149	94	60	1.79	VV
37	$D_{1,2}$	181	36	48	$D_{1,3}$	149	94	60	1.71	VV
38	$D_{1,2}$	181	36	60	$D_{1,3}$	149	94	60	1.68	VV
39	$D_{1,2}$	181	36	72	$D_{1,3}$	149	94	60	1.71	VV
40	$D_{1,2}$	181	36	84	$D_{1,3}$	149	94	60	1.79	VV

Table A1 (Continued) — Indexing, Coordinates, Polarizations, and Corresponding Free-Space
Propagation Losses for Transmitter-Receiver Locations on the ex-USS *Shadwell*

n	$D_{i,j}$	x_R (in)	y_R (in)	z_R (in)	$D_{i,j}$	x_T (in)	y_T (in)	z_T (in)	R_n (m)	Pol.
41	$D_{1,2}$	157	36	48	$D_{1,3}$	149	94	60	1.52	VV
42	$D_{1,2}$	247	20	48	$D_{1,3}$	149	94	60	3.13	VV
43	$D_{1,2}$	247	20	48	$D_{1,3}$	149	94	60	3.13	VV
44	$D_{1,2}$	285	28	48	$D_{1,3}$	149	94	60	3.85	VV
45	$D_{1,2}$	285	28	48	$D_{1,3}$	149	94	60	3.85	VV
46	$D_{1,2}$	285	28	48	$D_{1,3}$	149	94	60	3.85	VV
47	$D_{1,2}$	285	28	48	$D_{1,3}$	149	94	60	3.85	VV
48	$D_{1,4}$	323	24	48	$D_{1,3}$	149	94	60	4.77	VV
49	$D_{1,4}$	323	24	48	$D_{1,3}$	149	94	60	4.77	VV
50	$D_{1,4}$	323	24	48	$D_{1,3}$	149	94	60	4.77	VV
51	$D_{1,4}$	323	24	48	$D_{1,3}$	149	94	60	4.77	VV
52 (N)	$D_{1,4}$	323	24	48	$D_{1,3}$	149	94	60	4.77	VV
53	$D_{1,4}$	323	24	48	$D_{1,3}$	149	94	60	4.77	VV
54 (N)	$D_{1,2}$ (P)	261	28	90	$D_{1,3}$	149	94	60	3.39	VV
55 (N)	$D_{1,4}$ (P)	310	38	85	$D_{1,3}$	149	94	60	4.38	VV
56	$D_{1,4}$ (P)	310	38	85	$D_{1,3}$	149	94	60	4.38	VV
57	$D_{1,4}$ (P)	261	201	82	$D_{1,3}$	149	94	60	3.97	VV
58 (N)	$D_{1,8}$	261	453	48	$D_{1,3}$	149	94	60	9.56	VV
59	$D_{1,8}$	261	453	48	$D_{1,3}$	149	94	60	9.56	VV
60	$D_{1,8}$	261	453	48	$D_{1,3}$	149	94	60	9.56	VV
61 (N)	$D_{1,8}$ (P)	261	453	48	$D_{1,3}$	149	94	60	9.56	VV
62	$D_{1,8}$ (P)	261	429	94	$D_{1,3}$	149	94	60	9.01	VV
63	$D_{1,8}$ (P)	249	358	60	$D_{1,3}$	149	94	60	7.17	VV
64 (N)	$D_{1,8}$ (P)	249	358	60	$D_{1,3}$	149	94	60	7.17	VV
65 (B)	$D_{1,8}$ (P)	257	358	84	$D_{1,3}$	149	94	60	7.27	VV
66	$D_{1,8}$ (P)	257	358	84	$D_{1,3}$	149	94	60	7.27	VV
67 (Q)	$D_{1,8}$ (P)	264	358	48	$D_{1,3}$	149	94	60	7.32	VV
68	$D_{1,8}$	264	419	48	$D_{1,3}$	149	94	60	8.76	VV
69 (B)	$D_{1,8}$	264	419	48	$D_{1,3}$	149	94	60	8.76	VH
70	$D_{1,8}$	264	419	48	$D_{1,3}$	149	94	60	8.76	VH
71	$D_{1,12}$	93	741	48	$D_{1,3}$	149	94	60	16.50	VV
72	$D_{1,12}$	93	741	48	$D_{1,3}$	149	94	60	16.50	VV
73 (N)	$D_{1,12}$	93	741	48	$D_{1,3}$	149	94	60	16.50	VV
74 (B)	$D_{1,12}$	93	741	48	$D_{1,3}$	149	94	60	16.50	VV
75	$D_{1,12}$	93	741	48	$D_{1,3}$	149	94	60	16.50	VV
76 (B)	$D_{1,2}$	154	19	48	$D_{1,3}$	149	94	60	1.93	VV
77 (Q)	$D_{1,2}$	154	19	48	$D_{1,3}$	149	94	60	1.93	VV
78	$D_{1,2}$	154	19	48	$D_{1,3}$	149	94	60	1.93	VV
79	$D_{1,2}$	154	19	48	$D_{1,3}$	149	94	60	1.93	VV
80	$D_{1,2}$	154	19	48	$D_{1,3}$	149	94	60	1.93	VV

Table A1 (Continued) — Indexing, Coordinates, Polarizations, and Corresponding Free-Space
Propagation Losses for Transmitter-Receiver Locations on the ex-USS *Shadwell*

n	$D_{i,i}$	x_R (in)	y_R (in)	z_R (in)	$D_{i,i}$	x_T (in)	y_T (in)	z_T (in)	R_n (m)	Pol.
81(B)	$D_{1,2}$	154	19	48	$D_{1,3}$	149	94	60	1.93	VV
82	$D_{1,2}$	154	19	48	$D_{1,3}$	149	94	60	1.93	VV
83	$D_{1,2}$	154	19	48	$D_{1,3}$	149	94	60	1.93	VH
84	$D_{1,2}$	154	19	48	$D_{1,3}$	149	94	60	1.93	HH
85	$D_{1,2}$	154	19	48	$D_{1,3}$	149	94	60	1.93	HV
86	$D_{1,2}$	154	19	48	$D_{1,3}$	149	94	60	1.93	VV
87	$D_{1,2}$	154	19	48	$D_{1,3}$	149	94	60	1.93	VV
88	$D_{1,2}$	154	19	48	$D_{1,3}$	149	94	60	1.93	VV
89	$D_{1,2}$	154	19	48	$D_{1,3}$	149	94	60	1.93	VV
90	$D_{1,2}$	154	19	48	$D_{1,3}$	149	94	60	1.93	VV
91	$D_{1,1}$	0	292	48	$D_{1,3}$	149	94	60	6.30	VV
92	$D_{1,1}$	0	554	48	$D_{1,3}$	149	94	60	12.29	VV
93	$D_{1,1}$	-156	396	48	$D_{1,3}$	149	94	60	10.91	VV
94 (N)	$D_{1,14}$	-216	582	48	$D_{1,3}$	149	94	60	15.48	VV
95	$D_{1,14}$	-216	582	48	$D_{1,3}$	149	94	60	15.48	VV
96	$D_{1,14}$	-216	396	48	$D_{1,3}$	149	94	60	12.04	VV
97 (Q)	$D_{1,14}$	-216	396	48	$D_{1,3}$	149	94	60	12.04	VV
98	$D_{1,20}$	-216	150	48	$D_{1,3}$	149	94	60	9.38	VV
99 (N)	$D_{1,20}$	-216	150	48	$D_{1,3}$	149	94	60	9.38	VV
100 (N)	$D_{1,20}$	-216	150	48	$D_{1,3}$	149	94	60	9.38	VV
102	$D_{3,1}$	282	43	160	$D_{1,3}$	149	94	60	4.42	VV
103 (Q)	$D_{3,1}$	282	43	160	$D_{1,3}$	149	94	60	4.42	VV
104	$D_{2,3}$	285	178	-75	$D_{1,3}$	149	94	60	5.31	VV
105 (Q)	$D_{2,3}$	285	178	-75	$D_{1,3}$	149	94	60	5.31	VV
106	$D_{1,2}$	285	24	48	$D_{1,12}$	93	741	60	18.86	VV
107	$D_{1,2}$	285	24	48	$D_{1,12}$	93	741	60	18.86	VV
108	$D_{1,2}$	285	24	48	$D_{1,12}$	93	741	60	18.86	VV
109	$D_{1,2}$	285	24	48	$D_{1,12}$	93	741	60	18.86	VV
110	$D_{1,2}$	285	24	48	$D_{1,12}$	93	741	60	18.86	VV
111	$D_{1,2}$	285	24	48	$D_{1,1}$	0	292	60	9.94	VV
112	$D_{1,2}$	285	24	48	$D_{1,2}$	0	20	60	7.25	VV

Table A2 — Indexing and Open/Closed Door Configurations
for Transmitter-Receiver Locations on the ex-USS *Shadwell*

n	Open Doors	Closed Doors
1 (B)		1-28-1
2		1-28-1
3 (B)		1-28-1
4		1-28-1
5		1-28-1
6		1-28-1
7		1-28-1
8		1-28-1
9		1-28-1
10		1-28-1
11 (B)		1-28-1
12 (B)		1-28-1
13		1-28-1
14		1-28-1
15		1-28-1
16		1-28-1
17		1-28-1
18		1-28-1
19		1-28-1
20 (B)		1-28-1
21		1-28-1
22		1-28-1
23		1-28-1
24		1-28-1
25		1-28-1
26		1-28-1
27		1-28-1
28		1-28-1
29		1-28-1
30		1-28-1
31		1-28-1
32		1-28-1
33		1-28-1
34		1-28-1
35		1-28-1
36		1-28-1
37		1-28-1
38		1-28-1
39		1-28-1
40		1-28-1

Table A2 (Continued) — Indexing and Open/Closed Door Configurations
for Transmitter-Receiver Locations on the ex-USS *Shadwell*

n	Open Doors	Closed Doors
41	1-28-1	1-26-1
42	1-28-1;1-28-5	1-26-1
43	1-28-3;1-28-5	1-26-1;1-28-1
44	1-28-3;1-28-5	1-26-1;1-28-1
45	1-28-1;1-28-3;1-28-5	1-26-1
46	1-28-1;1-28-3	1-26-1;1-28-5
47	1-28-3	1-26-1;1-28-1;1-28-5
48	1-28-1;1-28-3;1-28-5	1-26-1
49	1-28-3;1-28-5	1-26-1;1-28-1
50	1-28-3	1-28-1;1-28-5
51		1-28-1;1-28-3;1-28-5
52 (S)		1-28-1;1-28-3;1-28-5
53		1-28-1;1-28-3;1-28-5
54 (S)	1-28-3	1-28-1;1-28-5
55 (S)		1-28-1;1-28-3;1-28-5
56	1-28-1;1-28-5	1-28-3
57	1-28-1;1-28-5	1-28-3
58 (S)	1-28-1	1-22-1;1-25-1;1-26-3;1-28-3;1-28-5
59	1-28-1	1-22-1;1-25-1;1-26-3;1-28-3;1-28-5
60	1-22-1;1-25-1;1-28-1;1-28-3;1-28-5	1-26-3
61 (S)	1-28-1;1-28-5	1-22-1;1-25-1;1-28-3
62	1-28-1;1-28-5	1-22-1;1-25-1;1-28-3
63	1-25-1;1-28-1;1-28-3;1-28-5	1-22-1
64 (S)	1-25-1;1-28-1;1-28-3;1-28-5	1-22-1 (Cracked)
65 (B)	1-25-1;1-28-1;1-28-3;1-28-5	1-22-1
66	1-25-1;1-28-1;1-28-3;1-28-5	1-22-1
67 (Q)	1-25-1;1-28-1;1-28-3;1-28-5	1-22-1
68	1-22-1;1-25-1;1-28-1;1-28-3;1-28-5	
69 (B)	1-22-1;1-25-1;1-28-1;1-28-3;1-28-5	
70	1-22-1;1-25-1;1-28-1;1-28-3;1-28-5	
71	1-15-1,3,7;1-22-1;1-25-1;1-28-1,3,5	1-26-3
72	1-15-3,7;1-22-1;1-25-1;1-28-1,3,5	1-15-1
73 (S)	1-15-7;1-22-1;1-25-1;1-28-1,3,5	1-15-1;1-15-3
74 (B)	1-15-1,7;1-22-1;1-25-1;1-28-1,3,5	1-15-3
75	1-15-1,7;1-22-1;1-25-1;1-28-1,3,5	1-15-3
76 (B)		1-28-1
77 (Q)		1-28-1
78		1-28-1
79		1-28-1
80		1-28-1

Table A2 (Continued) — Indexing and Open/Closed Door Configurations
for Transmitter-Receiver Locations on the ex-USS *Shadwell*

n	Open Doors	Closed Doors
81 (B)		1-28-1
82		1-28-1
83		1-28-1
84		1-28-1
85		1-28-1
86		1-28-1
87		1-28-1
88		1-28-1
89		1-28-1
90		1-28-1
91		1-15-1;1-20-2;1-26-1;1-28-1,5
92		1-15-1;1-20-2;1-26-1;1-28-1,5
93		1-15-1;1-20-2;1-26-1;1-28-1,5
94 (S)		1-15-1;1-16-2;1-20-2;1-26-1;1-28-1,5*
95	1-20-2	1-15-1;1-16-2;1-26-1;1-28-1,5*
96	1-20-2	1-15-1;1-16-2;1-26-1;1-28-1,5*
97 (Q)		1-15-1;1-16-2;1-20-2;1-26-1;1-28-1,5*
98	1-20-2;1-22-2;1-25-4	1-15-1;1-16-2;1-26-1;1-28-1,5*
99 (S)	1-22-2	1-15-1;1-16-2;1-20-2;1-26-1;1-28-1,5*
100 (S)		1-15-1;1-16-2;1-20-2;1-26-1;1-28-1,5*
102	1-28-3;1-28-5;Hatch to 01 Level	1-26-1;1-28-1;1-29-3
103 (Q)	1-28-3;1-28-5	1-26-1;1-28-1;1-29-3;Hatch to 01 Level
104	1-28-3;1-28-5;2-25-1	1-26-1;1-28-1;1-29-3
105 (Q)	1-28-3;1-28-5	1-26-1;1-28-1;1-29-3
106	1-15-3;1-20-2;1-22-1;1-25-1;1-28-3,5	1-15-1;1-28-1;1-29-3
107	1-20-2;1-22-1;1-25-1;1-28-3,5	1-15-1;1-15-3;1-28-1;1-29-3
108	1-15-1;1-20-2;1-22-1;1-25-1;1-28-3,5	1-15-3;1-28-1;1-29-3
109	1-20-2;1-22-1;1-25-1;1-28-3,5	1-15-1;1-15-3;1-28-1;1-29-3
110	1-22-1;1-25-1;1-28-3,5	1-15-1;1-15-3;1-20-2;1-28-1;1-29-3
111		
112		

*Indicates that all 01-level doors are closed in port passageway between frames 15 and 29

Appendix B

DERIVATION OF EFFECTIVE PROPAGATION LOSS

According to several sources,[B1,B2] the bistatic Friis transmission formula for free space is

$$P_{r1} = P_t G_t G_r \left(\frac{\lambda}{4\pi R}\right)^2 L_S, \tag{B1}$$

where

    P_{r1} is the received signal power,
    P_t is the transmitted power,
    G_r is the gain of the receiving antenna,
    G_t is the gain of the transmitting antenna,
    R is the distance between the transmitting antenna and the receiving antenna,
    λ is the wavelength at frequency f of the transmitted signal, and
    L_s is the combination of all losses in the transmitter and receiver.

The quantity $(\lambda/(4\pi R))^2$ is typically called the free-space propagation loss and is denoted L_0. Thus Eq. (B1) becomes

$$P_{r1} = P_t G_t G_r L_0 L_S. \tag{B2}$$

In more complex environments like ships, where several phenomena are simultaneously occurring, the received signal power P_{r2} is represented by

$$P_{r2} = P_t G_t G_r L_{SP} L_S, \tag{B3}$$

where the effective propagation parameter L_{SP},

$$L_{SP} = \prod_{\alpha=0}^{N} L_\alpha, \tag{B4}$$

is the product of all other propagation/scattering effects L_α For example, the effects may be attributable to multipath, waveguide structures, surface waves, and coaxial-cable structures. The nonnegative number N of effects depends on the particular electromagnetic situation. The simplest case occurs when $N = 0$, that is, when the transmitting and receiving systems are essentially in free space. In this special case, Eq. (B3) reduces to Eq. (B2).

Although the L_α are typically losses ($L_\alpha < 1$), the value of a particular L_α may be larger than unity. If $L_\alpha > 1$, then the impact of the corresponding physical phenomena is to enhance the radiated signal. As the reader can observe in the data for $l_{sp}(41)$ in Appendix D, this situation actually occurred. Apparently, multipath from the signal bouncing around compartments $D_{1,2}$ and $D_{1,3}$ caused the propagation factor l_{SP} to exceed the free-space propagation loss l_0.

On board the ex-USS *Shadwell*, received signal levels (denoted P_{S1}) were collected for various transmitter-receiver locations. In addition, a calibration measurement P_{S2} was taken, where the transmitter and receiver ports were connected directly. By Eq. (B3) and a simplified version of it,

$$P_{S1} = P_t G_t G_r L_{SP} L_S, \qquad P_{S2} = P_t L_S. \tag{B5}$$

Consequently,

$$\frac{P_{S1}}{P_{S2}} = G_t G_r L_{SP}. \tag{B6}$$

To determine L_{SP} in terms of measured quantities (that is, to determine $G_t G_r$), two additional calibration measurements subsequent to the *Shadwell* experiment were made in the Radar Division's Compact Range: one for the batwing dipole and one for the coaxially tipped probe. First, the receiving port was connected directly to the transmitting port, and a system calibration was performed that produced a unity gain (0 dBi) across the frequency spectrum. Then the antennas were attached to the appropriate ports, and the received power was measured when the transmitting and receiving antennas were separated by distance R_{C1}. The second part of the calibration was done for each receiving antenna. This procedure permitted the calculation of the ratio P_{C12} ($= P_{C1}/P_{C2}$). P_{C1} is the measured received power in the Compact Range at each of the 23 frequencies when the transmitter and receiver are separated by R_{C1}, and P_{C2} is the measured received power in the range at each of the 23 frequencies when the transmitting and receiving ports are directly connected. Since $P_{C2} = P_t L_S$ and

$$P_{C1} = P_t G_t G_r \left(\frac{\lambda}{4\pi R_{C1}}\right)^2 L_S, \tag{B7}$$

then

$$P_{C12} = G_t G_r \left(\frac{\lambda}{4\pi R_{C1}}\right)^2. \tag{B8}$$

Consequently, the product $G_t G_r$ is solvable in terms of measured quantities and is given by

$$G_t G_r = \left(\frac{4\pi R_{C1}}{\lambda}\right)^2 P_{C12}. \tag{B9}$$

Equations (B6) and (B9) are combined to obtain L_{SP} in terms of five known or measured quantities:

$$L_{SP} = \frac{P_{S1}}{P_{S2}} \left(\frac{\lambda}{4\pi R_{C1}}\right)^2 \frac{1}{P_{C12}}. \tag{B10}$$

REFERENCES

B1. D.K. Barton, *Modern Radar System Analysis* (Artech House, Inc., Norwood MA, 1988), Ch. 1, pp. 10-12.

B2. C.A. Balanis, *Antenna Theory Analysis and Design*, 2nd ed. (Wiley, New York NY, 1997), Ch. 2, pp. 86-90.

Appendix C

RAW RECEIVED POWER ON EX-USS *SHADWELL*

This appendix provides the raw received power measurements for data sets 1 through 112. These data were collected on the ex-USS *Shadwell* from 23 – 25 February 1998 with the bistatic measurement system that is described in the third section of this report. Each data set consists of 23 measured values of the power, one value for each frequency: 800 MHz, 900 MHz, 1 GHz,...,2.9 GHz, 3 GHz. The 23 ordered pairs (f, p_{s1}) of frequency and logarithmic power are connected by line segments for each data set. The resulting plot for the nth data set is designated by $p_{s1}(n)$, where n runs from 1 to 112.

Based on the analysis of Appendix E, error bars are plotted at each frequency. The curve for $p_{s1}(62)$ provides a clear example of what the error bars look like. In contrast to the plot of $p_{s1}(62)$, the error bars in many of the curves appear as a single horizontal line segment, because the received power is 40 dBm or more above the background noise level p_N, which is approximately –90 dBm (Fig. 11). When $p_{s1} - p_N \geq$ 40 dB, $0 \leq \varepsilon_U - \varepsilon_L \leq .174$ dB. Consequently, the upper and lower horizontal line segments of the error bar coalesce so that they appear as a single horizontal line segment.

Of all the data sets, $p_{s1}(41)$ has the largest values of power across the frequency band, because the transmitting antenna and the receiving antenna were separated by a mere 4 ft, with only free space between them. The implications of the strength of $p_{s1}(41)$ are discussed in Appendix D in the context of the effective propagation loss.

Raw Received Power for Data Sets 1 – 10
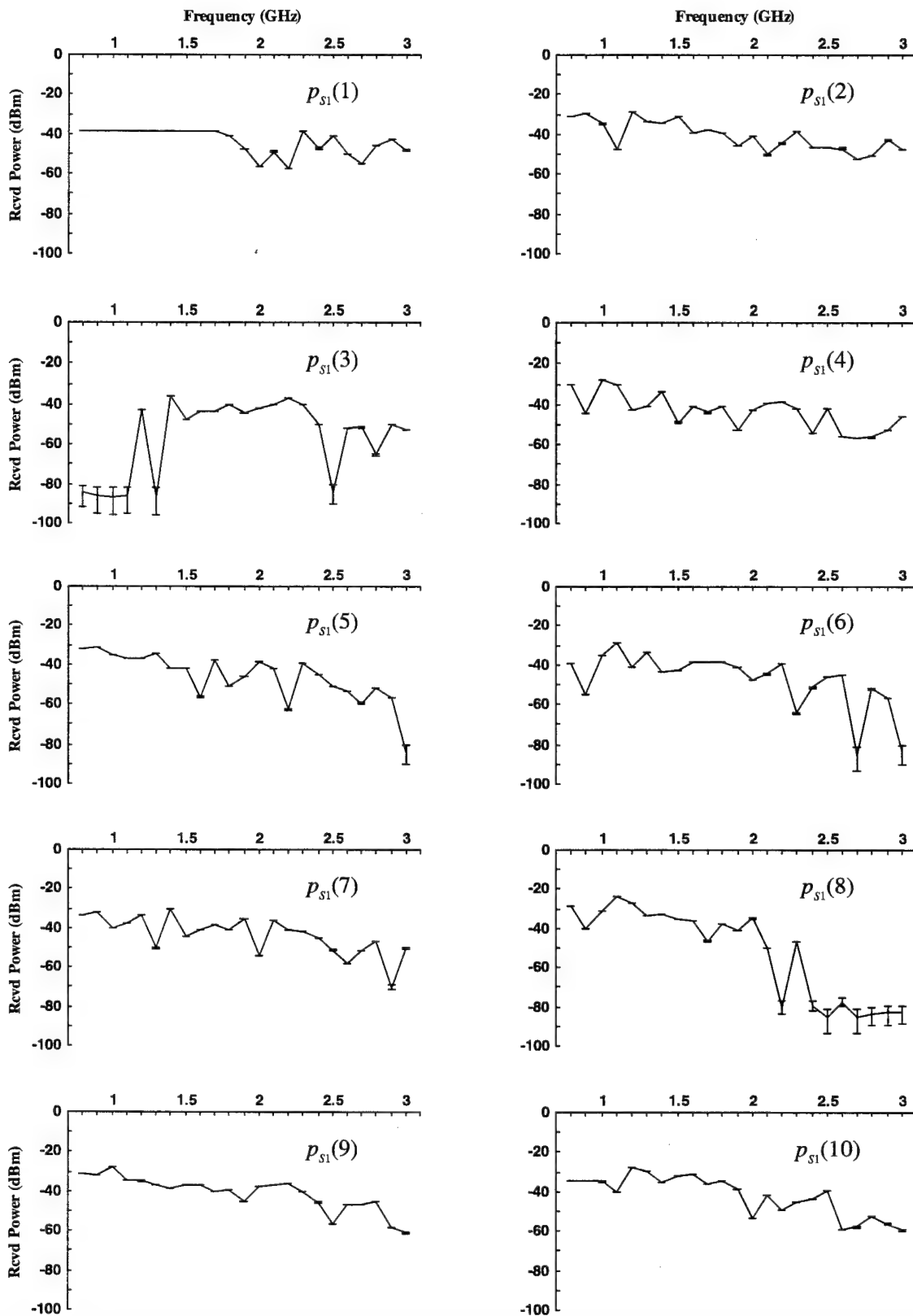
Raw Received Power for Data Sets 11 – 20
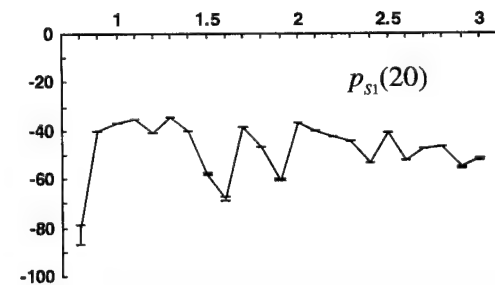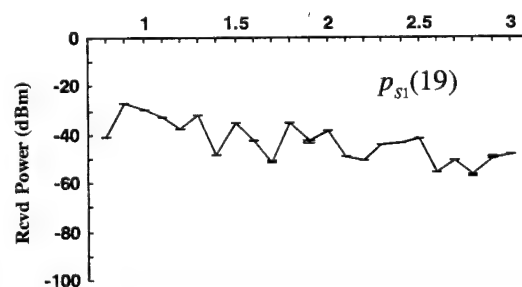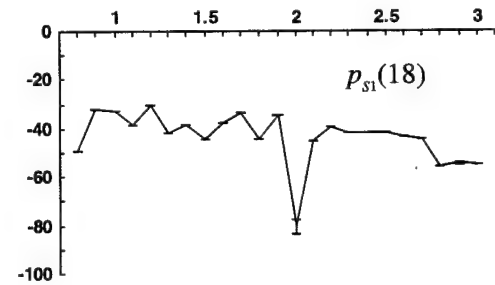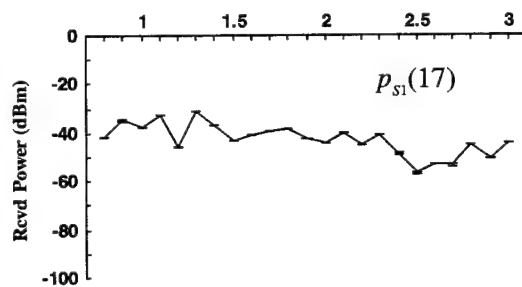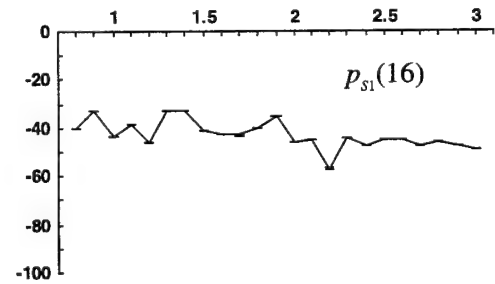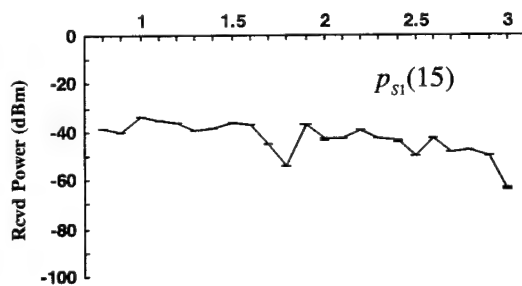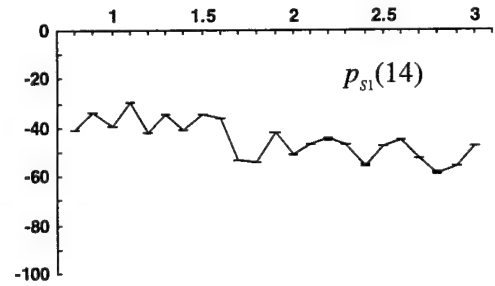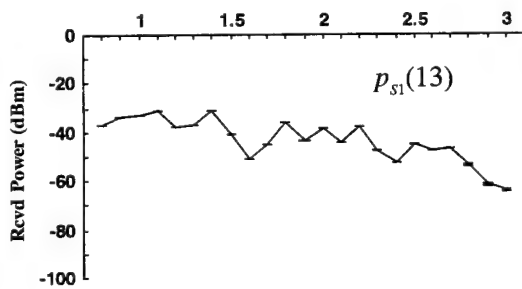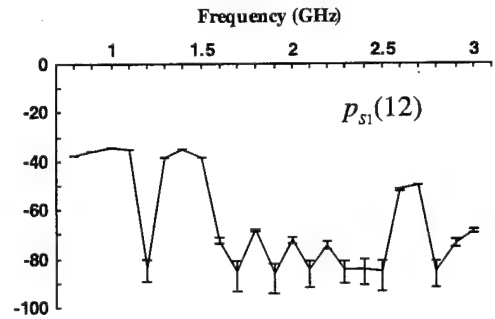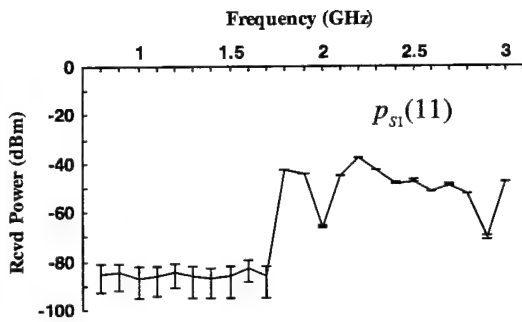
Raw Received Power for Data Sets 21 – 30
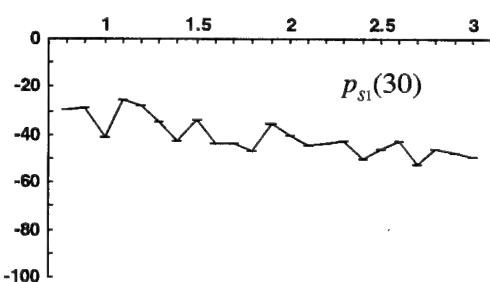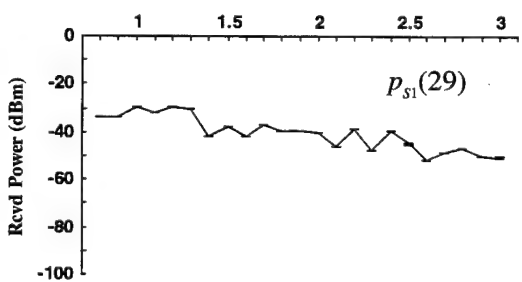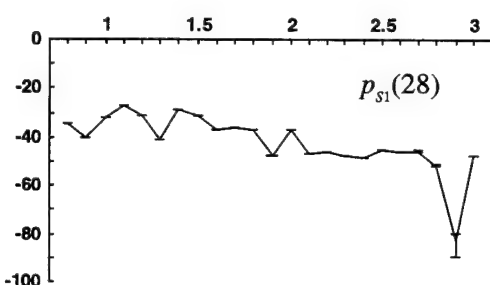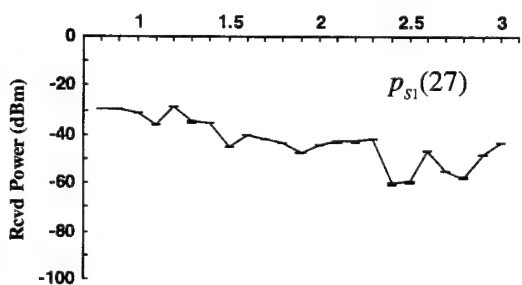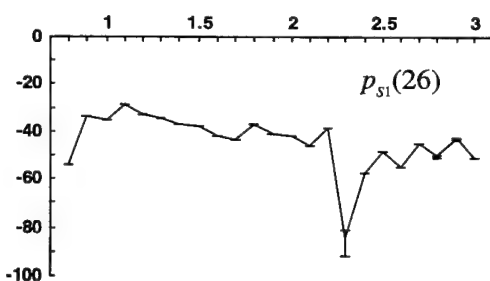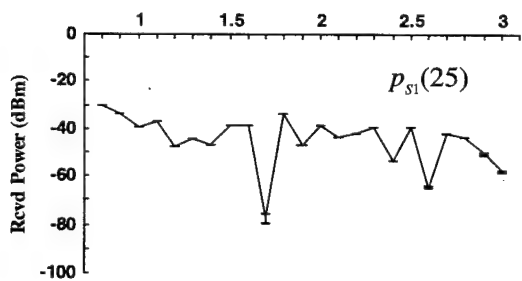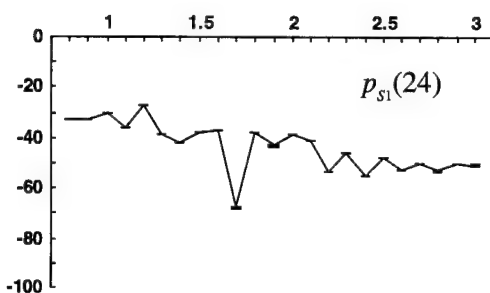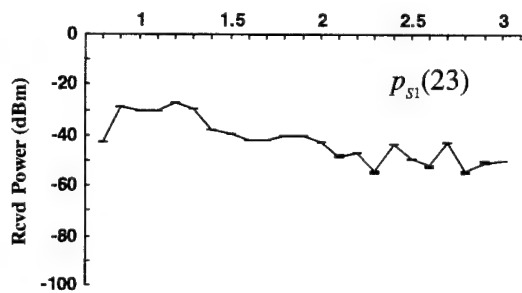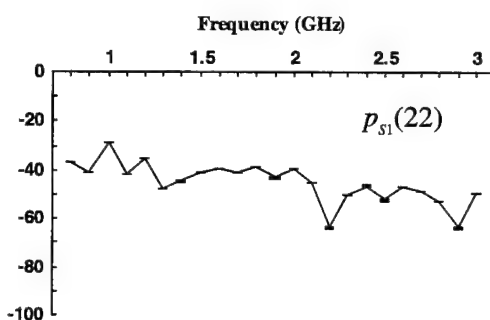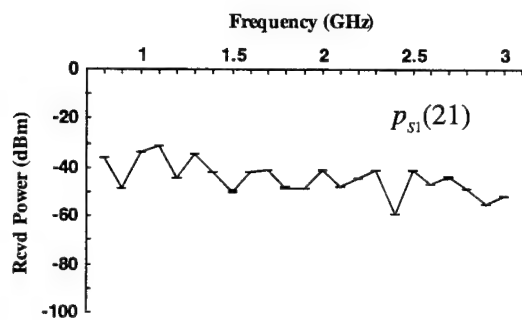
Raw Received Power for Data Sets 31 – 40
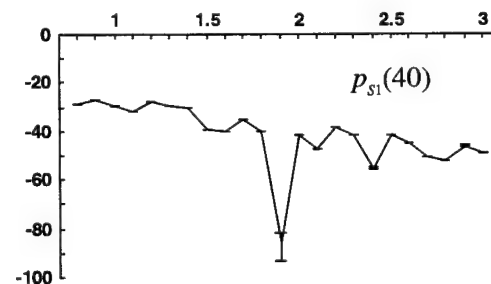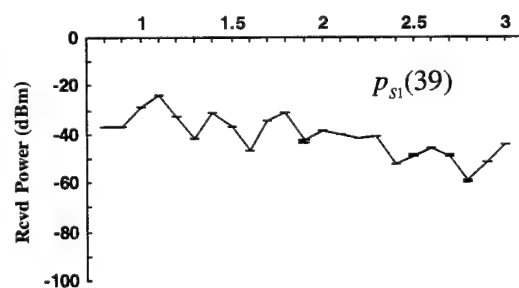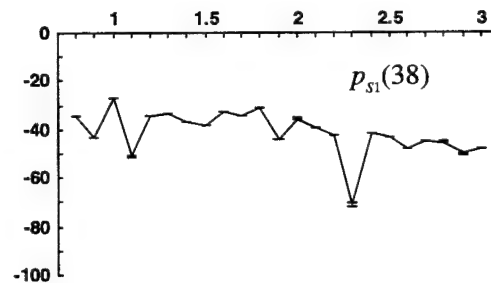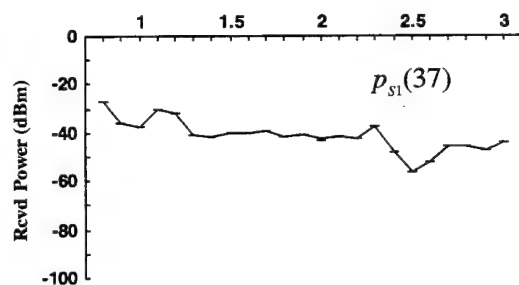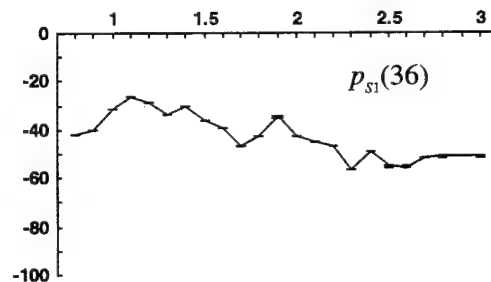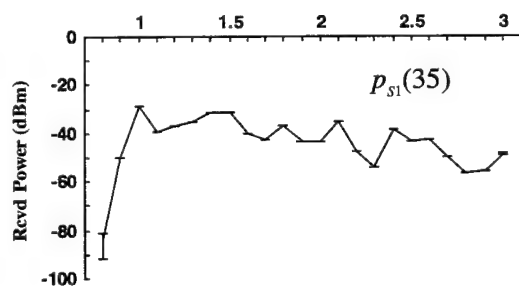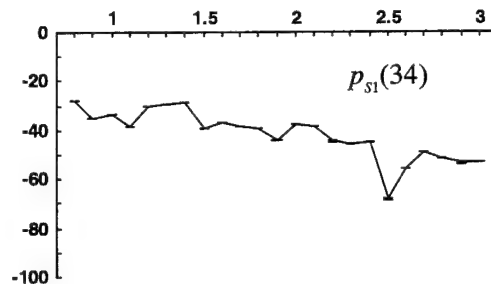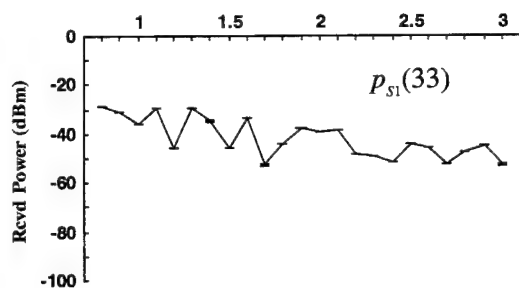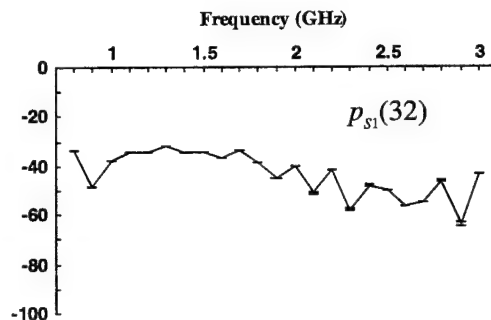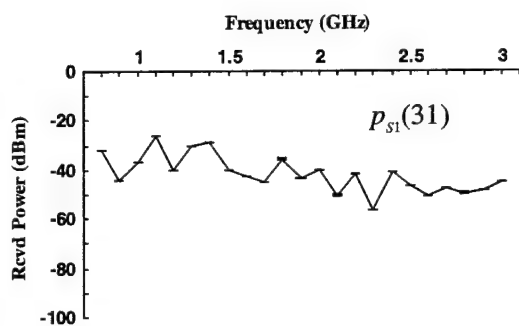
Raw Received Power for Data Sets 41 – 50
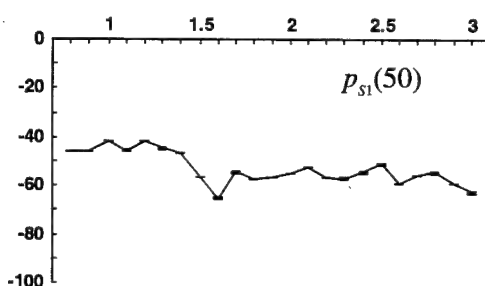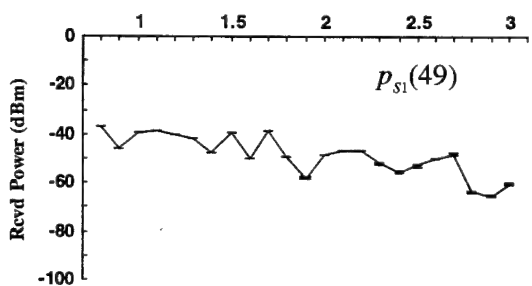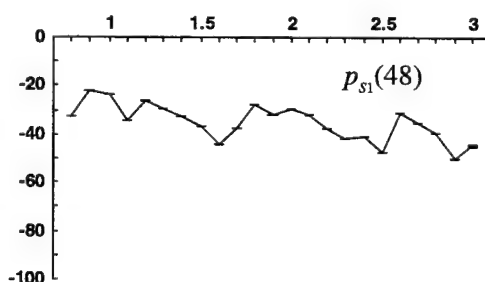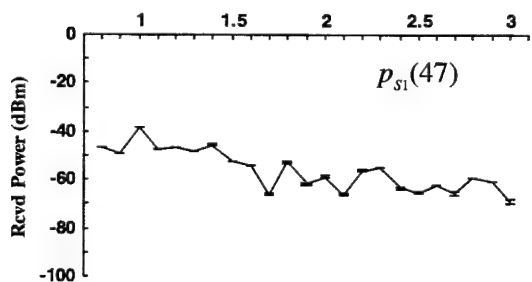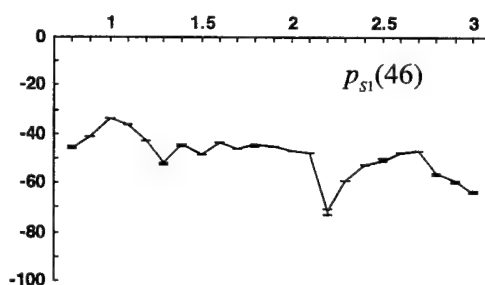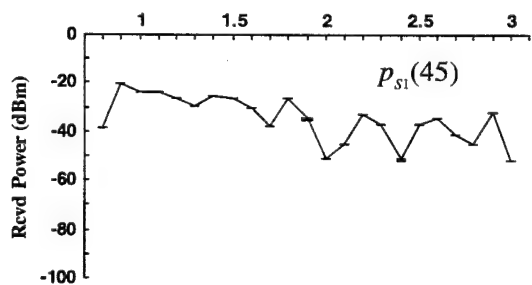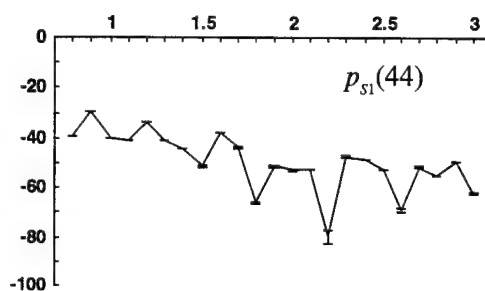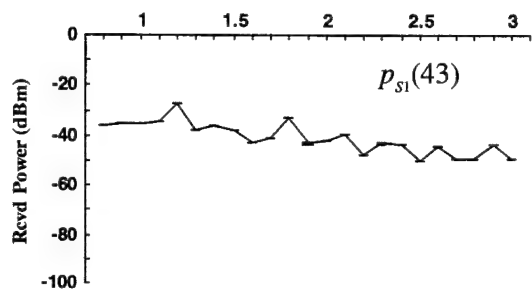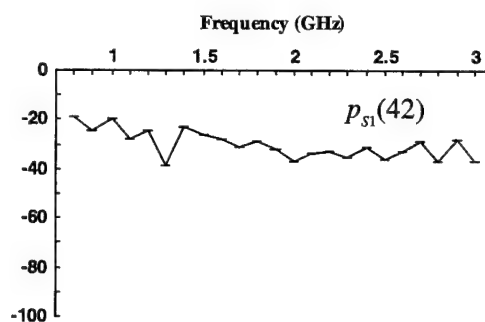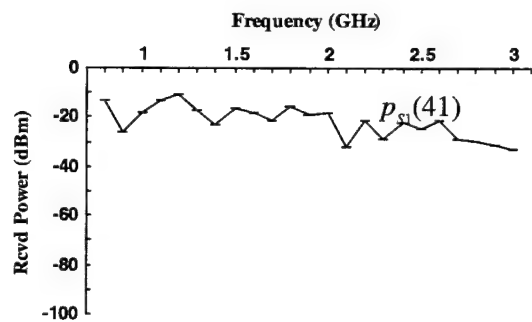
Raw Received Power for Data Sets 51 – 60
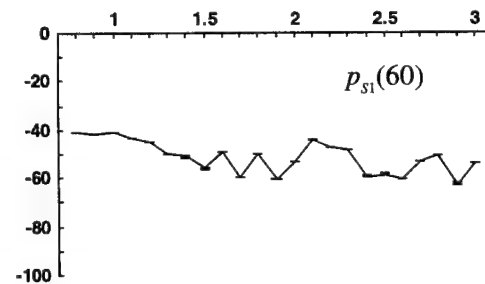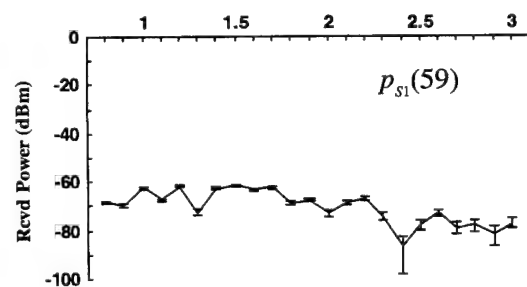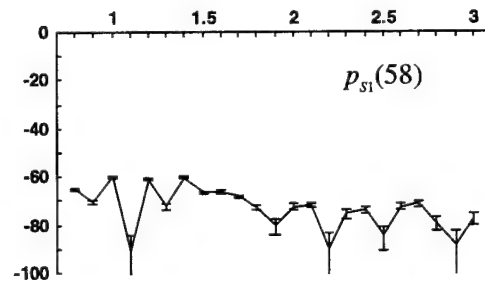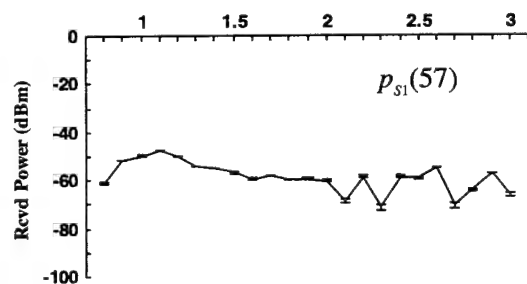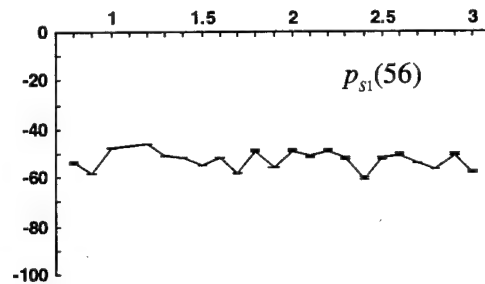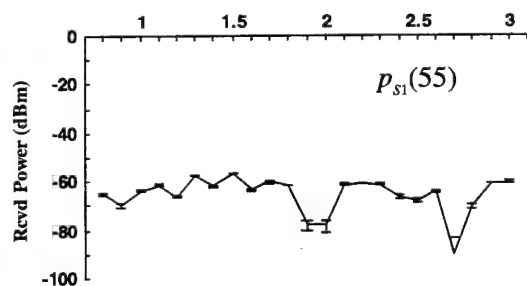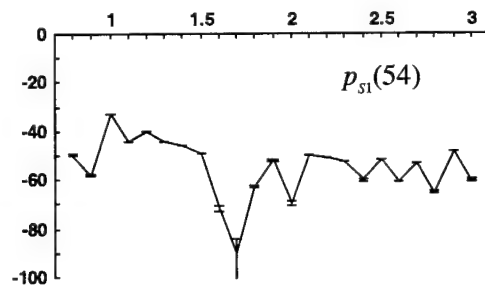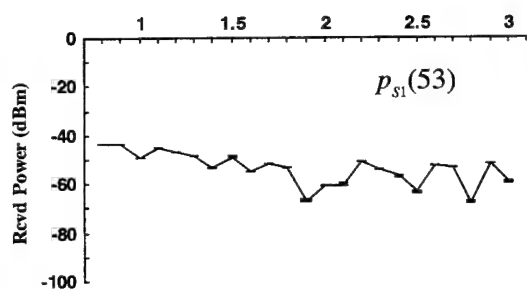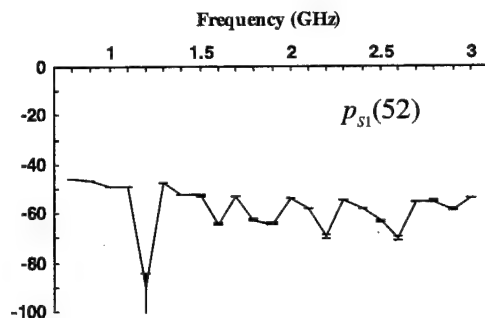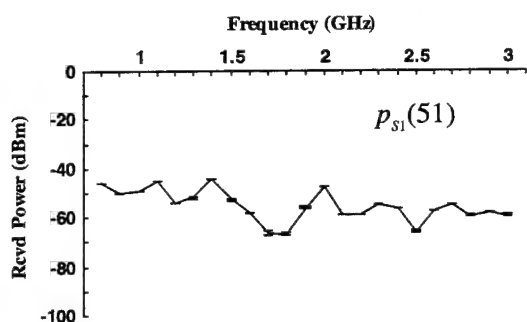
Raw Received Power for Data Sets 61 – 70
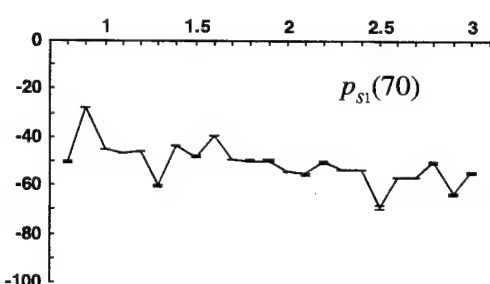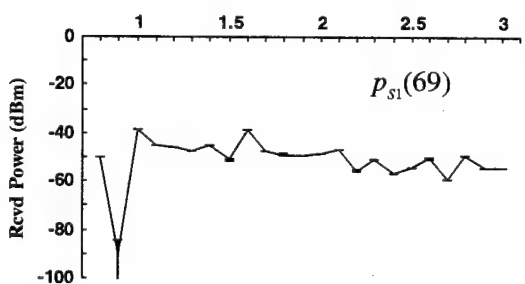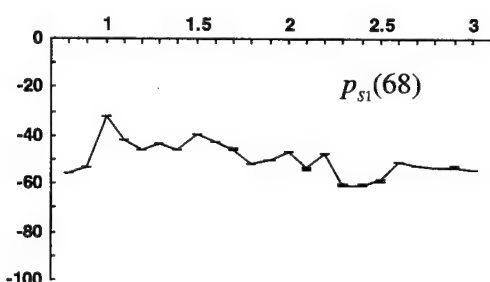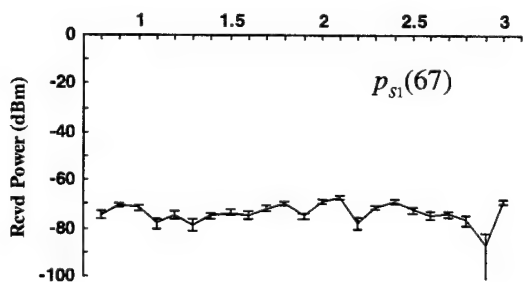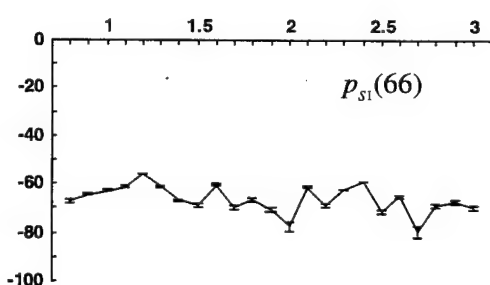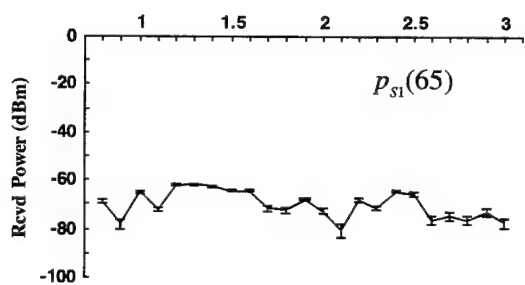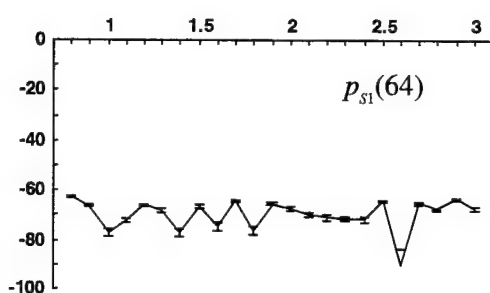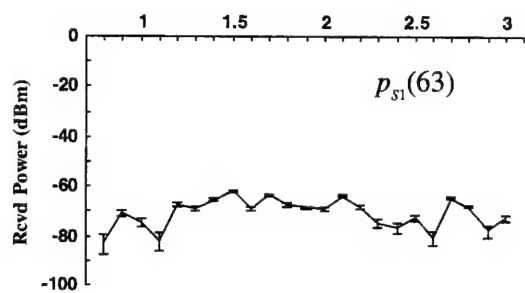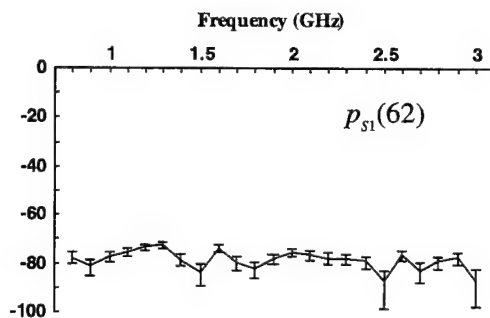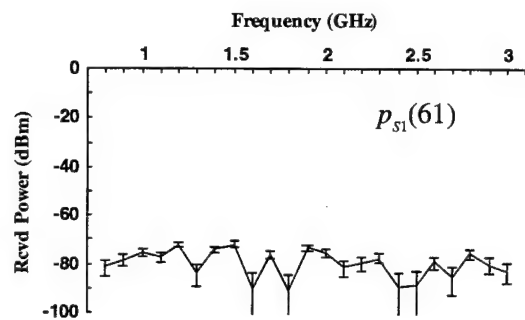
Raw Received Power for Data Sets 71 –80
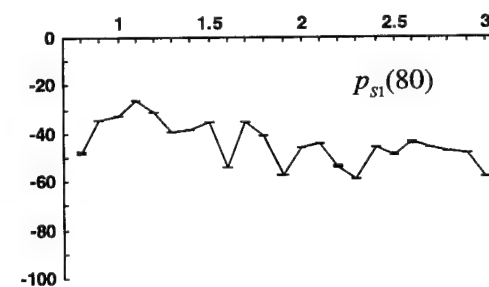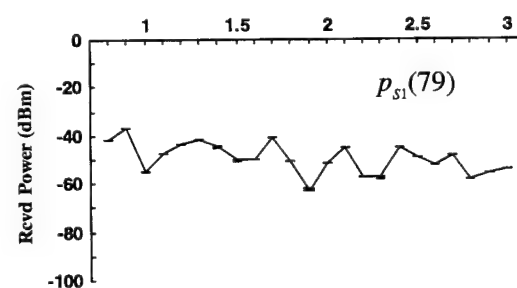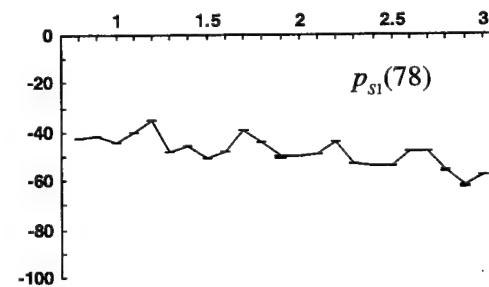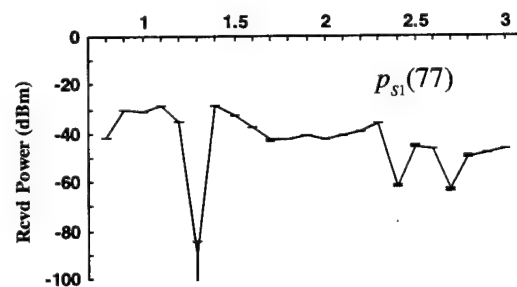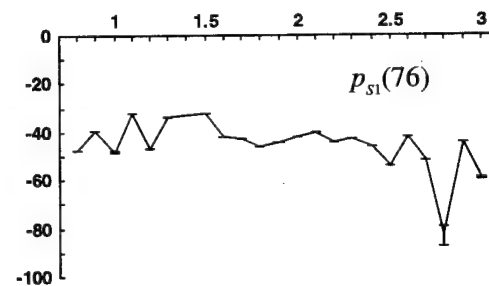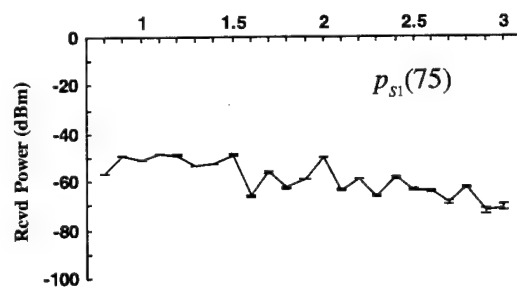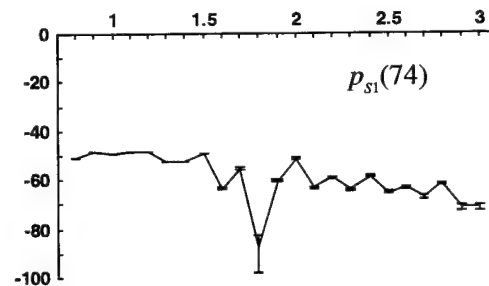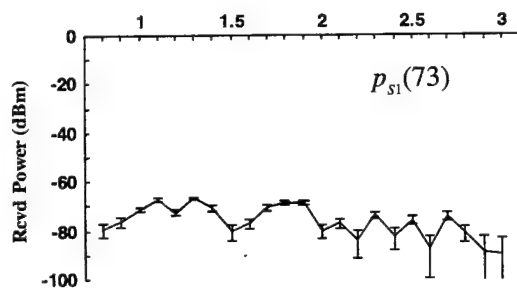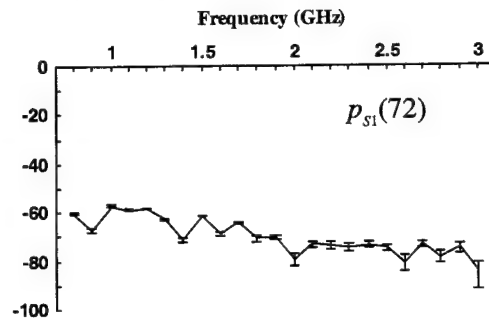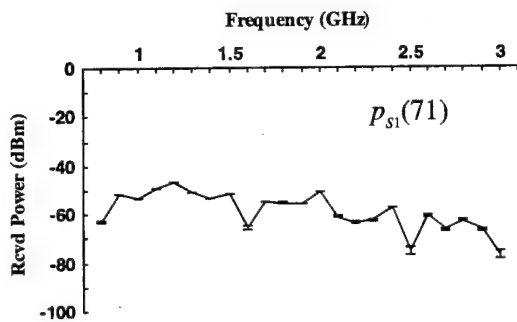
Raw Received Power for Data Sets 81 – 90
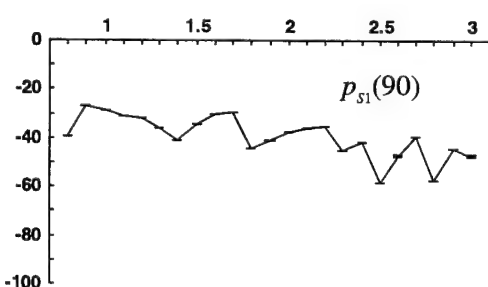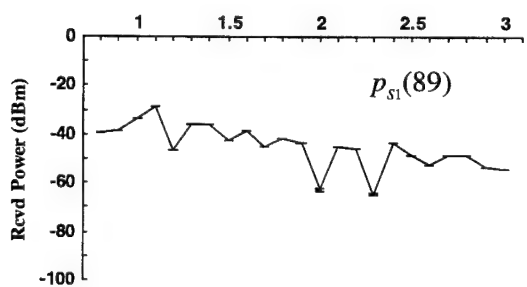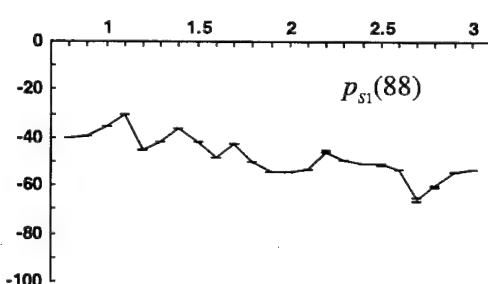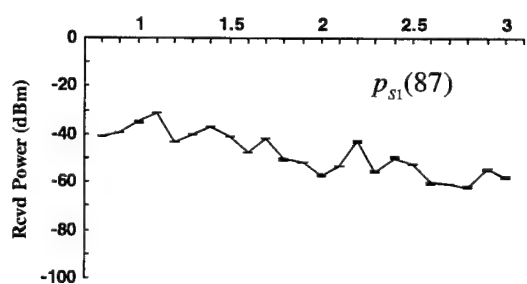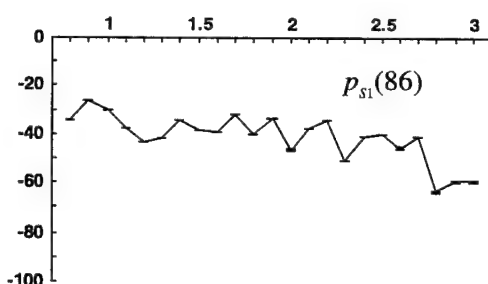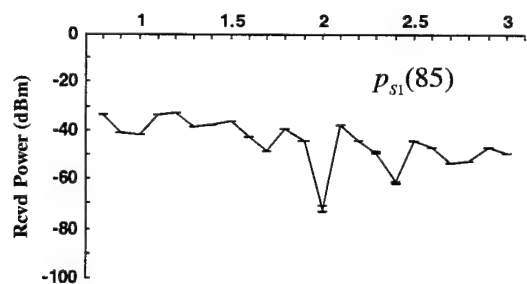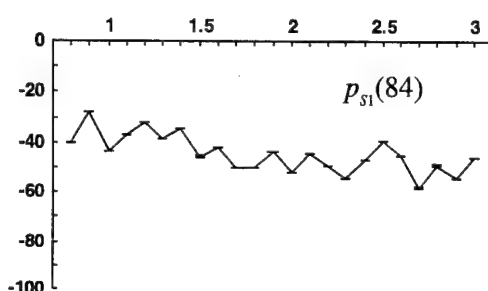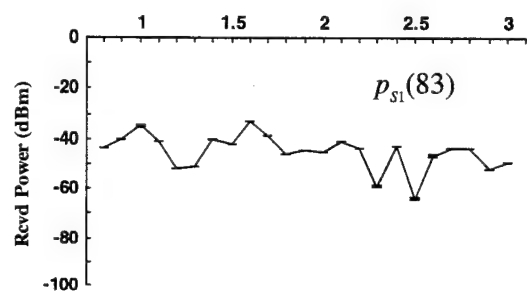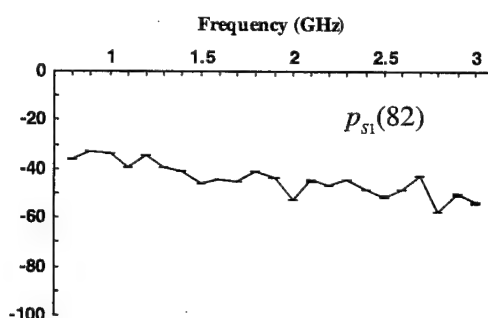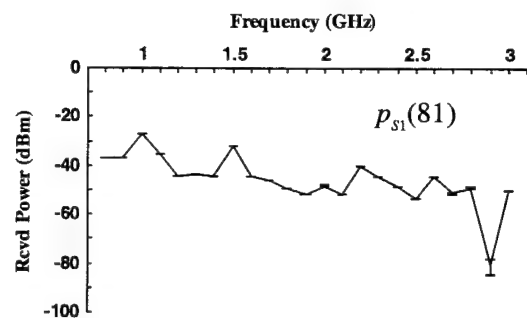
Raw Received Power for Data Sets 91 – 100
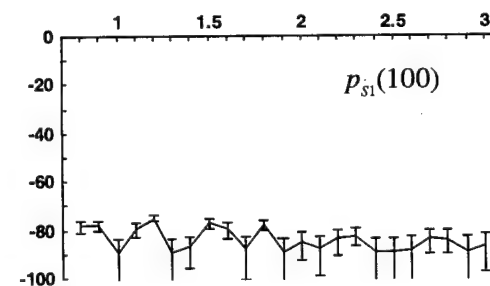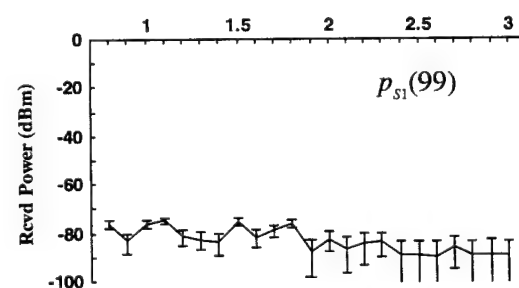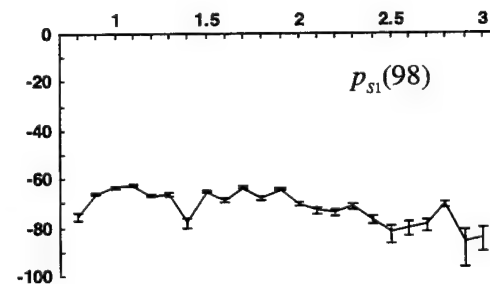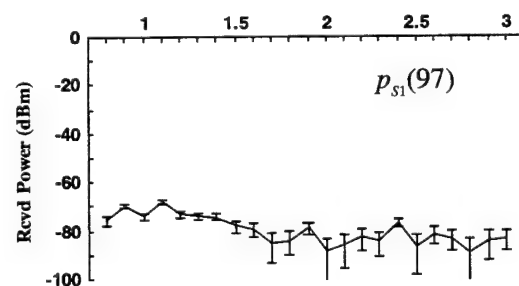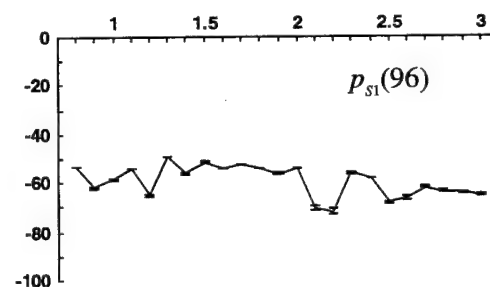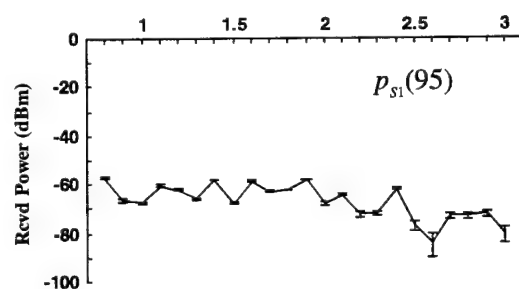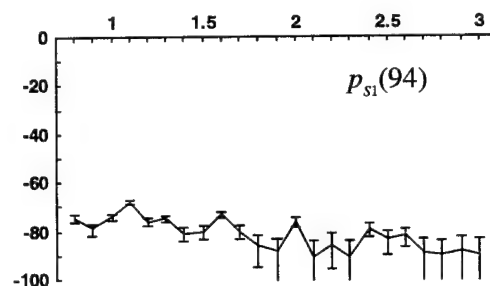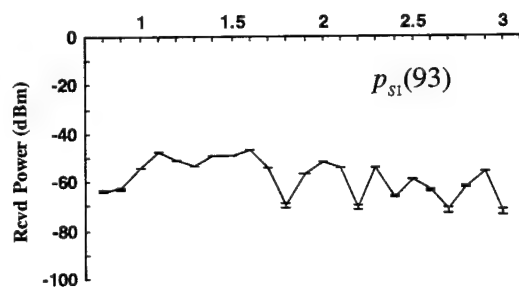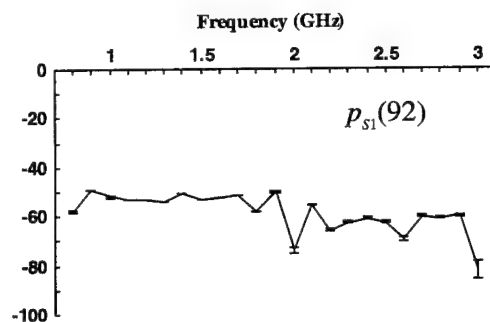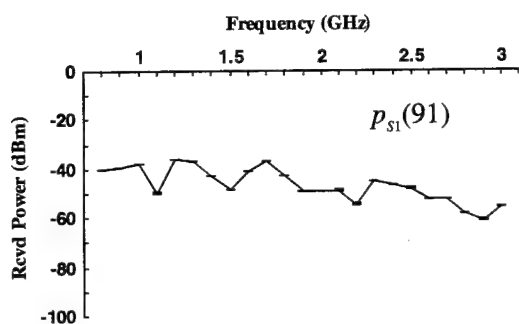
Raw Received Power for Data Sets 101 – 110
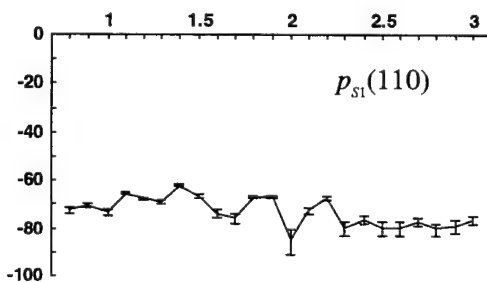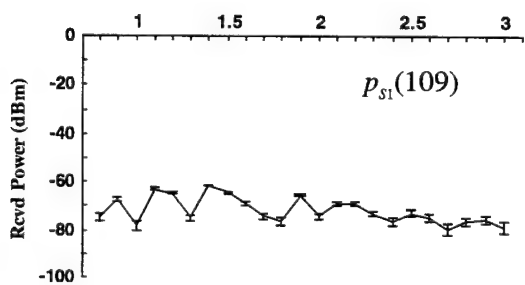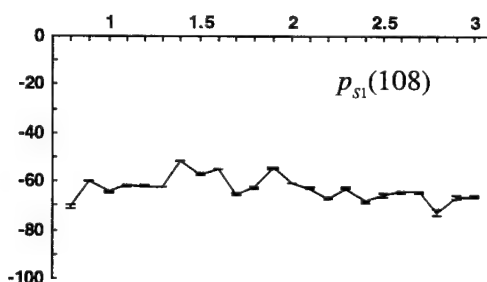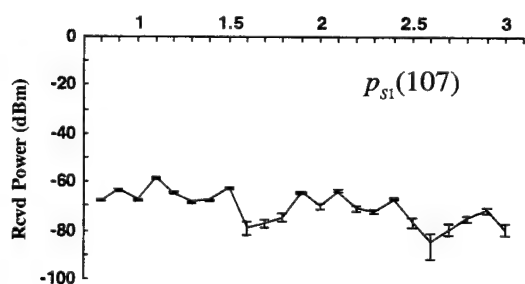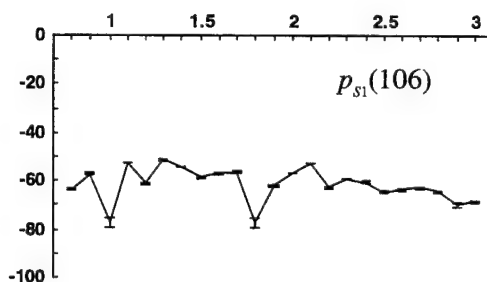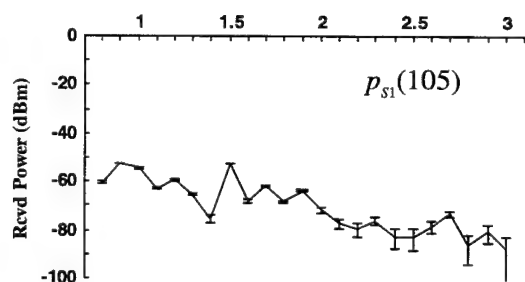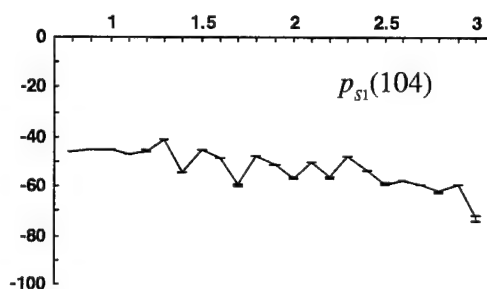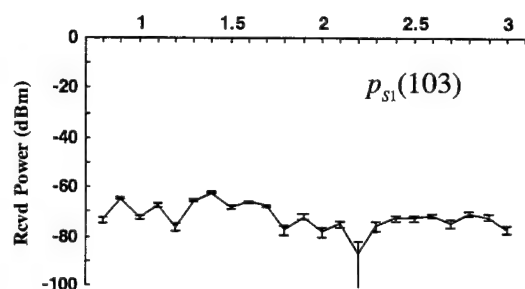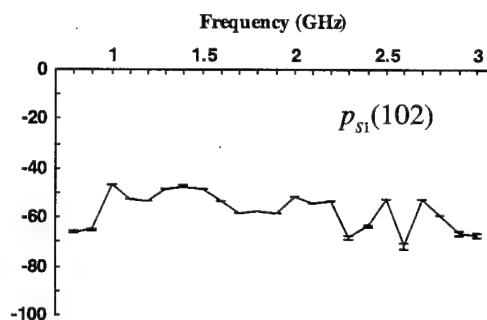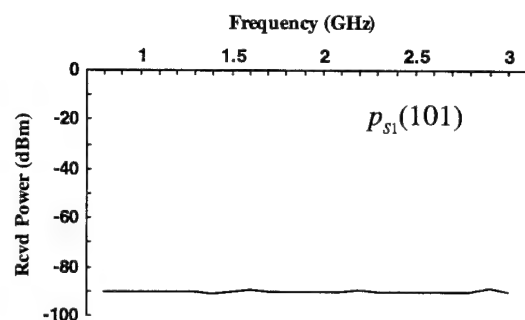
Raw Received Power for Data Sets 111 – 112
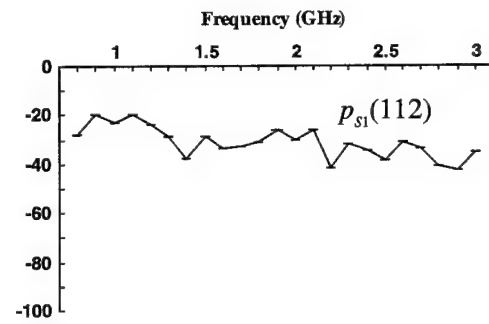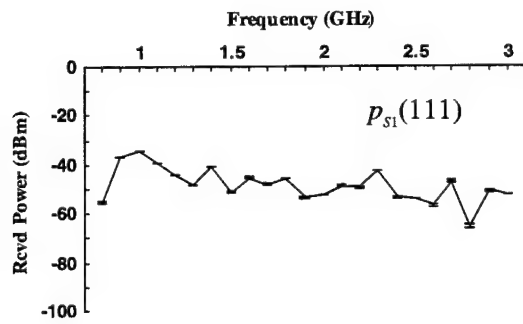
Appendix D

EFFECTIVE PROPAGATION LOSS FOR EX-USS *SHADWELL* MEASUREMENTS

This appendix provides the derived logarithmic effective propagation loss $l_{SP}(n)$ as defined by Eq. (2) for data sets 1 through 112, except for 101. The logarithmic free-space propagation loss $l_0(n)$, corresponding to the transmitter-receiver separations listed in Table A1 of Appendix A, is also included as the dashed curve for comparison.

For most measurements, $l_0(n)$ is substantially below $l_{SP}(n)$, which is what one might intuitively expect since L_{SP} is the product of several other effects L_α (see Eq. (B4) of Appendix B), including L_0. Generally, these effects tend to attenuate the received signal; however, for several data sets, they actually enhanced the signal return relative to the free-space propagation loss L_0: $n\varepsilon\{41, 42, 45, 48, 54, 56, 57, 60, 66, 68, 69, 70, 76, 81, 90, 111, 112\}$. A good example is the plot of $l_{SP}(41)$, which exceeds $l_0(41)$ at all except two frequencies. In this case, the transmitting antenna was located in $D_{1,3}$, and the receiving antenna was placed 4 ft away just outside open door 1-28-1 in $D_{1,2}$. For this configuration, the receiving antenna was in the near field of the transmitting antenna. Since the transmitting antenna was the omnidirectional disc-cone and since it was located equidistant from all four metallic bulkheads of $D_{1,3}$, the received signal had to have components from the transmitted signal that were scattered from the three bulkheads other than the one containing 1-28-1. Furthermore, these three signals probably arrived nearly in phase since the corresponding propagation paths of the scattered waves were roughly equal. In addition to the multipath from the bulkheads in $D_{1,3}$, the scattered signals from the aft bulkhead of $D_{1,2}$ were incident on the receiving antenna and undoubtedly contributed to elevating $l_{SP}(41)$ above $l_0(41)$. Evidently, the incident field on the receiving antenna was a superposition of several multipath fields, and this increased power of the received signal above what it would have been if the radiation had taken place in free space. Consequently, the increased power of the received signal (relative to the free-space signal) at short ranges in this confined metallic space must be caused in part by multipath.

Effective and Free-Space Propagation Losses for Data Sets 1 – 10
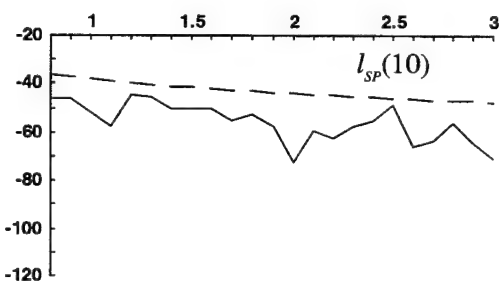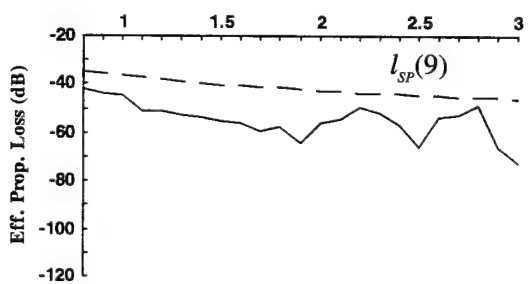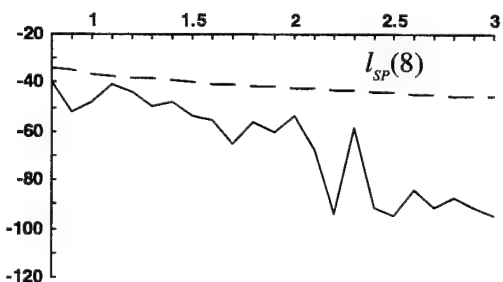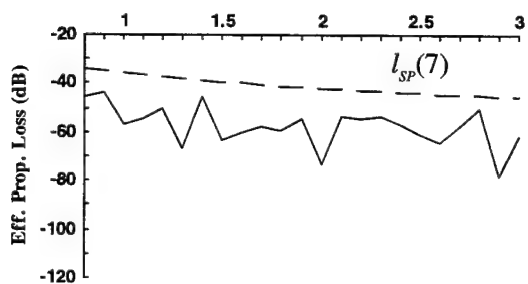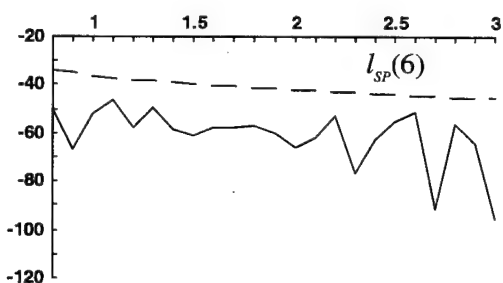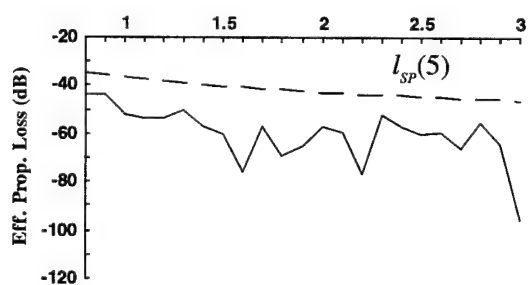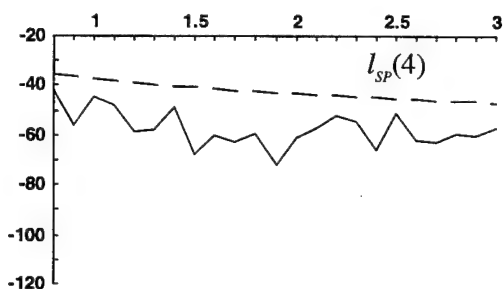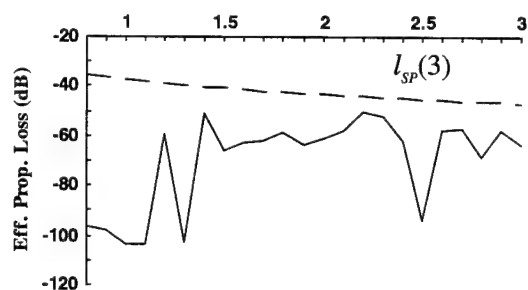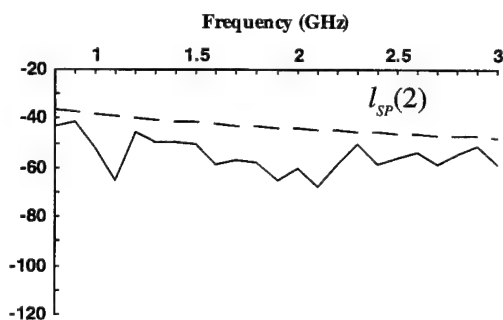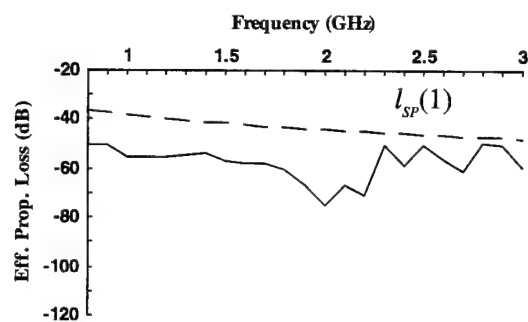
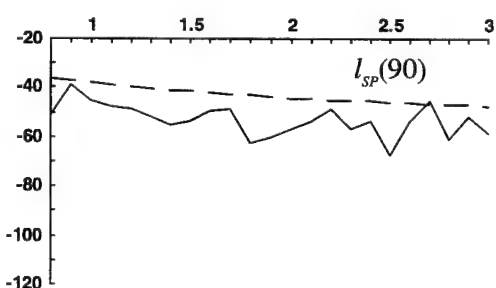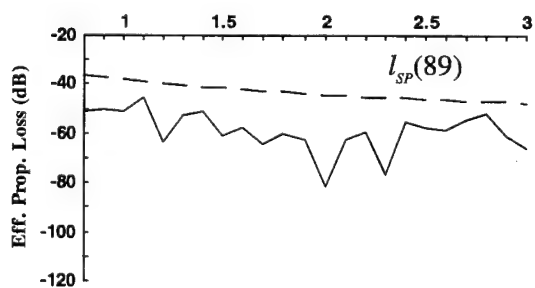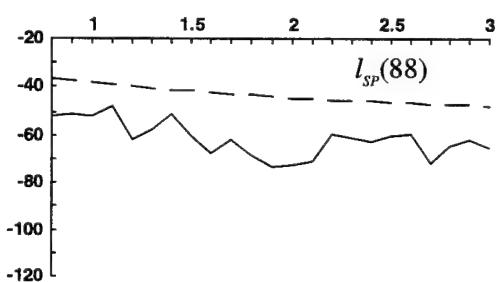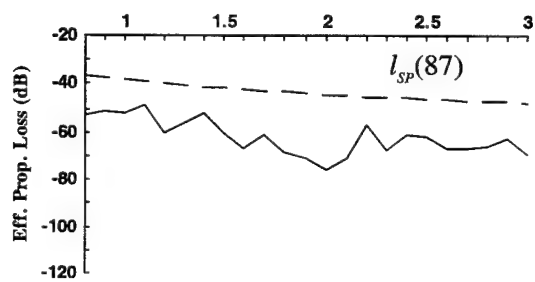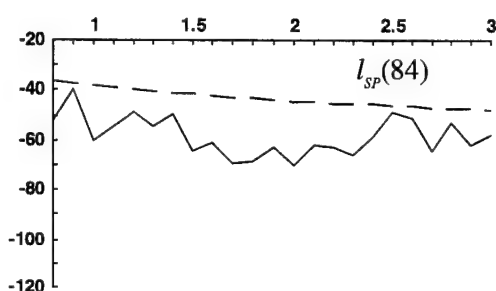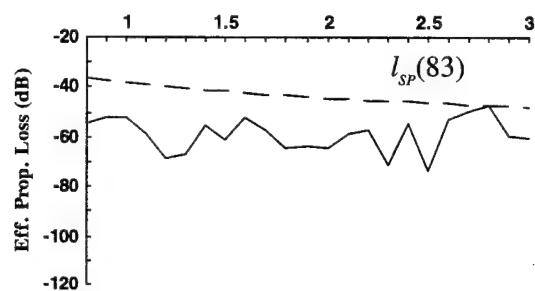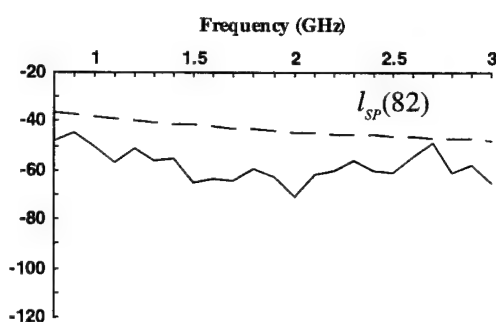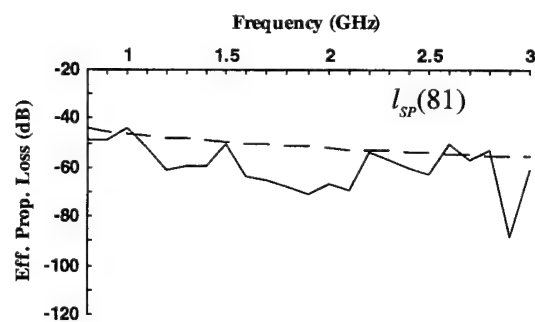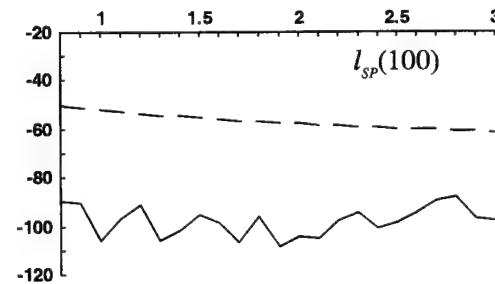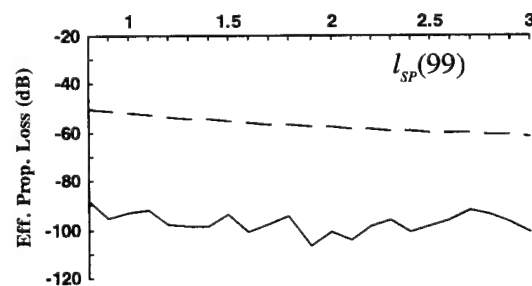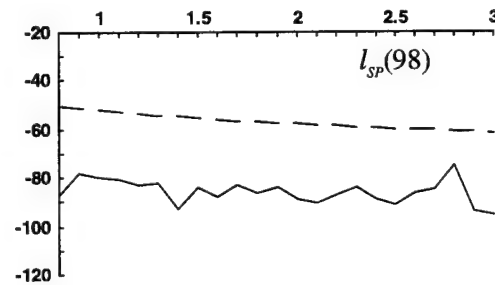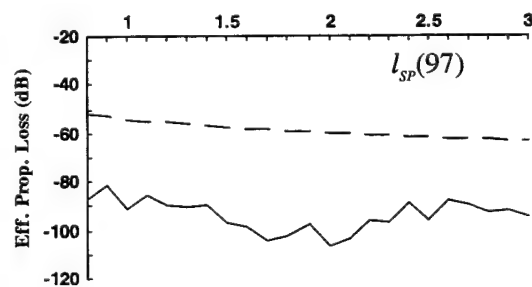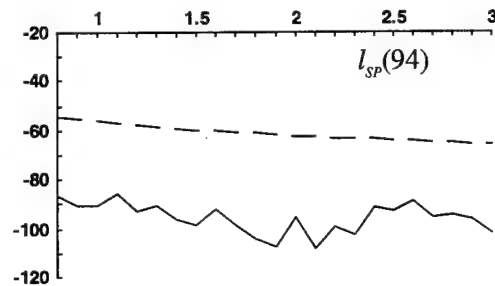Effective and Free-Space Propagation Losses for Data Sets 11 – 20
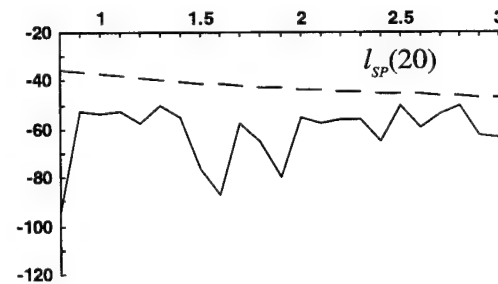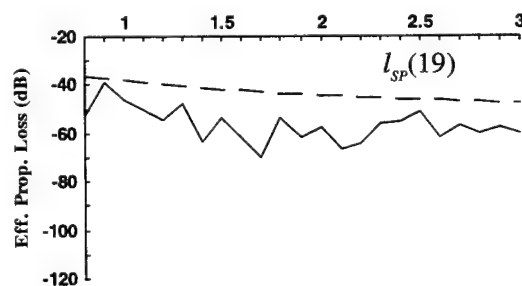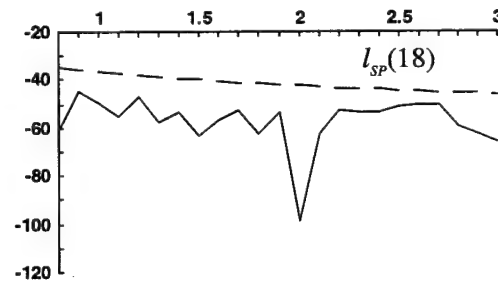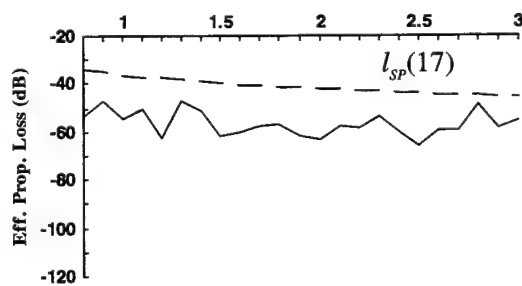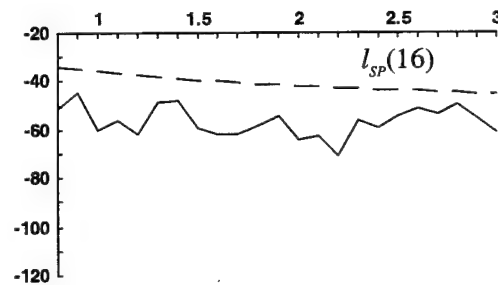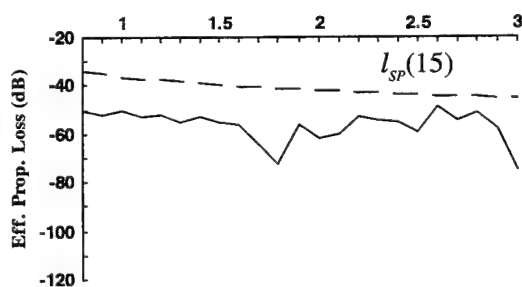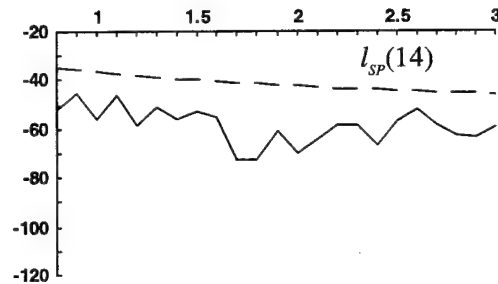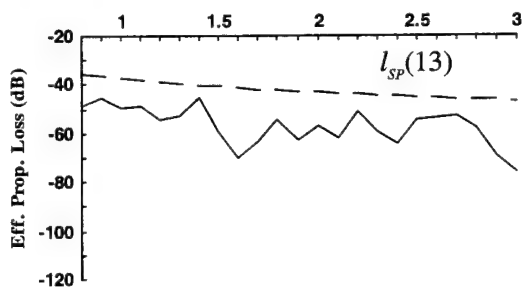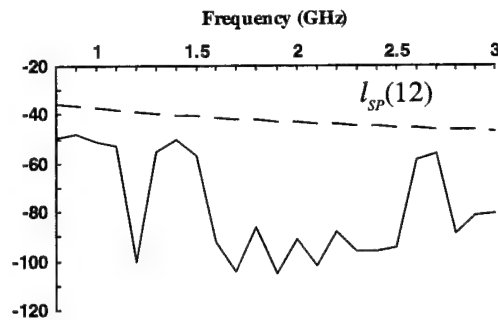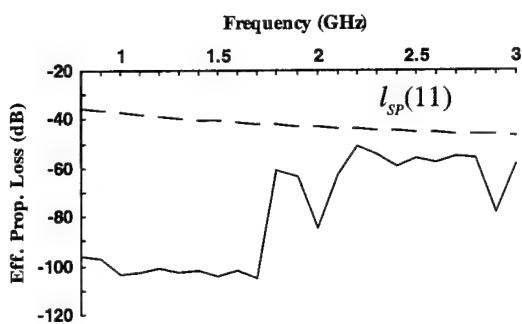
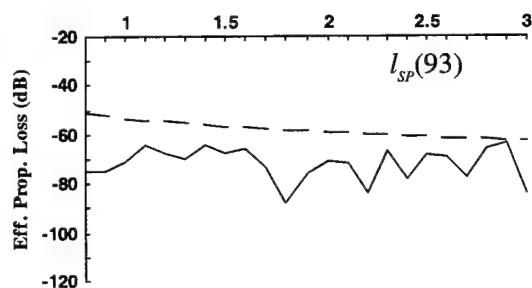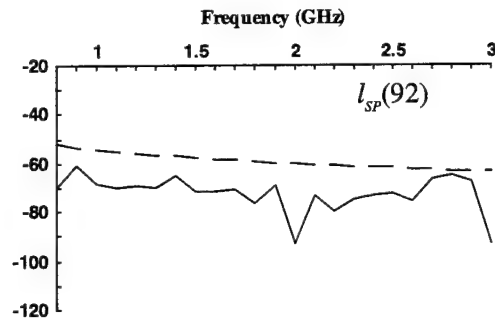### Effective and Free-Space Propagation Losses for Data Sets 21 – 30
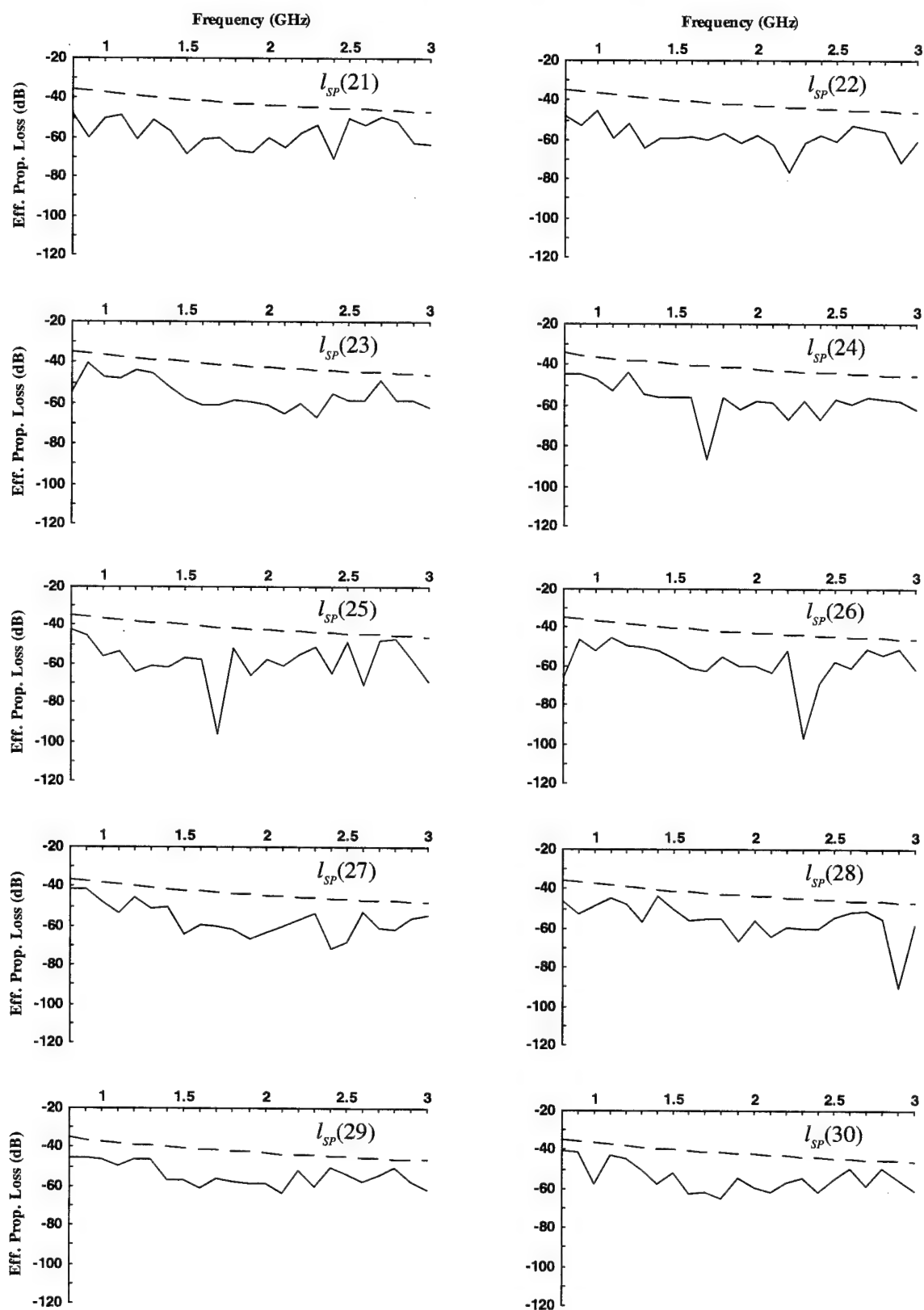
Effective and Free-Space Propagation Losses for Data Sets 31 – 40
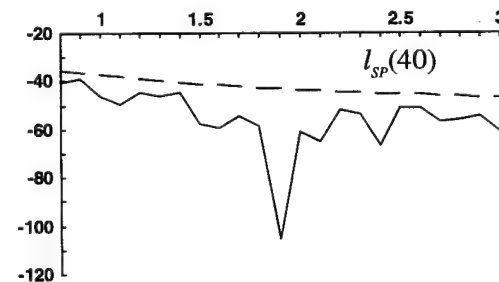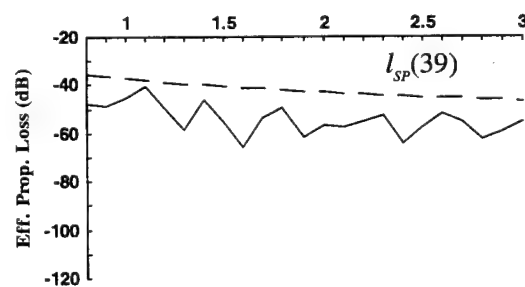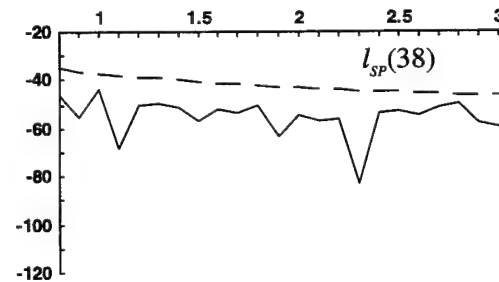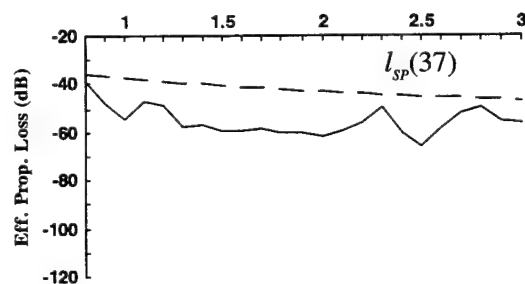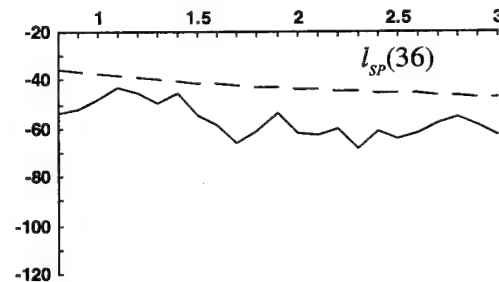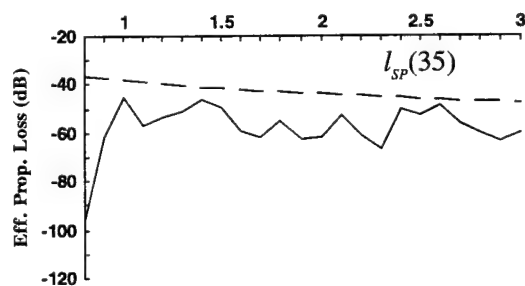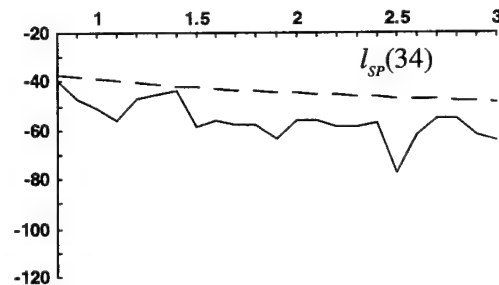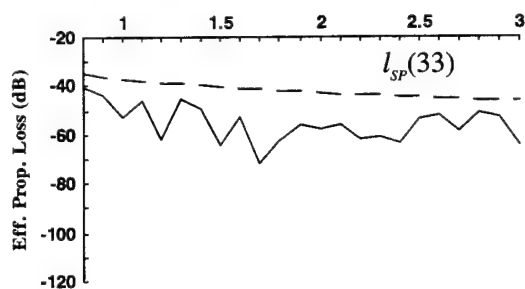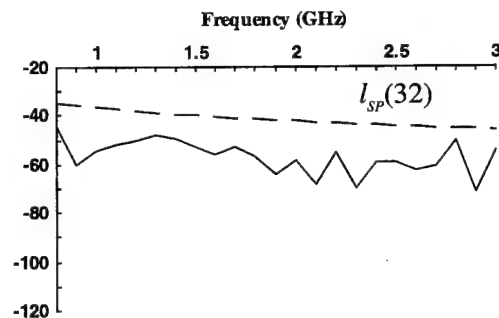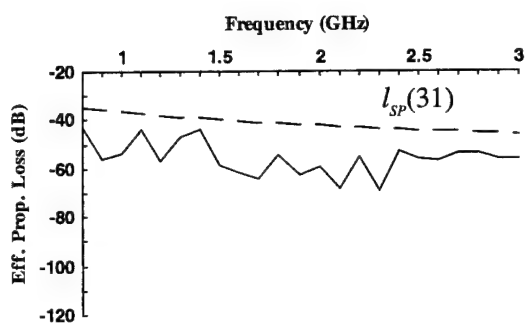
Effective and Free-Space Propagation Losses for Data Sets 41 – 50
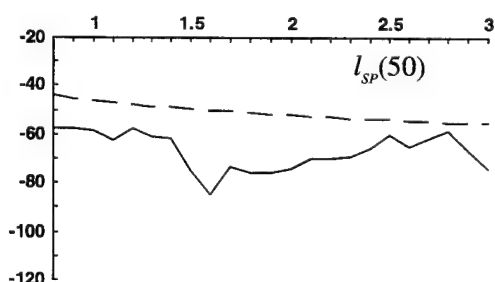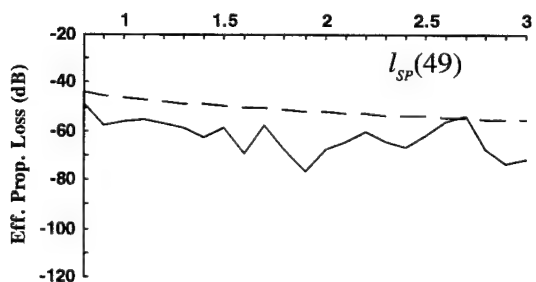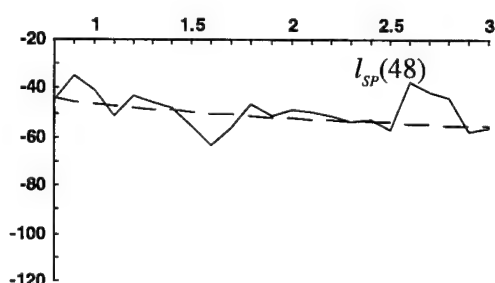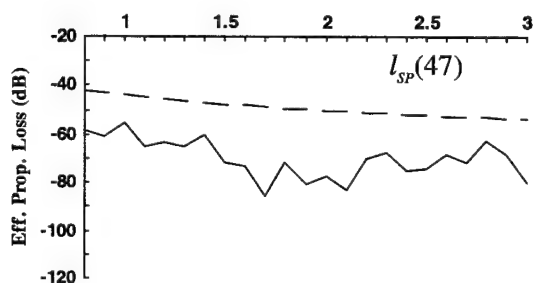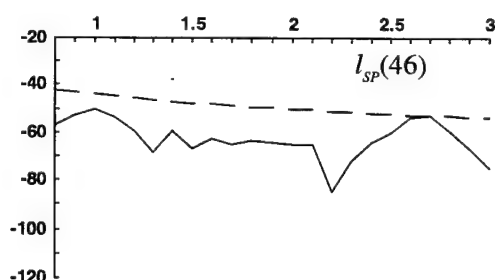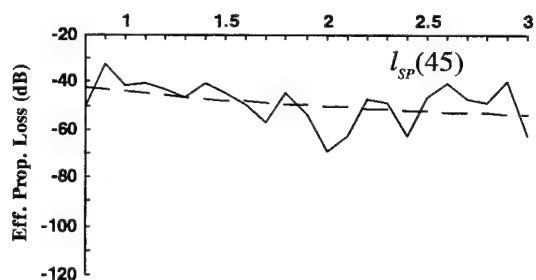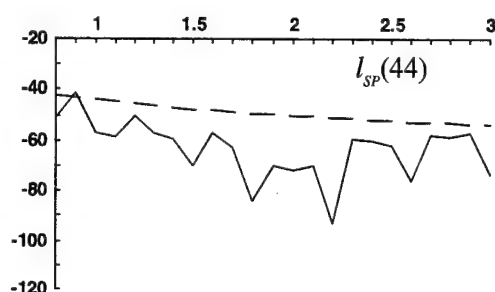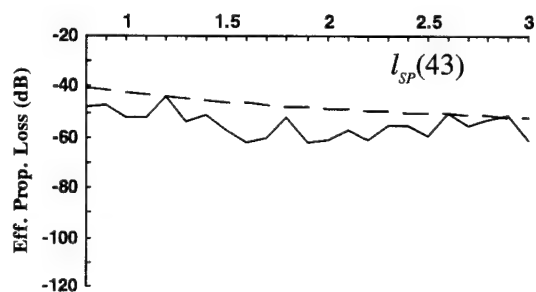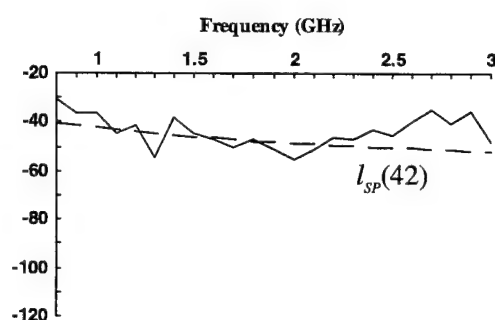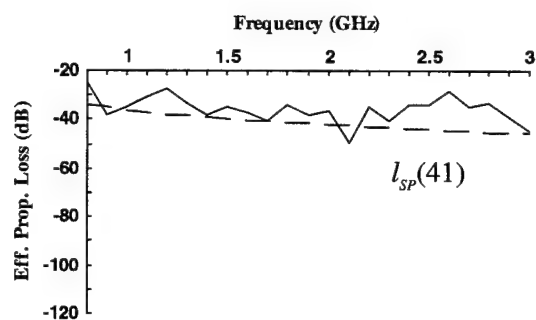
Effective and Free-Space Propagation Losses for Data Sets 51 – 60
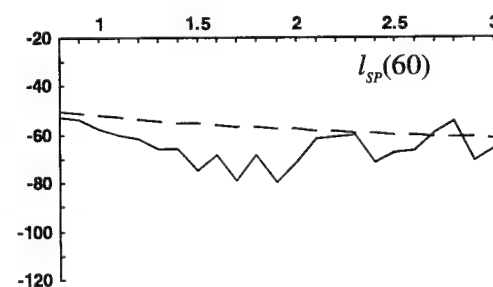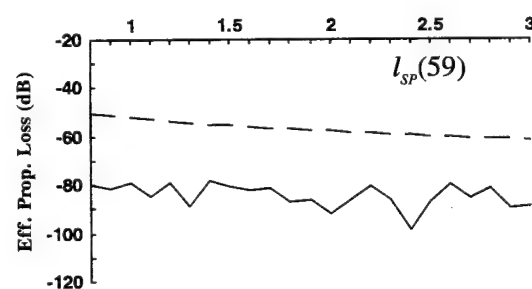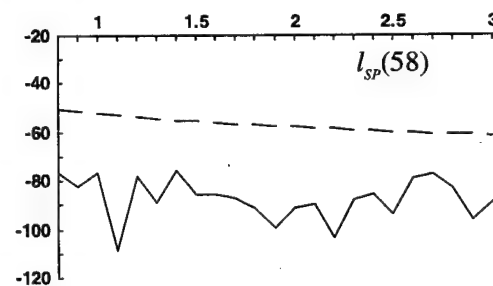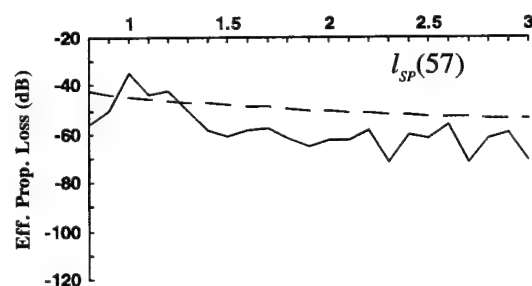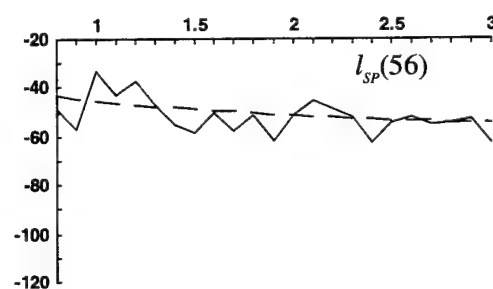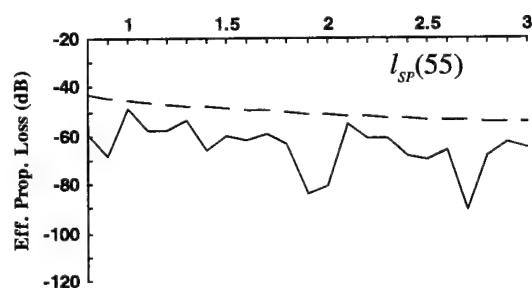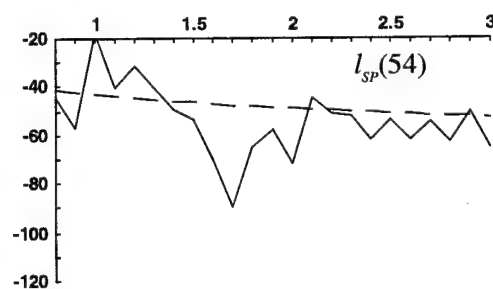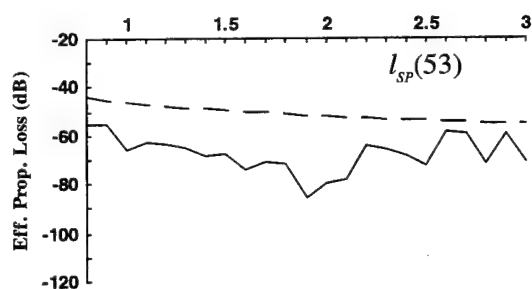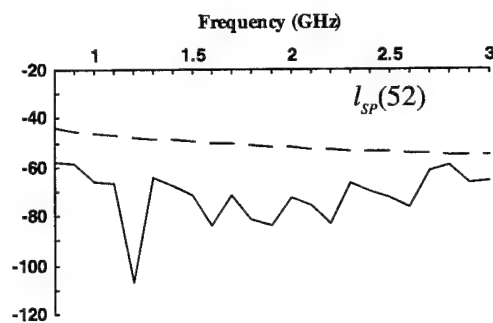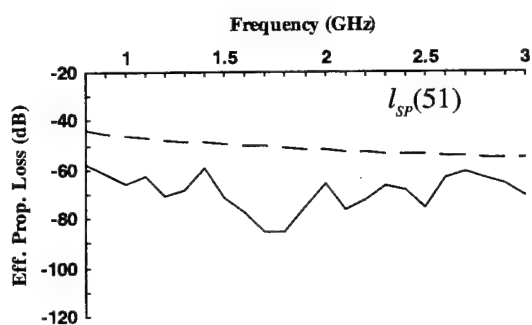
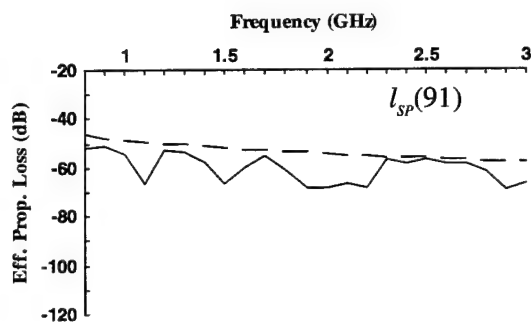### Effective and Free-Space Propagation Losses for Data Sets 61 – 70
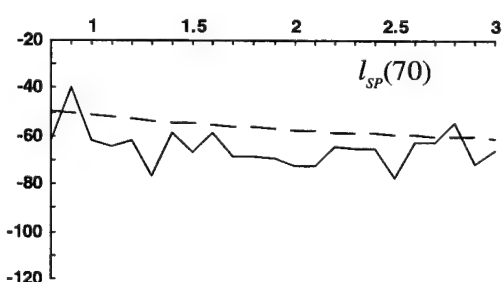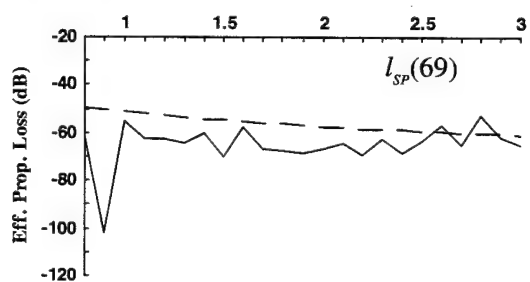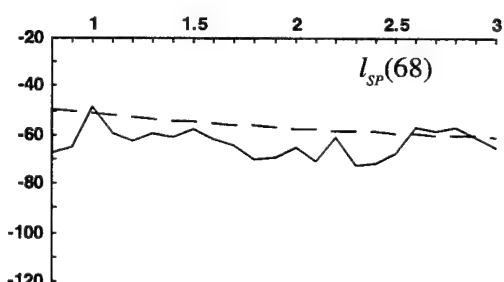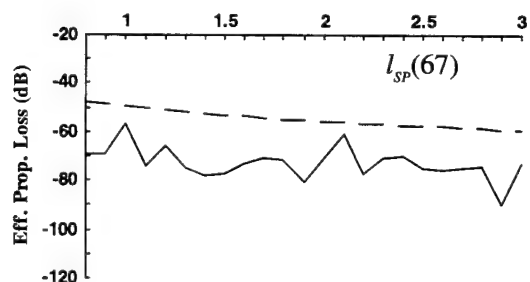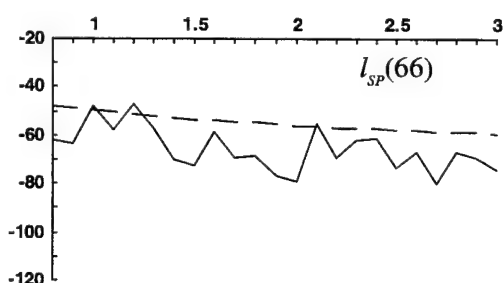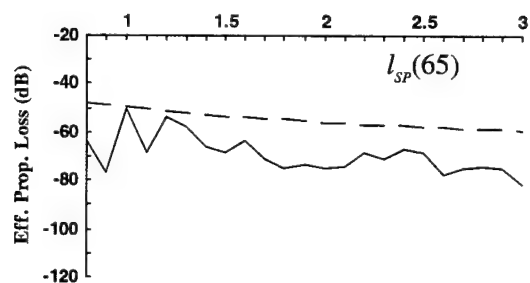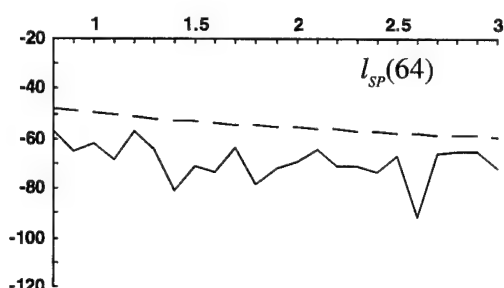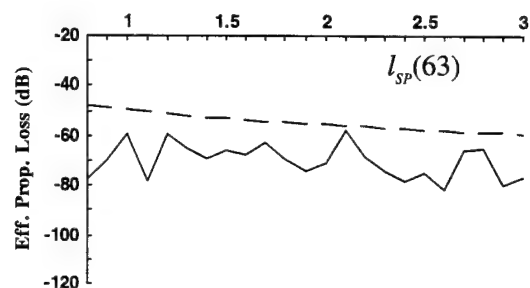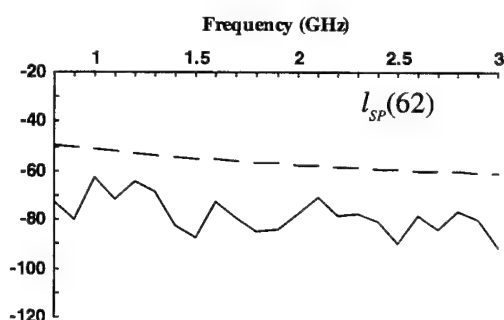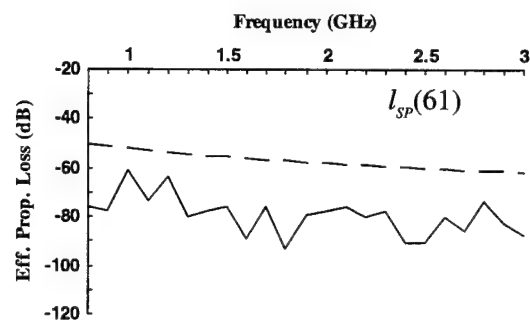
Effective and Free-Space Propagation Losses for Data Sets 71 – 80
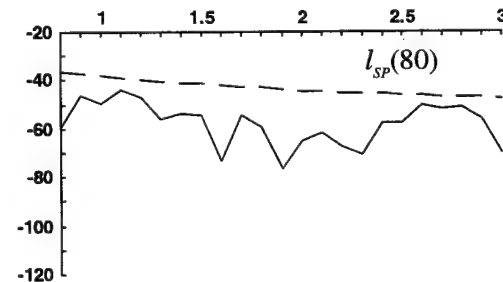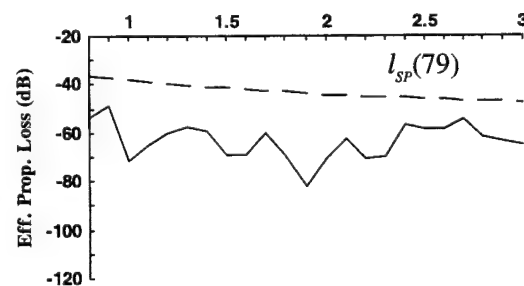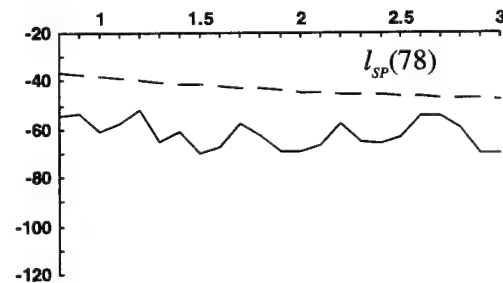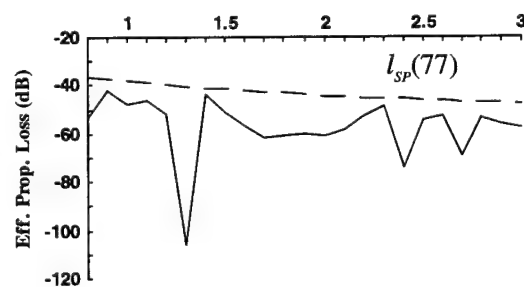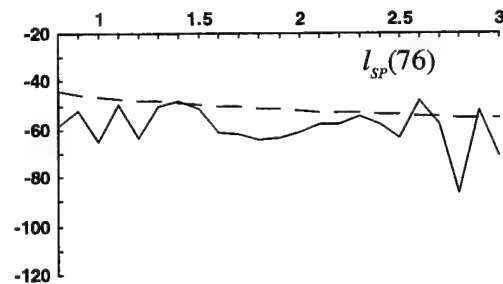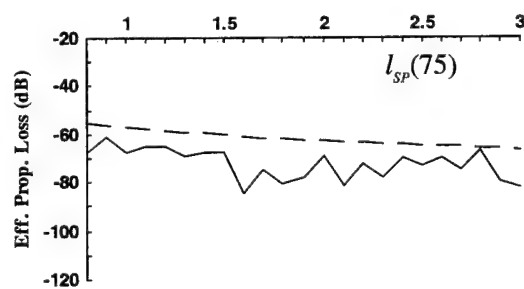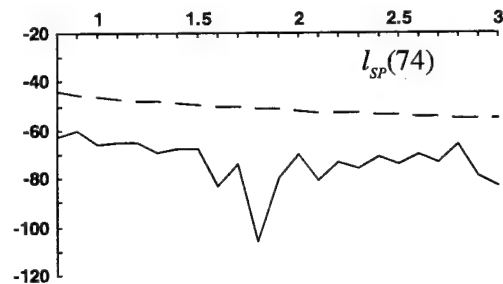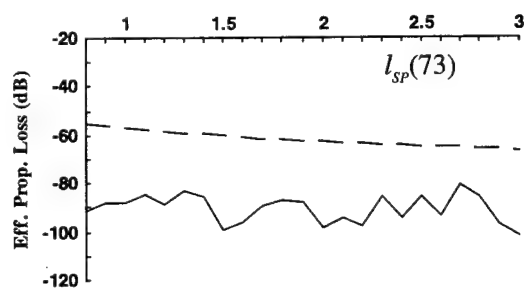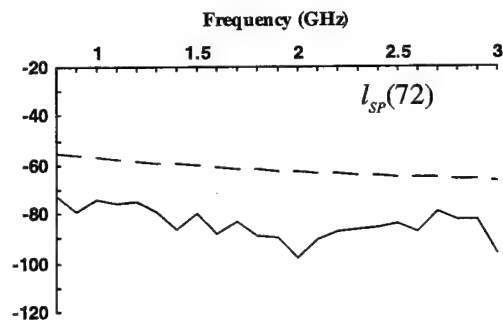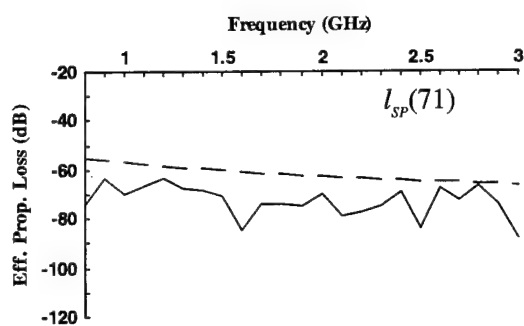
Effective and Free-Space Propagation Losses for Data Sets 81 – 90
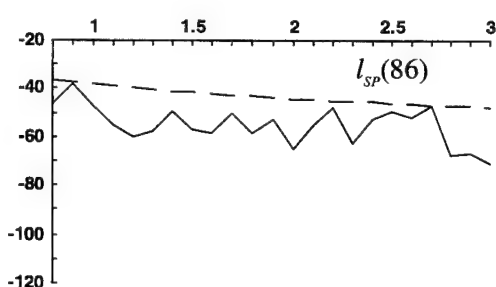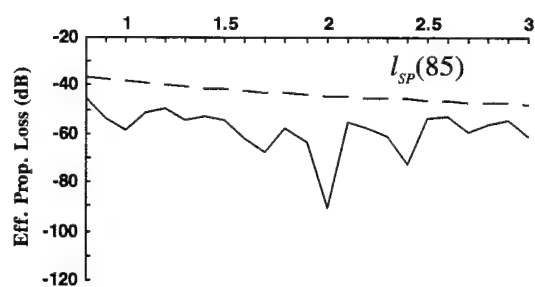
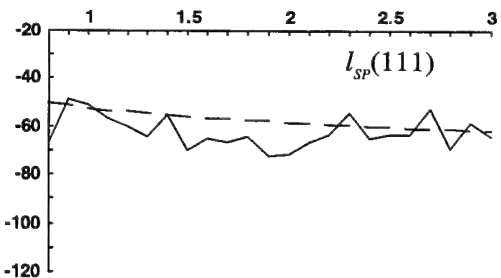## Effective and Free-Space Propagation Losses for Data Sets 91 – 100
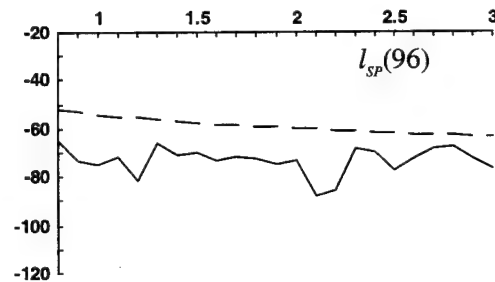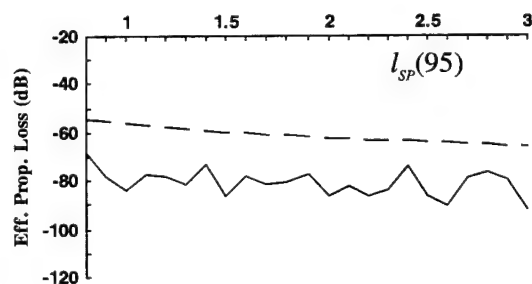
Effective and Free-Space Propagation Losses for Data Sets 102 – 111
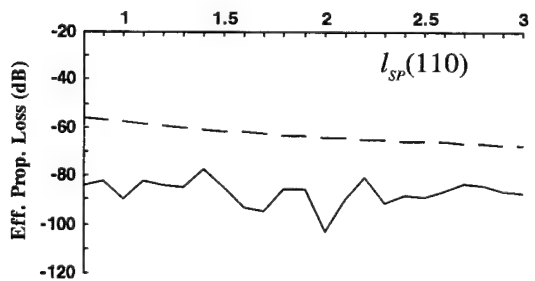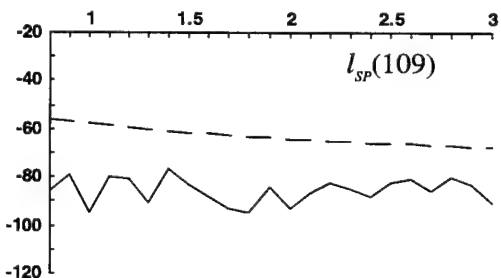
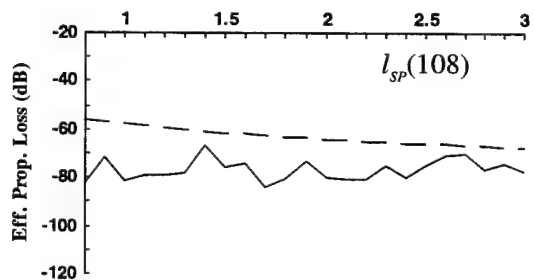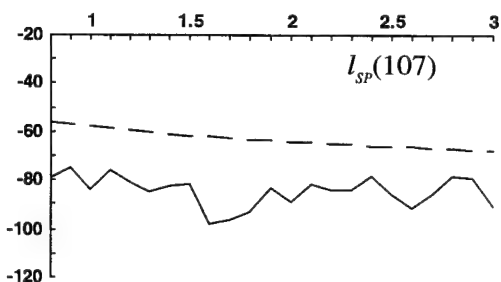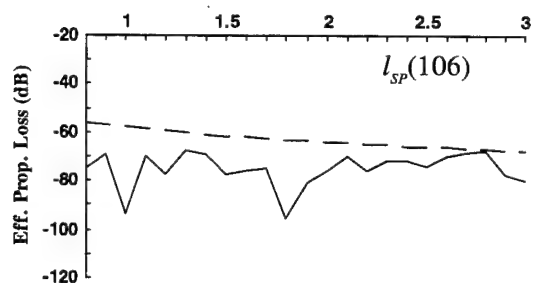## Effective and Free-Space Propagation Losses for Data Set 112

Appendix E

DERIVATION OF ERROR BARS FOR RECEIVED POWER

The purpose of this appendix is to determine error bars for the magnitude of the received measured power P_M of an arbitrary receiving system in the frequency domain. To accomplish this, first consider the corresponding receiv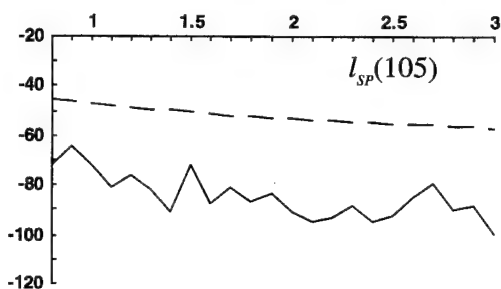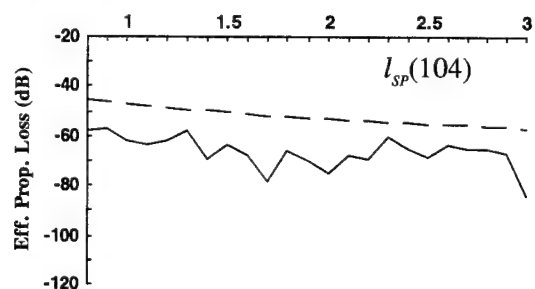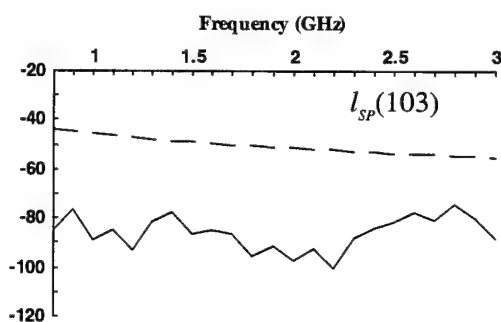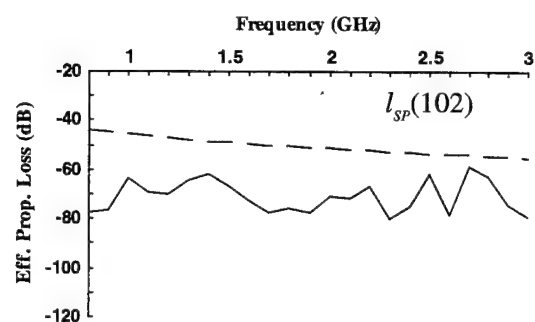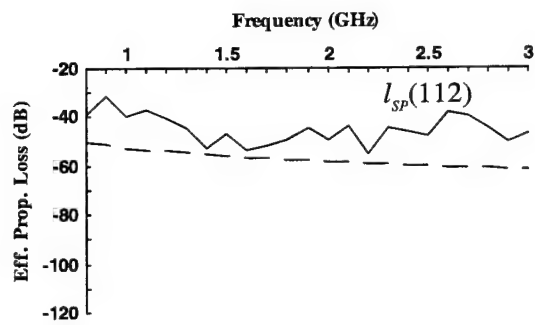ed voltage V_M. For a receiving system, V_M is generally the sum of the true incident voltage V_S across the receive terminals and the receiving system's background noise voltage V_N. The system noise is generated by several components of the receiver (amplifiers, cables, mixers, etc.). Because V_S, V_N, and V_M are complex phasors (Fig. E1), let

$$V_S = v_S e^{i\phi_S}, \quad V_N = v_N e^{i\phi_N}, \quad V_M = v_M e^{i\phi_M}, \tag{E1}$$

where v_l and ϕ_l are the magnitudes and phases, respectively, of the three voltages ($l = S,N,M$) (Fig. E1). Since the true voltage V_S is unknown, upper-bound and lower-bound curves are sought that depend on the two known measured quantities (V_M and V_N).
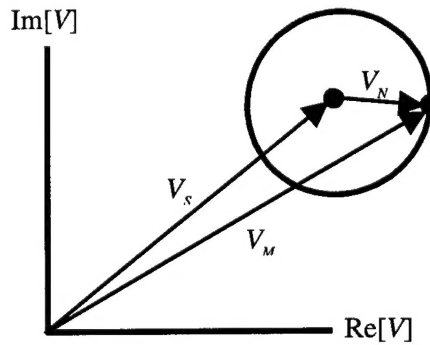
Fig. E1. — Phasor representation of the actual voltage V_S, the noise voltage V_N, and the measured voltage V_M in the complex V plane

Substitute Eq. (E1) into the expression, $V_M = V_S + V_N$, to obtain

$$\begin{aligned} v_M e^{i\phi_M} &= v_S e^{i\phi_S} + v_N e^{i\phi_N} \\ \Leftrightarrow v_S e^{i\phi_S} &= v_M e^{i\phi_M} - v_N e^{i\phi_N} \\ \Leftrightarrow v_S e^{i(\phi_S - \phi_N)} &= v_M e^{i(\phi_M - \phi_N)} - v_N. \end{aligned} \tag{E2}$$

Taking the magnitude of both sides of Eq. (E2) yields

$$v_S^2 = \left[v_M e^{i(\phi_M - \phi_N)} - v_N \right]\left[v_M e^{-i(\phi_M - \phi_N)} - v_N \right] = v_M^2 + v_N^2 - 2v_N v_M \cos(\phi_M - \phi_N),$$

$$\Rightarrow \tag{E3}$$

$$\left(v_M - v_N \right)^2 \leq v_S^2 \leq \left(v_M + v_N \right)^2.$$

Let R be the resistance in the equivalent network for the three voltages, and let P_l be the corresponding power (that is, $P_l = v_l^2 / R$). Equation (E3) becomes

$$\left(\sqrt{P_M} - \sqrt{P_N} \right)^2 \leq P_S \leq \left(\sqrt{P_M} + \sqrt{P_N} \right)^2. \tag{E4}$$

By inspection of (E4), the actual power P_S lies in the interval $[P_L, P_U]$, where

$$P_L = P_M \left(1 - \sqrt{\frac{P_N}{P_M}} \right)^2, \qquad P_U = P_M \left(1 + \sqrt{\frac{P_N}{P_M}} \right)^2. \tag{E5}$$

Both P_L and P_U are expressed in terms of the measured return P_M and the measured signal-to-noise ratio ($SNR_M = P_M / P_N$). For any subscript l and for SNR_M, let

$$p_l = 10 \log_{10} P_l, \qquad \alpha = 10 \log_{10} \left(P_M / P_N \right). \tag{E6}$$

Consequently,

$$p_L = p_M + \varepsilon_L, \qquad p_U = p_M + \varepsilon_U, \tag{E7}$$

where the upper error ε_U and the lower error ε_L are given by

$$\varepsilon_L = 20 \log_{10} \left| 1 - \sqrt{\frac{P_N}{P_M}} \right|, \qquad \varepsilon_U = 20 \log_{10} \left(1 + \sqrt{\frac{P_N}{P_M}} \right). \tag{E8}$$

Since P_N is the minimum detectable signal, values of P_M that are less than or equal to P_N have no relevance. In the remaining analysis, assume that $P_N < P_M$, which removes the absolute value in (E8). Further algebraic manipulation of (E8) yields

$$\varepsilon_L = 20 \log_{10} \left(1 - e^{\frac{-\alpha}{20 \log_{10} e}} \right), \qquad \varepsilon_U = 20 \log_{10} \left(1 + e^{\frac{-\alpha}{20 \log_{10} e}} \right). \tag{E9}$$

Both errors depend on α and are depicted in Fig. E2. Clearly, $\varepsilon_L < 0$ and $\varepsilon_U > 0$. Moreover, the magnitudes of the errors are unequal for all values, which is clear from the asymmetry in the figure for small values of α. However the magnitudes are approximately equal when α exceeds 30 dB (Table E1). The preceding analysis is modeled on the radar-cross-section work in Ref. E1, where bounds are determined for the

measured signal instead of bounds on p_s. Figure 13.12 in Ref. E1 is very similar to Fig. E2, but the values of the error bounds are slightly different because the emphasis is different.

The value of the true signal p_s minus the measured signal p_M ($p_s - p_M$) lies between the bounding curves of Fig. E2. Consequently, for a given value of p_M, one can associate an error bar with it by connecting ε_L and ε_U with a vertical line segment that passes through p_M. The actual signal p_{S1} will correspond to some point on the error bar. Because of the logarithmic scale, the error bar is not symmetric about p_M. Moreover, the error bar decreases as α increases. For reasonable measurement accuracy, one would like α to exceed 20 dB.
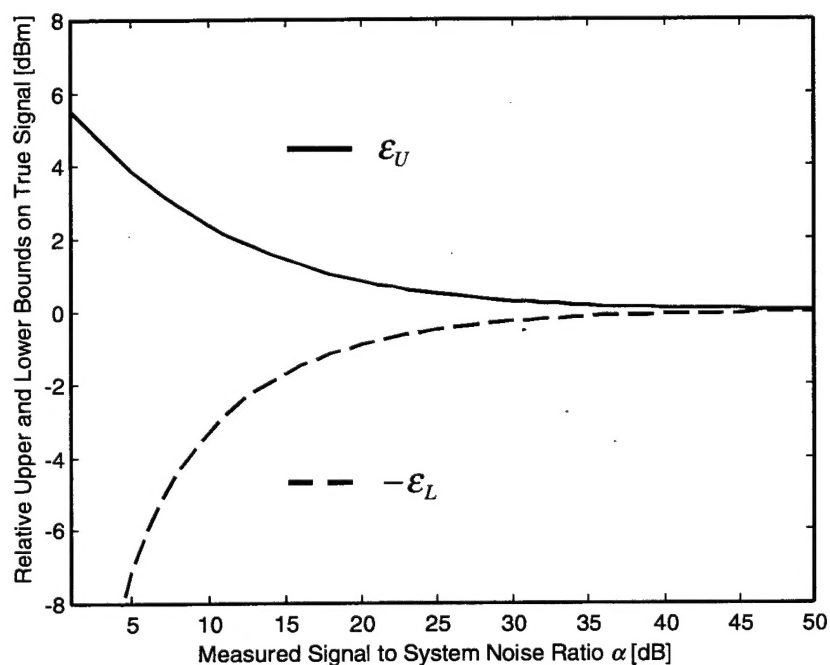

Fig. E2 — Relative upper bound ε_U and relative lower bound ε_L for the true received signal power vs the measured signal-to-noise ratio α given the measured signal power p_M and the noise p_N.

Table E1 – Error Bounds on Measured Signal p_M

α [dB]	ε_U [dB]	ε_L [dB]	$\varepsilon_U - \varepsilon_L$ [dB]
1	5.535	-19.271	24.806
5	3.876	-7.177	11.053
10	2.387	-3.302	5.688
15	1.422	-1.701	3.122
20	0.828	-0.915	1.743
25	0.475	-0.503	0.978
30	0.270	-0.279	0.550
35	0.153	-0.156	0.309
40	0.086	-0.087	0.174
45	0.049	-0.049	0.098
50	0.027	-0.028	0.055

REFERENCE

E1. J.S. Hollis, T.J. Lyon, and L. Clayton, *Microwave Antenna Measurements* (Scientific-Atlanta, Inc., Atlanta GA, 1970), Ch. 13.